Dissertation
submitted to the
Combined Faculties for Natural Sciences and for Mathematics
of the Ruperto-Carola University of Heidelberg, Germany
for the degree of
Doctor of Natural Sciences

presented by
Meeta Girish Kulkarni, M.Sc. Microbiology
born in Mumbai, India
Oral examination on 24 April 2012

Characterization of Butyrate response factor 2

and study of its role in

AU-rich element-mediated mRNA decay

Referees: Prof. Dr. Ingrid Grummt
Dr. Georg Stoecklin

I hereby declare that I have written the submitted dissertation myself and in this process have used no other sources or materials than those explicitly indicated.
The work was carried out in the German Cancer Research Center (DKFZ) Heidelberg in the group *"Posttranscriptional Control Of Gene Expression"* of Dr. Georg Stoecklin.

Heidelberg, February 2012 Ms. Meeta Girish Kulkarni

Summary

AU-rich element (ARE)-mediated mRNA decay (AMD) is a prominent mode of mRNA degradation considering 10-15 % of mRNAs in the cell contain AREs in their 3' untranslated region (UTR). AMD is majorly promoted by the Tris-tetraproline (TTP) family of proteins which bear extensive homology among each other. This family comprises TTP and Butyrate response factors (BRF) 1 and 2. These proteins bind to AREs in mRNA 3'UTRs and accelerate degradation of these mRNAs. In my study, I characterized the protein BFR2 and tried to determine its possible role in AMD. Results suggested that BRF2 degrades mRNAs in an ARE-dependent manner and that BRF2 binds to 14-3-3 protein in a phosphorylation-dependent manner. I performed a detailed interaction analysis of BRF2 with 14-3-3 as a possible means of AMD-regulation by BRF2. I could establish that the serine residues S123 and S257 in BRF2 are the binding sites for 14-3-3 and that simultaneous mutation of both sites was neccessary to abolish 14-3-3 binding. The kinase MK2 appeared to affect the BRF2-14-3-3 interaction. However, unlike observed for TTP and BRF1, overexpression of MK2 did not reduce AMD efficiency of BRF2. This could possibly imply that BRF2 is resistant to inactivation by stress-induced kinases. 14-3-3 binding mutants of BRF2 localized slightly more nuclear than BRF2 wildtype which was predominantly cytoplasmic. Upon arsenite stress, a fraction of nuclear wildtype BRF2 seemed to relocalize to the cytoplasm. All 14-3-3 binding mutants equally efficiently localized to processing bodies and to oxidative stress-induced stress granules with slightly different efficiencies. Preliminary co-immunoprecipitation experiments suggested an interaction between BRF2 and the mRNA deadenylation machinery. The fragments BRF2:aa1-275 (N-terminus + RNA binding region) and BRF2:aa97-275 (RNA binding region) both localized to the nucleus. This could be due to the absence of the nuclear export signal (NES) from the C-terminus. Interestingly, upon oxidative stress, BRF2:aa1-275 shifted to the cytoplasm, which hinted to the presence of an additional N-terminal NES that is active upon oxidative stress. In addition, the central RNA binding domain consisting of the two 14-3-3 binding sites and two zinc fingers appeared to be sufficient to cause AMD of ß-globin-ARE reporter mRNAs. However, despite being predominantly nuclear, the fragments BRF2:aa1-275 and BRF2:aa97-275 still promoted AMD. This opens up an interesting idea as to whether AMD could be nucleus-associated.

Zusammenfassung

Durch AU-reiche Elemente (ARE) vermittelter mRNA Abbau (AMD) ist eine bedeutende Form des mRNA Abbaus in der Zelle, da 10-15 % aller mRNAs ein ARE in ihrer 3' untranslatierten Region (UTR) beinhalten. Diese mRNAs kodieren für Proteine, die an wichtigen zellulären Prozessen beteiligt sind, beispielsweise Zellwachstum und -erhaltung, Entwicklung, Transkription, Entzündung oder Apoptose. AMD wird hauptsächlich von Proteinen der Tristetraprolin (TTP) Familie, bestehend aus TTP, BRF1 und BRF2 vermittelt, die mRNA Abbau durch Bindung an AREs in der 3'UTR beschleunigen. Trotz ihrer beträchtlichen Homologie zeigen die Proteine der TTP Familie unterschiedliche Eigenschaften. In meiner Doktorarbeit habe ich das Protein BRF2 charakterisiert und seine mögliche Funktion in AMD bestimmt. Meine Experimente deuten darauf hin, dass der mRNA Abbau durch BRF2 von AREs abhängt, und dass BRF2 abhängig von seinem Phosphorylierungsstatus an 14-3-3 bindet. Die Interaktion von BRF2 und 14-3-3 habe ich als eine mögliche Form der Regulation der AMD-Aktivität von BRF2 genauer untersucht. Ich konnte zeigen, dass 14-3-3 über die Bindestellen Serin123 und Serin257 an BRF2 bindet, und dass es notwendig ist, beide Serine zu mutieren, um diese Interaktion zu verhindern. Die Kinase MK2 scheint die Phosphorylierung von BRF2 und damit die Bindung an 14-3-3 zu beeinflussen, da diese Interaktion in Anwesenheit einer inaktiven Form von MK2 reduziert ist. Anders als für TTP und BRF1 scheint MK2 die AMD-Effizienz von BRF2 nicht zu beeinträchtigen. Dies könnte darauf hinweisen, dass BRF2 resistent gegenüber der Inaktivierung durch Stress-induzierte Kinasen ist. 14-3-3 Bindungsmutanten von BRF2 zeigen verglichen mit dem vorwiegend zytoplasmatischen BRF2 Wildtyp eine stärkere Kernlokalisation. Nukleäres BRF2 verlagert sich durch Arsenit-Stress teilweise ins Zytoplasma. Alle 14-3-3 Bindungsmutanten lokalisieren mit gleicher Effizienz in processing bodies und zeigen leicht unterschiedliche Lokalisation in Arsenit-induzierten stress granules. Erste Co-Immunopräzipitationen weisen auf eine Interaktion zwischen BRF2 und der mRNA Deadenylierungs-Maschinerie hin. Die Fragmente BRF2:aa1-275 (N-Terminus + RNA-Bindungsregion) und BRF2:aa97-275 (RNA Bindungsregion) zeigen beide Kernlokalisation. Ein Grund dafür könnte das fehlende nukleäre Exportsignal (NES) am C-Terminus sein. Interessanterweise verschiebt sich BRF2:aa1-275 unter oxidativem Stress ins Zytoplasma, was auf ein weiteres N-terminales NES hinweist, welches unter oxidativem Stress aktiv ist. Außerdem scheint die zentrale RNA-Bindedomäne, die aus den zwei 14-3-3 Bindestellen und zwei Zinkfingern besteht, ausreichend zu sein, um AMD von ARE-Reporter mRNAs zu bewirken. Obwohl mBRF2:aa97-275 hauptsächlich nukleär vorkommt, löst die Mutante immer noch AMD aus. Dies eröffnet das neue interessante Konzept, dass AMD Kern-assoziiert sein könnte.

Contents

1 Introduction **3**

1.1 Control of mRNA levels in the cell . . . 3
1.2 Degradation of mRNA . . . 4
1.3 Cytoplasmic RNA granules: . . . 8
1.3.1 Processing bodies: . . . 9
1.3.2 Stress granules: . . . 10
1.4 AU-rich elements (AREs) . . . 12
1.5 ARE-binding proteins (AUBPs) . . . 13
1.5.1 HuR . . . 13
1.5.2 AUF1 . . . 14
1.5.3 The TTP family of proteins . . . 15
1.5.4 TTP . . . 16
1.5.5 BRF1 . . . 19
1.5.6 BRF2 . . . 21
1.6 Aim of the study . . . 22

2 Results: BRF2 promotes ARE-mediated mRNA decay **23**

2.1 BRF2 mRNA levels are elevated in SlowC cells . . . 23
2.2 Stable over-expression of BRF2 in SlowC cell lines . . . 25
2.3 Transient over-expression of BRF2 destabilizes ARE-containing mRNAs . . . 28
2.4 DISCUSSION . . . 29

3 Regulation of BRF2 activity **37**

3.1 BRF2 binds to 14-3-3 protein . . . 37
3.1.1 BRF2 interaction with 14-3-3 is dependent on phosphorylation . . . 37
3.1.2 BRF2 binds to 14-3-3 via serine residues S123 and S257 . . . 39
3.2 Regulation of AMD efficiency of BRF2 . . . 42
3.2.1 S123,257A mutations do not alter AMD efficiency of BRF2 . . . 42
3.2.2 S125,259P mutations do not alter AMD efficiency of BRF2 . . . 43
3.3 Cellular localization of 14-3-3 binding site mutants of BRF2 . . . 43
3.4 DISCUSSION . . . 45

4 Kinase(s) involved in phosphorylating BRF2 **57**
4.1 PKBα and MK2 kinases may affect BRF2 binding to 14-3-3 . . 57
4.2 Effect of inhibitors of the PKB and MK2 kinase pathways . . . 58
4.3 Effect of siRNA-mediated knockdown of MK2 59
4.4 MK2 does not alter AMD-efficiency of BRF2 60
4.5 DISCUSSION 60

5 BRF2 interacts with the deadenylation machinery **67**
5.1 BRF2 interacts with Not1 and Caf1a 67
5.2 DISCUSSION 67

6 Truncation mutants of BRF2 **71**
6.1 Cellular localization of truncated versions of BRF2 72
6.2 AMD-efficiency of truncated mutants of BRF2 72
6.3 DISCUSSION 73

7 Outlook and future directions **77**
7.1 Summary 77
7.2 Future directions: 78

8 Materials and methods **83**

Bibliography **95**

Bibliography **97**

List of Figures

1.1 Homology between the TTP family members 15
1.2 The SlowC cell line 20

2.1 mRNA levels of BRF1 and BRF2 in HTwt16 and SlowC cells . . 24
2.2 Endogenous BRF1 and BRF2 proteins in various cell lines . . . 25
2.3 Polyclonal antibodies against BRF1 and BRF2 26
2.4 The GFP-IL3 reporter mRNA 27
2.5 FACS and Northern blotting analyses of stable BRF2 clones . . 31
2.6 Expression of BRF1 or BRF2 protein in respective stable clones 32
2.7 FACS profiles of stable SlowC-BRF2 clones: Attempt II. 33
2.8 Expression of BRF2 protein in stable SlowC-BRF2 clones after serial passages 34
2.9 BRF2 degrades mRNAs in an ARE-dependent manner 35
2.10 Putative AU-rich elements in BRF2 3'UTR 36

3.1 The GFP binder system 38
3.2 BRF2 binds to 14-3-3 in a phosphorylation-dependent manner . 39
3.3 14-3-3 binding sites TTP, BRF1, and BRF2 40
3.4 BRF2-S123,257A mutant shows reduced binding to 14-3-3 . . . 49
3.5 Anisomycin treatment causes a slight increase in 14-3-3 binding to BRF2-AA 50
3.6 BRF2-S125,259P mutant shows reduced binding to 14-3-3 . . . 51
3.7 AMD efficiency of BRF2-AA mutant as compared to BRF2 wildtype 52
3.8 BRF2-PP mutant degrades ARE-containing mRNAs with equal efficiency as wildtype BRF2 53
3.9 BRF2 wildtype and its 14-3-3 binding site mutants localize to P bodies 54
3.10 BRF2 wildtype and its 14-3-3 binding site mutants localize to oxidative stress-induced stress granules 55
3.11 Cellular localization of BRF2 wildtype and its 14-3-3 binding site mutants 56

4.1 MK2 and PKB kinases may affect 14-3-3 binding to BRF2. . . . 63

4.2 Effect of chemical inhibitors to MK2 and PKBα kinase pathways on 14-3-3 binding to BRF2 64
4.3 siRNA knockdown of MK2 65
4.4 MK2 does not modulate AMD efficiency of BRF2 66

5.1 BRF2 interacts with the deadenylation machinery 69

6.1 BRF2 truncation mutants 71
6.2 Cellular localization of BRF2 truncation mutants. 74
6.3 AMD efficiency of truncation mutants of BRF2. 75
6.4 Putative NES in N-terminus of BRF2 76

1 Introduction

The central dogma of molecular biology indicates that genetic information flows from DNA to RNA to proteins. DNA can be present in the active form, euchromatin; or the inactive form, heterochromatin. RNA can be controlled at the level of transcription, localization, storage, or translation. Lastly, proteins could be controlled at the levels of expression, activity, stability, or localization. All the above modes of regulation are to ensure that the final product, proteins, are expressed in a timely manner and only in the exact quantities required. Considering the scope of my project, I will briefly explain the process of mRNA degradation and thereforth focus on adenylate/uridylate-rich element (ARE)-mediated mRNA decay.

1.1 Control of mRNA levels in the cell

In complex eukaryotes, a majority of DNA is transcribed; however, only a fraction of these transcripts get translated [1, 2]. mRNA gets transcribed in the nucleus. Subsequently, it is exported to the cytoplasm where it faces different fates depending on what protein complex loads onto it. These fates can be broadly categorized as: translation, translational suppression till the mRNA attains a desired localization in the cell, or deadenylation followed by storage/degradation. Controlling levels of mRNA is an efficient way of controlling the proteome. The range of stability of mRNAs varies greatly; the half-lives ranging from 20 mins for labile mRNAs to more than 24 hrs for some stable mRNAs [3]. Short-lived mRNAs can elicit temporary but potent responses to different stimulii like growth, inflammation, oxidative or nutrient deprivation stress, etc. Moreover, the cell has evolved pathways to eliminate aberrantly processed mRNAs or mRNAs originating from mutated genes. Taken together, the half-life of each mRNA is decided based on its quality and its function after which it is destined to undergo degradation. There exist multiple surveillance mechanisms where damaged mRNAs are rapidly scavenged, namely, Nonsense-mediated decay (NMD) where the transcripts harbour a premature stop codon (PTC), Nonstop mRNA decay (NSD) where transcripts lacking a stop codon are degraded, No-go mRNA decay (NGD) where mRNAs with stalled translation elongation are degraded (reviewed in [4]). An additional type of mRNA

decay is ARE-mediated RNA decay (AMD) where factors bind to specific cis-acting elements in the 3'UTR of mRNA and thus target it for degradation. Though the pathways targeting the mRNAs for degradation are diverse, all the above pathways converge after the mRNA recognition step and thereforth follow similar steps towards degradation, i.e., deadenylation, decapping, and endo/exoribonuclease digestion of the mRNA body. Eukaryotic mRNAs bear modifications at the 5' and the 3' end, and proteins binding to these structures offer protection to the mRNA body and render it inaccessible to exonucleases. Therefore, once an mRNA is destined for degradation, the initial steps involve removal of these modifications to prepare the mRNA body for the ribonuclease action. The following is a concise description of the important steps common to most degradation pathways of mRNA degradation.

1.2 Degradation of mRNA

1.2.0.1 Deadenylation

The polyA tail interacts with polyA binding protein (PABP) present in the cytoplasm. This interaction supports translation and protects the mRNA from a 3'-5' exoribonuclease activity [5]. The process of deadenylation involves progressive shortening of the polyA tail. However, after successful deadenylation, the mRNA can revert back to getting re-adenylated and can enter active translation. Hence, deadenylation is a fairly reversible process [6, 7]. There are three main deadenylases in present in eukaryotic cells; the polyA-specific ribonuclease (PARN), the polyA nuclease 2 (PAN2)-PAN3 deadenylase complex, and the Ccr-Caf1-Not deadenylation complex.

The polyA ribonuclease (PARN): belongs to the DEDD (Asp-Glu-Asp-Asp motif) family of nucleases. It is a nucleo-cytoplasmic shuttling protein although mainly localized to the nucleus [8]. It requires $Mg^{+2}$and a free 3' hydroxyl group for action and releases solely 5'-AMP [9]. Although known for deadenylating polyA tails, it has also been shown to degrade polyU tails at a ~10-fold lower efficiency [10]. Since polyU tails are majorly found in oocytes [11], this finding might support the role of PARN in embryogenesis [12]. The cap binding protein 80 (CBP80) binds to PARN inhibiting it from deadenylating nascent pre-mRNA [13] in untreated conditions. Moreover, in conditions of DNA damage where deadenylation is transiently but strongly inhibited, the cleavage stimulation factor 1 (CstF1) interactes with PARN inhibiting its activity [14]. Nuclear PARN decreases the stability of ARE-containing mRNAs, such as c-myc, c-fos, and c-jun, keeping their levels low in non-stress conditions [14, 15, 16]. The levels of these mRNAs therefore increase transiently due to an inactive PARN in UV-induced DNA damage conditions [17, 18, 19].

The PAN2-PAN3 deadenylation complex: PAN2 and PAN3 are active as a heterodimer where PAN2 is catalytic and PAN3 is the regulatory subunit. This deadelylase complex is majorly cytoplasmic, requires a free 3' hydroxyl group for action, and releases 5'-AMP as the product. PAN is activated on interaction with PABP, unlike for PARN and the Ccr4-Caf1-Not complex which are inhibited by PABP [20, 21, 22]. In higher eukaryotes, PAN is the first in line to act on polyA tails, reducing them to a length of ~100 nt from 200-250 nt, thus performing only incomplete deadenylation [22]. This implies that a second deadenylase follows the activity of PAN and takes the deadenylation to completion [8]. PAN complex is known to be regulated by ARE sequences in the 3' untranslated region (UTR) of mRNAs [22].

The Ccr4-Caf1-Not complex: Along with PAN, the Ccr4-Caf1-Not complex is responsible for cytoplasmic mRNA deadenylation, although unlike PAN, the Ccr4 exoribonuclease in the Ccr4-Caf1-Not complex is inhibited by PABP [8]. In its function, the Ccr4-Caf1-Not complex further deadenylates the mRNAs which are partially deadenylated by PAN and reduces the polyA tails from ~100 nt to ~8-12 nt [5]. Collart et al. [23] have reviewed the components of the Ccr4-Caf1-Not complex in detail. The complete complex is ~1.9 MDa in size [24] and consists of the Not 1-4 and Not10, Ccr4a/b, Caf1a/b, TAB182, and C2ORF29. Not1 was suggested to act as a platform onto which the other components of the complex load. Ccr4 is a 3' to 5' exoribonuclease, the activity of which depends on the length of the polyA tail. It interacts with Not1 via Caf1, which is also an exoribonucease. Similar to Ccr4, the activity of Caf1 is dependent on the length of the polyA tails [25].

1.2.0.2 Decapping

Decapping is a process by which the 5' m^7G cap is removed from the mRNA body thus making the mRNA body accessible to exoribonucleases. Unlike deadenylation, decapping is an irreversible process [26]. The decapping complex consists of the Dcp1 and Dcp2 proteins, of which Dcp2 exhibits the decapping activity while Dcp1 acts as an enhancer of Dcp2 activity [27]. Dcp2 activity requires the 7-methyl group on the cap and the 5' body of the mRNA. Incidentally, phosphorylation of Dcp1 and Dcp2 governs efficiency of P body and stress granule formation [28, 29].

1.2.0.3 Degradation of the mRNA body:

Xrn1 exoribonuclease: is a ~175 kDa enzyme which is highly specific for mRNAs bearing 5' monophosphate generated by the decapping action of Dcp1/2 [30, 31, 32] and cleaves mRNA in a 5' to 3' direction. Xrn1 is also involved in

degrading endonucleolytic mRNA cleavage products from the NMD and NGD mRNA degradation pathways [33, 34, 35, 36] or 5' monophosphorylated mRNAs generated by Argonaute-catalysed endonucleolytic cleavage during RNA interference [37, 38, 39].

Exosome: is a 12-subunit complex which contributes to 3' to 5' exoribonucleolytic activity. The exosome has been implicated in the AMD [40, 41] and the NMD pathways [42].

A list of proteins involved in mRNA degradation has been included below.

Table 1.1: Proteins involved in mRNA decay

Protein	**Domains**	**Function**	**Localization**	**Refs**
Deadenylation				
Pan2	DEDD (3'- 5' Exo)	initial deadenylation, distributive, activated by PABP1	C, PB	[8, 43]
Pan3	-	co-factor of Pan2	C, PB	[43]
Ccr4	Exo III (3'- 5' Exo)	terminal deadenylation, processive, inhibited by PABP1	N, C, PB	[8, 44, 45, 46]
Caf1, Pop2	Exo III (3'- 5' Exo)	terminal deadenylation, processive, inhibited by PABP1	N, C, PB	[43, 44, 46, 25, 47]
Not1	-	scaffold of the Ccr4-Caf1-Not complex	N, C, PB	[47, 48]
Not2	-	n.d.	N, C, PB	[47, 48]
Not3	-	n.d.	N, C, PB	[47, 48]
Not4	RING finger	E3 ligase	N, C, PB	[48, 49]
Tob2		interacts with Caf1, enhances deadenylation	C, PB	[50]
PARN	DEDD (3'- 5' Exo)	Nuclear in somatic cells, cyto-plasmic in oocytes, embryonal development	N, C	[51]
Nocturnin	Exo III (3'- 5' Exo)	circadian expression	C	[47, 52]
Decapping				
Dcp2	Nudix	decapping enzyme	C, PB	[53, 54, 55, 56]

Table 1.1: Proteins involved in mRNA decay

Protein	**Domains**	**Function**	**Localization**	**Refs**
Dcp1	-	enhancer of decapping	C, PB	[54, 55, 56]
Rck, Dhh1	DEAD helicase	RNA helicase, enhancer of decapping	C, PB	[45, 56, 57, 58, 59]
Edc3, Lsm16	-	enhancer of decapping, PB aggregation	C, PB	[60, 61]
Edc4, Hedls, Ge-1	-	enhancer of decapping	C, PB	[60, 62]
Lsm1-7	Sm	binds mRNAs with short poly(A) tails, enhancer of decapping	C, PB	[63, 45, 56, 61, 64, 54]
Pat1	-	connects deadenylaiton with decapping, enhancer of decapping, PB aggregation	C, PB	[65, 66, 67, 68]
Ro52		enhancer of decapping, E3 ligase	C, PB	[69]
Nudt16	Nudix	decapping enzyme	C	[70, 71]
5'-3' Decay				
Xrn1	5'-3' exonulcease	5'-3' exonulcease	C, PB	[72, 73]
Xrn2	5'-3' exonulcease	5'-3' exonulcease	N	[74, 75]
3'-5' Decay				
Rrp44, Dis3, EXOSC11	RNase II, S1, PIN endonuclease	active 3'-5' exonulcease and endonuclease of the exosome	N	[76, 77, 78]
Dis3L1			C	[79]
Rrp6, PmScl-100, EXOSC10	DEDD (3'- 5' Exo)	3'-5' exonulcease	N, C	[40, 80, 42]

Table 1.1: Proteins involved in mRNA decay

Protein	Domains	Function	Localization	Refs
Rrp41, Ski6, EXOSC4	RNase PH (inactive)	exosome core	N, C	[40, 78, 80]
Rrp42, EXOSC7	RNase PH (inactive)	exosome core	N, C	[78, 80]
Rrp43, Oip2, EXOSC8	RNase PH (inactive)	exosome core	N, C	[40, 78]
Rrp45, PmScl-75, EXOSC9	RNase PH (inactive)	exosome core	N, C	[40]
Rrp46, EXOSC5	RNase PH (inactive)	exosome core	N, C	[40, 80]
Mtr3, EXOSC6	RNase PH (inactive)	exosome core	N, C	[40, 80]
Rrp4, EXOSC2	KH, S1	RNA binding	N, C	[40, 78, 80]
Rrp40, EXOSC3	KH, S1	RNA binding	N, C	[40, 80]
Csl4, EXOSC1	S1	RNA binding	N, C	[40, 80]
Endonucleolytic cleavage				
Ago2	RNase H	cleavage of siRNA-mRNA duplex	C, PB, SG	[81, 82, 83, 84, 85]
Smg6	PIN endonuclease	cleavage of NMD targets	C, PB	[35, 34, 86]
Zc3h12a	PIN endonuclease	cleavage of IL-6 and IL-12b mRNA within stem-loop	C	[87]

1.3 Cytoplasmic RNA granules:

Cytoplasmic granules containing RNA are a common feature in plants, yeast, and mammalian cells. Processing bodies and stress granules are examples

of such structures and are suggested to offer a site for temporary storage of mRNAs and/or mRNA degradation. These granules are formed as a byproduct of mRNA metabolism or in response to stress-inducing cues. Both these structures exist independently but have an overlapping set of components [88].

1.3.1 Processing bodies:

Processing bodies (P bodies): are small cytoplasmic foci that include proteins required for mRNA degradation. Though the concept of P bodies was consolidated a lot later, XrnI exoribonuclease was first shown to have a punctate cytoplasmic localization [72]. Studies in the years later revealed many other mRNA degradation-related proteins to be a part of P bodies. These proteins have roles that span all the important steps in mRNA degradation, namely, deadenylation, decapping, and final degradation of the mRNA body. The arguement that mRNA degradation takes place in P bodies has been strengthened by the following observations. It has been shown that P bodies fail to form on inhibition of deadenylation. Ccr4 and Caf1 proteins which play a prominent role in deadenylation appear essential for the formation of P bodies, since knockdown of these proteins led to failure of P-body formation. On the other hand, P bodies show an increased size when 5' to 3' mRNA degradation is blocked by knockdown of XrnI. In these cases the mRNA destined for degradation or the decay intermediates accumulate inside P bodies [56, 45]. Blocking decapping produced the same effect [56]. The exosome components have, to date, not been observed in P bodies.

Function: P bodies have been linked with the degradation of many short-lived mRNAs. These mRNAs comprise those with premature termination codons (PTCs) degraded by the NMD pathway, those with AREs in their 3'UTR degraded by the AMD pathway, and those mRNAs which undergo microRNA (miRNA)-induced silencing. This is supported by the fact that some proteins prominently involved in these pathways localize to P bodies; NMD: Upf1-3, Smg5-7 [89, 86, 90]; AMD: Tristetraprolin family members, HuD [63, 91, 92]; and miRNA-induced mRNA silencing: Ago1-4, GW182 [81, 82, 93, 94]. Proteins involved in AMD and miRNA-induced silencing pathways localize more or less readily to P bodies. However, a study has indicated that P bodies were not required for NMD [95]. Localization of mRNAs to P bodies was reversible and these mRNAs held the potential to re-enter translation. This was shown in *S. cerevisiae* where disassembly of P bodies on stress recovery corresponded to re-entry into translation [96]. This assigns an mRNA-storage function to P bodies.

Assembly and dissasembly: Studies in *S. cerevisiae* [61] and *C. albicans* [97] provided evidence that P body assembly is greatly governed by the enhancer

of decapping 3 (Edc3) protein. Edc3 interacts with itself, and with Dcp2 and Rck to form a scaffold. Another contributing protein with a similar function is Pat1 which networks multiple P body proteins [98, 65, 67]. Lsm4 was implicated in the assembly of P bodies and was suggested to form aggregates by virtue of a Q/N (glutamine and asparagine)-rich domain present in its C terminus [61]. Such a domain was later found to be a feature of many P body proteins [99]. Stimulii determining assembly and disassembly of P bodies have hitherto been poorly understood, although some studies describe the cues involved. P body dynamics appear to be closely related to the stages of growth. Stationary phase *S. cerevisiae* cells were observed to have large P bodies that stored mRNAs till growth resumed [96]. In *C. albicans*, P bodies were observed during hyphal developent and an edc3 deletion mutant exhibited a dramatic reduction of P bodies accompanied by defective filamentation [97]. Recent reports demonstrate that phosphorylation of the S315 on Dcp1a by the kinase JNK led to reduced number of P bodies in mammalian cells and that localization of XrnI and Edc4 was determined by Dcp1a. Prolonged JNK activation led to dispersal of P bodies [28]. Phosphorylation of Dcp2 on S137 by Ste20 kinase, affected its decapping activity, triggered accumulation of this Dcp2 in processing bodies, and promoted efficient formation of stress granules in *S. cerevisiae*. Ste20 kinase activates mitogen-activated protein kinase (MAPK) cascades [29]. Poliovirus infection elicited degradation of XrnI, Dcp1a, and Pan3, and eventually disrupted P bodies in these cells correlating with expression of viral proteases [100]. Intact microtubules were required for motility of P bodies and drug-induced disruption of microtubules led to an increase in the number of P bodies [101].

1.3.2 Stress granules:

Stress granules (SGs): are cytoplasmic mRNP complexes which form when translation initiation is impaired. Hindered translation initiation could be attributed to reasons like stress-induced reduction in translation initiation, drug-based prevention of translation initiation, knockdown of initiation factors, or over-expression of proteins that inhibit translation (reviewed in [88]).

Function: SGs are implicated in translational repression [102], protecting mRNAs from deadenylation during stress responses [103, 104, 105], possibly accumulating components in SGs to reduce the components in cytosol [88], and increasing the local concentration of components to possibly accelerate mRNP assembly on stress recovery [88]. It is a plausible idea that on stress recovery the initiation complex loads onto the mRNA while inside the SGs, although translation might not be initiated due to the lack of 60S ribosomal subunit [106, 88]. This model could also explain presence of proteins like DDx3, Pbp1,

HuR, Lin28 [107], and proteins which promote translation from internal ribosomal entry sites (IRES) sequences being present in SGs. These proteins promote stress-tolerant translation of specific mRNAs [108, 109, 110, 111]. SGs seem to play a role in sequestering pro-apoptotic proteins, so as to minimize their activity in modest stress conditions from which recovery is possible. RACK1 interacts with MTK1 kinase thus activating it leading to induction of apoptosis. Sequestering RACK1 in SGs prohibits this interaction and thus activation of apoptosis, Similarly, anti-apoptotic proteins like Ribosomal S6 inase 2 (RSK2) and FAST bind to the Q/N-rich domains of TIA-1. This overcomes TIA-1-induced translation repression and stimulates expression of anti-apoptotic factors [112]. ADAR-1, a dsRNA editing enzyme, has recently been shown to be a component of SGs following various stresses. This might indicate that SGs could be a site for RNA editing [113].

Assembly and disassembly: Response to stress results in abortive translation initiation where the polysomes are reduced to complexes with 48S ribosomes. Primary aggregation in SGs is attributed to aggregation of these free 48S complexes that include translationally stalled mRNAs. Along with this pool of mRNAs, there exist many proteins which have undergone posttranslational modifications. These modifications include phosphorylation, eIF2α [114]; the lack of phosphorylation [115, 116, 117, 118, 119] ; O-Glc-NAc modification [120], ubiquitination [120, 121]; acetylation, HDAC6 deacetylase mutants were defective in SG formation [121]; methylation or the ability to bind methyl groups via Tudor mRNA-binding domains [122, 123, 124]. These posttranslational modifications facilitate assembly of SGs with the existing proteins rather than requiring *de novo* protein synthesis. Similar to that seen in P bodies, proteins with Q/N-rich prion-like domains are constituents of SGs [125] Aggregation of prion domains can be reversed by expression of heat shock proteins [126]. An intact microtubule network is required for formation of SGs, although microtubule depolymerization still results in SGs of smaller size [127, 121, 128, 129, 130]. Moreover, dynein and kinesin motors have been implicated in assembly and disassembly, respectively, of SGs [130]. During recovery from stress, disassembly of SGs correlates with translational recovery, although translation initiation does not require complete disassembly of SGs [131]. On the other hand, translational repression does not require formation of SGs [130]. Staufen, which stabilizes mRNA-polysome interaction, inhibits SG assembly [132], and phosphorylation of growth factor receptor-bound protein 7(Grb7) during stress recovery enables SG disassembly [133]. Recent work in *S. pombe* showed presence of stress-induced RNA granules containing homologs of various mammlian P-body and stress granule components. Contrary to that in mammalian cells, PABP was observed in these stress-induced granules. On glucose deprivation, PABP-containing foci accumulated accompanied by translational downregulation, both in a PKA-dependent manner. On ex-

posure to hyperosmosis, non-phosphorylatable eIF2α did not block granule formation but merely delayed it and a similar delay was seen in the disassembly process. Since PKA mutants are capable of forming granules and eIF2α on hyperosmotic shock, it suggests of the presence of at least two independent pathways of stress-induced granule formation on glucose starvation [134].

Several reports indicate that P bodies and SGs are dynamically linked structures [135, 63, 88]. These two types of cytoplasmic RNA granules have been observed to physically interact with each other and this crosstalk indicates of cycling of mRNP components between polysomes, P bodies and SGs [6]. Many P-body components accumulated in SGs during stress, however the viceversa has not been observed [135]. In studies carried out in *S. cerevisiae*, blocking P body formation led to inhibition of SG formation. Blocking SG assembly did not affect P-body assembly [135, 120]. Moreover, SGs and P bodies can be spatially completely independent and there can be a direct delivery of mRNAs from polysomes to SGs without being routed via P bodies [63, 120].

With this, I have described the mRNA degradation process and the cytoplasmic RNA granules where the fate of mRNAs is decided. A critical step, however, is the targeting of specific mRNAs for degradation, without affecting the global mRNA pools. It is noteworthy that the fate of various eukaryotic mRNAs is controlled by cis-acting regulatory elements present in their 3'UTRs.

1.4 AU-rich elements (AREs)

A prominent example of cis-acting elements that determine mRNA stability are the adenylate/uridylate-rich elements (AREs) which have been estimated to be present in 10-15% of all transcripts [136]. AREs are present in the 3'UTR of mRNAs encoding proteins that require tight regulation. AREs comprise well-defined repeats of AUUUA or a nonamer UUAUUUAUU present in a U/AU-rich context. UUAUUUAUU or its variation UUAUUUAWW (where W=A/U) are considered to be the minimally functional motifs and two overlapping copies of such a nonamer exert the maximum effect on the stability of the mRNA [137, 138, 139, 140, 141]. The pentamer AUUUA is inactive as an ARE, unless located in an AU-rich context. On bioinformatical analyses of AU-rich labile mRNAs, WWWUAUUUAUWW was found to be the 13-base consensus motif which was located specifically in the 3'UTR [142]. Different ARE sequences were bionformatically categorized to five classes; classes I-V, which include mRNAs whose 3'UTRs have five, four, three, two, and one AUUUA pentamer, respectively, with a flanking AU context [143], and longer AREs were linked to shorter half-lives of the mRNA [144, 145].

Functional AREs exist as linear non-structured motifs or as stem-loop struc-

tures. The sequence motif NNUUNNUUU for HuR binding is functional as a linear structure and as a linear segment within a secondary structure, the latter proving to be more efficient [146, 147, 148, 149]. TTP was shown to bind with high affinity to WWWUAUUUAUWW, but also could bind to motifs as small as UAUUUAU and UUAUUUAUU. Adenylate residues in the ARE are a requisite for TTP binding, unlike HuR which is able to bind to a U-rich tract [150, 151, 152]. Apart from the conservation amongst the ARE sequences, a general observation was that 3'UTRs bearing AREs are longer than those devoid of them [136, 153, 154, 155]. Since longer 3'UTRs tend to offer more miRNA targets, it could be hypothesized that miRNAs and AREs act synergistically in regulating mRNA stability and/or translation [156].

1.5 ARE-binding proteins (AUBPs)

The cis-acting AREs in the 3'UTR are further assisted by trans-acting proteins called the ARE-binding proteins (AUBPs). Barreau et al. [157] compiled information on characteristics of binding of prominent AUBPs with AREs belonging to different classes in order to perceive a pattern in their interactions. However, no particular interaction specificity was observed between the types of AUBPs and AREs. Most AREs were able to bind more than one AUBP, and likewise the AUBPs were seen to bind to different AREs regardless of the class the AREs belonged to. However, much of the data considered for this study was derived from *in vitro* analyses such as UV-crosslinking or electrophoretic mobility shift assays (EMSA) and only a few studies covered interactions between endogenous mRNAs and proteins. All the same, this study brought forth the idea of redundancy, synergism, and antagonism existing between AUBPs in binding to AREs in different circumstances. AUBPs regulated the stability, and in some cases the translation efficiency, of the target mRNAs (discussed in subsequent sections). A compiled version of all the different AUBPs and their target ARE-mRNAs is published in [157]; however, only a selected few are described hereforth.

1.5.1 HuR

The embryonic-lethal abnormal vision (ELAV) family of proteins consists of four closely related proteins; human antigenR (HuR), HuC, HuD, and Hel-N1 [158]. HuR has been implicated in stability of ARE-mRNAs. It is a predominantly nuclear protein, though undergoes nucleo-cytoplasmic shuttling [159, 160]. It could be by virtue of this shuttling that HuR helps export of c-fos mRNA out of the nucleus [161]. HuR binds to AREs and increases

stability and translation of mRNAs involved in growth and proliferation [162]. Knockdown on HuR in MCF7 breast cancer cells decreases the growth potential of cells which was attributed to decreased transcript and protein levels of cyclin D1[163]. HuR exists in three different polyadenylated variants, 1.5 kb testis-specific form, 2.4kb ubiquitously expressed form and a differentiating neuron-specific 6.0 kb isoform. The 6.0 kb isoform is less stable than the 2.4 kb isoform and is also less expressed. Moreover, neuronal HuB, HuC, HuD, as well as HuR itself, when overexpressed, bind to the polyadenylation site of the 2.4-kb mRNA leading to alternative polyadenylation generating an extended HuR 3'-UTR that is translationally less active [164]. HuR was seen to be associated with regulation of growth on exposure to hypoxic stress [165, 166]. CoCl2-induced hypoxic stress led to caspase-dependent cleavage of HuR. The HuR-cleavage product-1 thus formed strongly associated with the 3'UTR of c-myc mRNA, blocked its translation, and as a result reduced cell viability. HuR, along with AUF1 as a co-factor, binds to a stem-loop structure in the 3'UTR of p16 mRNA and destabilizes the mRNA by recruiting the RISC complex [167]. In a recent interesting study, Zheng et al. cloned p53 HuR-binding site in the 3'UTR of adenoviral vector encoding the luciferase reporter gene. On transfecting this modified vector into rat submandibular glands or salivary cells, higher luciferase activity was noticed, ~4-fold compared to that obtained with the CMV promoter [168].

1.5.2 AUF1

AUF1, also termed as heterogenous nuclear ribonucleoprotein D (hnRNPD), is essentially a nuclear protein and was the first of the AUBPs to be identified. The AUF1 family consists of four proteins arising from alternative splicing of a common pre-mRNA; AUF1-p37, -p40, -p42, and -p45 [169]. AUF1 has been shown to stabilize some ARE-mRNA targets, e.g., parathyroid hormone mRNA [170], as well as destabilize some ARE-mRNAs, e.g., IL-3 mRNA [171], tumor necrosis factor α (TNFα), Granulocyte macrophage colony stimulating factor (GM-CSF), etc [172]. AUF1-p45, which is the longest of the four isoforms and bears the 'GY' elements, binds to tristetraprolin (TTP) via the GY elements and increases the mRNA-binding efficiency of TTP by ~5 fold [173]. AUF1 has also been implicated in the hypoxic stress response. von Hippel Lindau (VHL) protein, product of a tumor suppressor gene, controls oxygen-responsive gene expression at transcriptional and posttranscriptional levels. VHL is actively involved in destabilizing the vascular endothelial growth factor (VEGF) mRNA in normoxic conditions. VEGF bears an ARE in the 3'UTR which is the binding site for AUF1 and/or HuR. VHL interacts indirectly with VEGF mRNA via AUF1 and HuR proteins and cause destabilization of VEGF mRNA. In hypoxic conditions, VHL levels in the cell are lowered but AUF1

and HuR continue to bind to VEGF mRNA, thus stabilizing the mRNA [174]. AUF1 knockout mice exhibit symptoms of severe endotoxic shock due to high expression of TNFα and IL-1ß [175].

1.5.3 The TTP family of proteins

The TTP family consists of four proteins; TTP, Butyrate response factor 1 (BRF1), BRF2, and BRF3. These proteins are characterized by the presence of two zinc finger motifs with a strictly defined intra-finger spacing $CX_8CX_5CX_3H$ (where X=any amino acid). The interfinger spacing is 18 amino acids and there is a conserved amino acid lead-in sequence (R/K)YKTEL located immediately before the first cysteine of each finger [176]. Any alterations in this zinc finger setup interferes with the RNA binding capacity of these proteins [177]. The domain including the two zinc fingers is called the TZF domain, and there exists >70% homology in this domain amongst the TTP family members [176]. The overall homology between the proteins can be seen in Figure 1.1. TTP, BRF1, and BRF2 when over-expressed induce apoptosis by the mitochondrial death pathway [178].

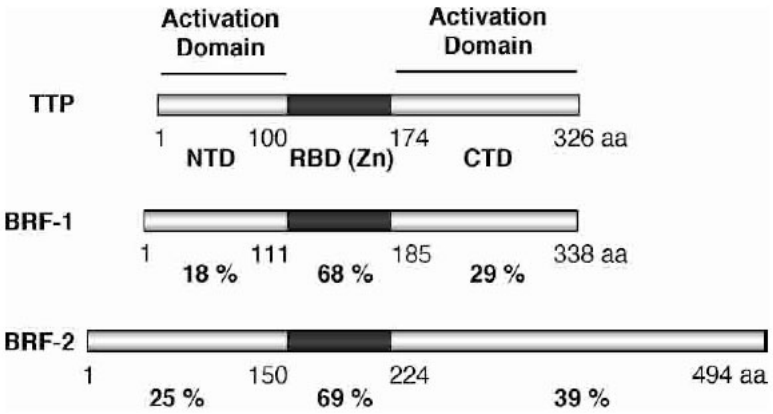

Figure 1.1: Homology between the TTP family members. Figure reproduced from Lykke-Anderson et al. [179]

BRF3 has been the last addition to this family and has yet to be studied in detail. BRF3 cDNA coded for a 725 amino acid protein, and included 38 consecutive repeats of the motif GAALAP or a related variant in its C-terminus. BRF3 is a rodent-specific protein and BRF3 transcripts were initially detected only in the placenta and extraembryonic tissues in the mouse [180]. Recent studies in mouse adipocytes demonstrated presence of BRF3 transcripts at

low levels [181]. Unlike seen with the other TTP family members [182], mouse BRF3 when exogenously expressed in HEK293 cells showed an exclusively cytoplasmic localization, even on treatment with CRM-1-dependent nuclear export inhibitor, LeptomycinB. This protein held the capacity to promote deadenylation and degradation of ARE-containing mRNAs [180].

1.5.4 TTP

TTP is a basic proline-rich protein which contains three PPPG repeats [183]. TTP is a phosphoprotein which is induced by several mitogens including serum, platelet derived growth factor (PDGF), fibroblast growth factor (FGF), phorbol 12-myristate 13 acetate (PMA), insulin, 12-o-tetradecanoyphorbol-13-acetate (TPA) [176, 183, 184, 181], etc. Carrick et al. performed time-course studies to check for the response of TTP to lipopolysaccharide (LPS) induction. Stimulation of human monocytes caused a rapid induction of TTP mRNA, reaching 16-fold higher levels in 60 mins of the treatment, as compared to the unstimulated controls. The levels of TTP exhibited a sharp decline over the next 2 hrs to plateau at a new level which slightly higher than the initial unstimulated level [185]. Incidentally, TTP mRNA is labile in unstimulated cells (t1/2=17 mins) but gains more stability on serum stimulation of cells (t1/2=45 mins), as seen from experiements in fibroblasts [186]. TTP is known to negatively regulate its own expression by virtue of an ARE in its 3'UTR [187, 188]. Evidence suggests that apolipoprotein-1 (AP-1), a major component of high-density lipoprotein, was shown to suppress LPS-induced inflammation via increasing expression of TTP [189].

TTP knockout mice were characterized by myeloid hyperplasia, associated with cachexia, erosive arthritis, dermatitis, conjunctivitis, and auto-immune reactions. The myeloid progenitors were insensitive to growth factors. Almost all above effects could be negated by administering anti-TNFα antibodies, thus suggesting that TNFα was a target of TTP [190]. TTP knockout mice developed defects in the hematopoietic stem-progenitor cell compartment, there were increases in the frequemcies of short-term hematopoietic stem cells (HSCs), multipotent progenitors, and granylocyte-monocyte progenitors, although no long-term defects were observed [191].

TTP promotes degradation of mRNAs that contain an ARE in their 3'UTR. TTP binds to a nonameric ARE, UUAUUUAUU [141] in the 3'UTRs of its target mRNAs. This binding greatly depends on the integrity of the zinc fingers and cysteine to arginine mutations in any of the two zinc fingers abolishes the binding of TTP to the target mRNAs. Furthermore, this zinc finger mutant acts in a dominant negative manner [192]. Studies were carried out in HeLa cells using ß-globin mRNA reporters harbouring the ARE from

TNFα or GM-CSF [193]. TTP was shown to perform the function of recruiting these ARE-containing reporter mRNAs to P bodies, since depletion of TTP hampered the localization of ARE-mRNAs to the P bodies. Besides, over-expression of TTP slightly enhanced the amounts of ARE-mRNA in the P bodies when compard to untransfected or control-transfected cells. Expression of a dominant-negative RNA-binding mutant, TTP-F126N, hampered ARE-mRNA recruitment to P bodies. Individual over-expression of the N-terminal domain (NTD), the C-terminal domain (CTD), or the RNA-binding domain (RBD) were not suffiicient to deliver ARE reporter mRNAs to the P bodies. The NTD or the CTD along with the RBD was required to recruit the ARE-mRNAs to P bodies; however, artificial tethering of the NTD or the CTD to the ARE-mRNA proved sufficient. Accumulation of ARE-mRNAs in P bodies was enhanced when a component of the mRNA decay machinery was rendered limiting. Taken together, the RBD performed the function of binding to the target mRNA and the NTD or the CTD were important in delivering the ARE-mRNAs to the P bodies [193]. In unstressed COS7 cells, TTP localized to P bodies and SGs. In fact, exogenous expression of TTP increases the interactions between these two cytoplasmic RNA bodies [63]. TTP also co-localized with SGs in COS7 cells on experiencing energy starvation by the action of FCCP, a mitochondrial inhibitor. However, on induction of oxidative stress by exposure to arsenite, TTP failed to get recruited to stress granules. MAPK-activated protein kinase-2 (MK2), which is one of the kinases induced by oxidative stress, induced complex formation between TTP and 14-3-3, and such complexes were excluded from SGs [194]. Incidentally, the TTP:14-3-3 complex bound to but did not degrade the ARE-mRNA[194]. This hindered AMD-efficiency was attributed to failure to recruit the deadenylation machinery [195, 196] to the phosphorylated TTP.

Thus, TTP recruits ARE-mRNAs to the possible sites of mRNA degradation. TTP also facilitates the further steps in mRNA degradation. Lai et al. [197] via *in vitro* analyses proved that TTP promotes deadenylation of target ARE-mRNAs by employing the PARN deadenylase. Since then, studies have shown that TTP binds to the decapping machinery (Dcp2, Edc3) via the NTD [60], to the deadenylation machinery (Ccr4-Caf1-Not complex) via the CTD [198] and to PAN2 [195] to eventually enable mRNA degradation. To date, TTP has been shown promote AMD of numerous endogenous mRNA targets involved in inflammation (TNFα, COX-2, GM-CSF, Interleukins (IL)-2, IL-3, IL-6, IL-8, IL-10, IL-12), cell cycle control (c-myc, c-fos), carcinogenesis, angiogenesis (VEGF), development (pituitary homeobox 2), protein glycosylation (1,4-galactosyl transferase), etc (reviewed in [199, 157]). TTP was also shown to control some target mRNAs by repressing their translation and in this it is aided by the RcK protein [200].

TTP has been shown to bind to the ARE and destabilize TNFα mRNA

[190, 201]. On LPS induction, p38 MAPK is stimulated and it phosphorylates the downstream kinase MK2. Activated MK2 deactivated TTP, prevented association of TTP with the TNFα ARE, thus stabilizing the TNFα mRNA. Furthermore, MK2 also stabilized TTP mRNA causing an increase in cellular TTP levels [202]. On LPS induction in MK2 defficient mice, the levels of TNFα mRNA or its secretory properties were not changed, but the TNFα protein levels were severely reduced. This indicates that MK2 affects translation of TNFα [203], and it was later demonstrated that this activity was dependent on the ARE in TNFα [204]. When TTP is removed from this MK2-defficient system, TNFα levels were elevated resembling the TTP-defficient system. This could mean that MK2 and TTP together control the biosynthesis of TNFα. An additional tratment with a p38 inhibitor demonstrated that TNFα and TTP biosynthesis was also controlled by an additional kinase in absence of MK2 [202]. It is noteworthy that in the same system, IL-6 biosynthesis is controlled only at the level of mRNA stability and not its translation.

As explained before, inducibility is one way of regulating TTP activity in the cells. Additionally, after induction, TTP is also controlled posttranslationally. Kinases from some of the major signaling pathways in the cell have TTP as their downstream target. These kinases include ERK mitogen-activated protein kinase (ERK-MAPK), p38 MAPK, JNK, GSK3ß, PKA, PKB, and PKC [205, 206, 207, 208, 209, 210]. Mutational studies revealed that phosphorylation of TTP at the serine residues S52 and S178 contributed significantly to the downregulation of its activity, and that these residues were a target of the MK2 [194]. The residues flanking S52 and S178 are similar in sequence to the RSXpSXP or RXXXpSXP motifs which form optimal binding sites for 14-3-3. 14-3-3 is an abundant adaptor protein that modulates activity of its target proteins. TTP gets phosphorylated on S52 and S178 and binds to 14-3-3 as seen by electrophoretic mobility shift assays (EMSAs) performed in RAW264.7 cells, and conversion of both these serines together to alanines was required to abolish 14-3-3 binding to TTP [194]. Interaction of TTP with 14-3-3 enhances cytoplasmic localization of TTP, protects TTP from dephosphorylation, and prevents degradation of TTP by the proteasome [211, 212, 213]. When the stabilizing signal dissipates, phosphatase PP2A dephosphorylates TTP and activates it and renders it capable of degrading transcripts and limiting their expression [214].

14-3-3 proteins:

14-3-3 is an abundant modulator of activity of many proteins and exists in nine homologous family members in mammals (alpha, beta, gamma, delta, epsilon, eta, sigma, tau, and zeta). It binds to target proteins that bear the optimal binding motif for 14-3-3, RSXpSXP and/or RXXXpSXP, where the serines are pre-phosphorylated [215, 216, 217]. More recently, a new consensus

motif has been included. Ganguly et al. reported of six known interacting proteins with a novel carboxy terminal, pS/pT-X(1-2)-COOH motif (where X is not a proline) [218]. This SWTX motif overrides the RKR motif which is the endoplasmic reticulum localization signal and redirects membrane proteins to the cell surface [219, 220]. All the same, some recent studies indicate that phosphorylation is necessary but not sufficient for 14-3-3 binging and that more anchor residues might be required to stabilize the interaction [221]. Computational approaches have suggested that $> 90\%$ of the 14-3-3 binding sites lie in disordered regions of their target proteins [222]. Since 14-3-3 sites are usually present as a pair, Johnson et al suggested that 14-3-3 might act in integration of signals from different pathways, specially if both the binding sites are phosphorylated by different kinases [223].

SMG7 protein has been implicated in the dephosphorylation of UPF1 from the NMD pathway [224]. The N-terminal of SMG7 contains a 14-3-3-like-domain. In SMG7, there exist residues which resemble the phosphoserine binding residues of 14-3-3. Mutation of these residues impairs binding of SMG7 to UPF1 and the recruitment of UPF1 to cytoplasmic RNA foci. The same set of residues is seen in SMG5 and SMG6 [225].

1.5.5 BRF1

BRF1 was identified through a genetic screen designed to identify novel AUBPs. Stoecklin et al. [226] generated a reporter plasmid which consisted of a GFP reporter gene, flanked by the 5'UTR and the ARE-containing 3'UTR of human IL-3 gene. This reporter was stably transfected into HT1080 cells leading to several clones, one of which was HTwt16. HTwt16 are wildtype cells where AMD is efficient, hence the reporter ARE-mRNA is degraded, and consequently the GFP expression is low. The amount of GFP expressed could be estimated by performing fluorescence-activated cell sorting (FACS). These HTwt16 cells were then subjected to 8-12 rounds of random chemical mutagenesis by exposure to ICR191, which is a frameshift mutagen. Of the surviving population, 3 clones showed high levels of GFP expression, implying impaired AMD efficiency. Cells from one of these clones, SlowC, led to an ~8-fold increase in the half life of ARE-containing reporter mRNA. SlowC was subjected to gene complementation assays to determine which gene was responsible for the impaired AMD [227]. To this end, the SlowC cells were infected with a retroviral cDNA library which was generated using size-fractionated cDNA from HT1080 cells. Clones showing lower levels of AMD compared to that seen in SlowC cells were chosen via FACS. Figure 1.2 depicts the FACS profiles of the HTwt16, SlowC, and CM1 clone. As seen in the FACS profiles, the GFP intensity was plotted along the X-axis. HTwt16 shows low levels of GFP

which is a signature of wildtype cells with efficient AMD. The SlowC cells have impaired AMD efficiency, hence showed higher levels of expressed GFP. CM1 displayed lower GFP intensity as compared to that seen in SlowC cells, indicating restored AMD. Adjacent to the FACS profiles are the GFP-IL3 reporter mRNA decay experiments which demonstrate the difference in half-lives of the GFP-IL3 reporter mRNA in HTwt16, SlowC, and the CM1 cell lines. The gene responsible for restoring AMD activity of CM1 cells was later identified to be BRF1. The genotype of SlowC was analysed and it was observed that both copies of BRF1 in SlowC cells harboured out-of-frame stop codons which occur after 73 and 123 amino acids in the two BRF1 alleles. Phenotypic analyses revealed the absence of a full-length BRF1 protein. Thereforth, SlowC cells have been treated as a homozygous knockout for BRF1 gene. This SlowC cell line has been used in the study described in this thesis.

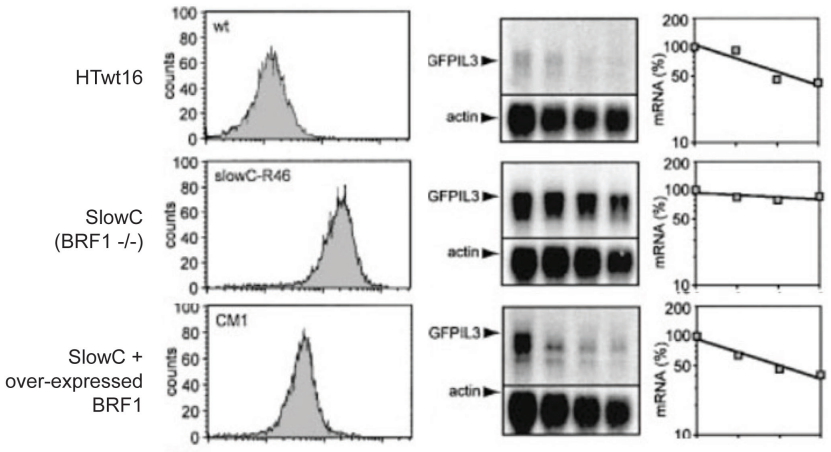

Figure 1.2: The SlowC cell line. HT1080 cells were stably transfected with a plasmid construct consisting of GFP reporter gene located between the IL-3 5' UTR and the ARE-containing 3' UTR of IL-3. The resultant cell line, HTwt16, was subjected to ten rounds of random chemical mutagenesis. Clones were selected based on increase in GFP intensity on performing FACS analyses. Gene complementation assay was carried out by transfecting clones with retroviral-cDNA library (cDNA was generated using HT1080 genomic DNA). Clones over-expressing BRF1 protein was identified as being able to restore AMD efficiency. Both alleles of BRF1 were sequenced to reveal premature stop codons. Figure reproduced from Stoecklin et al. [227].

Stumpo et al [228], created a BRF1 knockout mouse. All knockout embryos died in utero by embryonic day 11 (E11). Two-thirds of these deaths were attributed to failure of chorio-allantoic fusiion. In the remainder embryos, by E10.5 the placentas showed decreased cell division and atropy of trophoblast

layers. Neural tube defects were seen which were a consequence of placental abnormalities. Fibroblasts derived from knockout embryos had normal levels of fully polyadenylated compared to deadenylated GM-CSF mRNA and the mRNA turnover rate was normal. Bell et al. [229] investigated the placental defects of BRF1 knockout mice in greater detail. Expansion of primitive erythroid cells appeared hampered. Defective development of the mutant mice was due to elevated expression of VEGF-A in embroys and in the mutant embryonic fibroblasts cultured under normoxic or hypoxic conditions. VEGF-A mRNA decay rates remained unaltered. The increase in levels of VEGF-A protein was associated with enhanced association of VEGF-A mRNA with polysomes, indicating that BRF1 controls translation of VEGF-A mRNA. Another study revealed that BRF1 destabilized Stat5b mRNA and this resulted in a drastic decrease in formation of erythroid colonies indicating the role of BRF1 in hematopoiesis [230]. BRF1 mRNA levels were controlled by parathyroid hormone (PTH) and bone morphogenetic protein 2 (BMP-2) in mouse osteoblasts [231].

BRF1 activity is regulated in a manner very similar seen in TTP. In BRF1, serines S92 and S203 are phosphorylated by MK2 and Protein kinase-Bα (PKBα) enzymes, result in BRF1 binding to 14-3-3 and its ARE-mRNA destabilizing activity is impaired [232, 211, 233]. Furthermore BFR1 has been shown to recruit ARE-mRNA to P bodies [193].

1.5.6 BRF2

The Blackshear group attempted to create BRF2 knockout mice. In their first attempt, the mice still produced a BRF2 protein which lacked the first exon but expressed the second exon along with a significant portion of the single intron. rest of the protein taking a AUG in the intron as an initiation codon. The homozygous F1 progeny were healthy, but the females were sterile despite having a normal reproductive system. The death of homozygous F2 generation embryos occured due to arrest at the two-cell stage, which is a characteristic of maternal mRNA defficiency [234]. The same group later generated a BRF2 complete knockout mouse. Homozygous BRF2 knockout mice died within ~2 weeks of birth. All the knockout mice necropsied, had pallor of skin often accompanied by hemorrhage, usually in the intestines. There was an overall defect in hematopoietic development with significantly decreased levels of red blood cells, white blood cells, hemoglobin, and hematocrit. Myeloid and megakaryocyte populations appeared reduced [235]. Mutations in the BRF2 gene have been observed in many leukemia patients / cell lines [236]. Double knockout mice with a conditional deletion of BRF1 and BRF2 underwent defective thymopoiesis and developed T-cell acute lymbhoblastic leukemia (T-

ALL). Notch-1, which plays and important role in thymopoiesis and bears a nonameric ARE in the 3'UTR, was suggested to be a target. [237].

1.6 Aim of the study

The TTP family is a prominent part of the AUBPs. Although bearing high homology amongst each other, there are some significant differences, mostly regarding cellular presence. Carrick et al. established that the cellular mRNA levels of the TTP family members vary in different tissues and cell lines [238]. Serum and LPS have been known to rapidly induce TTP [185]. However, there are divided views about BRF1 and BRF2, indicating their upregulation [185] or downregulation (W.S. Lai and P.J. Blackshear, unpublished data, mentioned in [173]) on LPS treatment. Nevertheless, the change in BRF1 and BRF2 levels, if any, was marginal and not comparable to that of TTP. Insulin was shown to upregulate TTP mRNA and protein levels to a considerable extent [181, 183]; however, BRF1 and BRF2 mRNA levels were downregulated [181].

TTP, BRF1, and BRF2 can promote degradation of ARE-mRNAs in an *in vitro* setup with comparable efficiencies. However, it is clear from the differences in the respective knockout mice that each member has distinct functions and is active in a highly temporal manner. It also says that one member of the TTP family cannot be substituted by another in the *in vivo* context. The endogenous ARE-mRNA target specificities are different. A similar observation is regarding the SlowC cells, where TTP and BRF2 are possibly unaltered but still the AMD remains impaired. This points out to a higher level of regulation amongst the three members. Only limited information is available on BRF2. Hence, it would thus be interesting to question the role of BRF2 in the cell and investigate the regulation of its activity.

2 Results: BRF2 promotes ARE-mediated mRNA decay

2.1 BRF2 mRNA levels are elevated in SlowC cells

SlowC cells lack functional BRF1 protein [227]. Over-expression of BRF1 in SlowC cell lines restores the AMD capacity of these cells. The questions arose as to a) why the endogenous level of BRF2 was not sufficient to compensate for AMD and whether BRF2 was needed in amounts higher than the endogenous levels, b) whether BRF1 stabilizes BRF2, and therefore in absence of BRF1, eventually BRF2 too is destabilized, and c) whether BRF1 and BRF2 are functional as a heterodimer. I tried to address some of the questions in the following section.

The first question I asked was whether BRF1 regulates levels of BRF2. If it did, SlowC cells which lack BRF1 should show altered levels of BRF2 as compared to HTwt16. I measured the mRNA levels of the BRF1 and BRF2 genes in HTwt16 and SlowC cells to find out the effect of the absence of BRF1 on BRF2 mRNA levels. I performed RT-qPCR using two sets of primers each to determine BRF1 and BRF2 mRNA levels Figure 2.1. Nucleolin mRNA was used as an internal control against which the mRNA levels of BRF1 and BRF2 were normalized. Three independent biological repeats and three technical repeats PCR were performed. For each set of primers, mean mRNA level of the gene in HTwt16 was used as reference and set to 100%. Thus, BRF1 and BRF2 mRNA levels in SlowC were respectively represented as a percentage of BRF1 and BRF2 mRNA levels in HTwt16.

Both BRF1 alleles in SlowC contain premature stop codons; therefore, BRF1 mRNA levels remain unchanged. This finding was confirmed by RT-qPCR data as seen in [Figure 2.1]. Additionally, I observed a nearly 2-fold increase in the SlowC BRF2 mRNA levels when compared to those in HTwt16. Whether this difference holds true at the protein level remains to be probed.

Estimation of protein levels of both the above genes in SlowC cells, which would be the ideal experimental design, was not possible due to the lack of

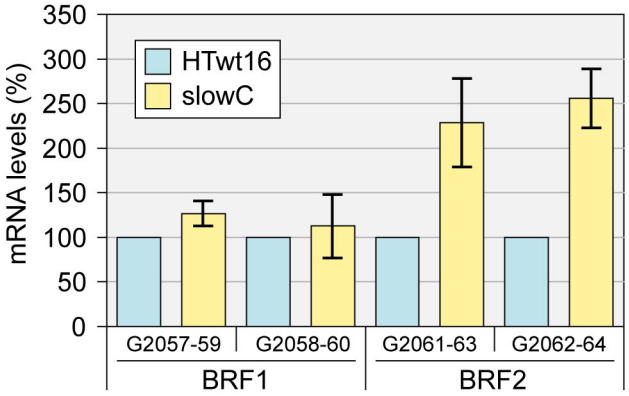

Figure 2.1: mRNA levels of BRF1 and BRF2 in HTwt16 and SlowC cells. mRNA levels of BRF1 and BRF2 in HTwt16 and SlowC cells were quantified byRT-qPCR using two distinct sets of primers per experimental gene. Values were normalized against nucleolin mRNA. Values are mean ± s.e.m of three technical replicates and three independent biological repeats.

antibodies that are highly specific towards BRF1 or BRF2. The existing rabbit polyclonal antibody [239] did not give conclusive results. Figure 2.2:Panel A shows a western blot where I analysed lysates from different cell lines as indicated for endogenous BRF1/2 protein expression. The filled arrow shows the possible position of BRF1; this band is seen in HT1080 lysate (Lane 5) and is missing from SlowC (Lane 6) confirming the absence of BRF1 in SlowC. Apart from this, BRF1 is detected in the U2OS cells. The empty arrow shows a band of low intensity which may correspond to BRF2. Panel B shows HA-BRF2 over-expressed in HTwt16 and SlowC cells (Lanes 9,10, respectively). Transient expression consistently shows HA-BRF2 to run between 60-70 kDa, while the predicted molecular weight of BRF2 is 51 kDa. I attempted raising polyclonal antibodies against mutually heterologous regions in BRF1 and BRF2. However, the obtained antibodies could detect only over-expressed BRF1 and BRF2 Figure 2.3.

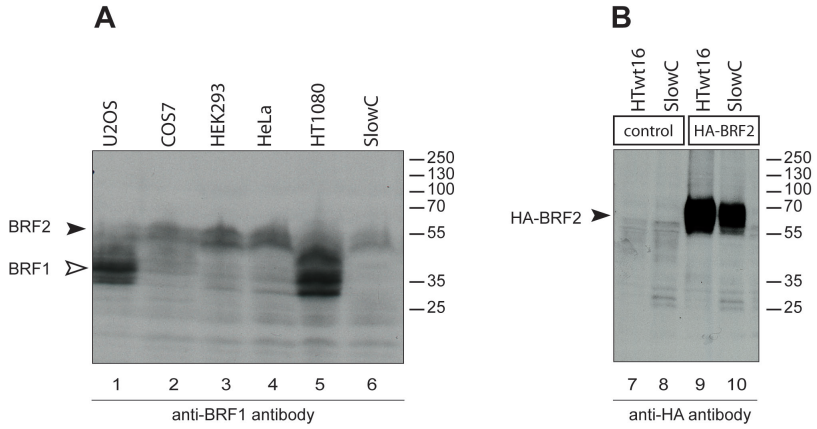

Figure 2.2: Protein levels of BRF1 and BRF2 in different cell lines. Panel **A**: Laemmli lysates of indicated cell lines were resolved on 10% polyacrylamide gels, subjected to western blotting, and probed with a polyclonal antibody against BRF proteins [239]. Panel **B**: HA-BRF2 transiently over-expressed in HEK293 cells.

2.2 Stable over-expression of BRF2 in SlowC cell lines

Assuming that BRF2 protein is upregulated ~2-fold in SlowC cells, why does this increase not restore the AMD capacity of the SlowC cells? To address this question, I initially tested whether BRF2 promotes mRNA degradation in an ARE-dependent manner. To this end, I used SlowC cells which encode a stably transfected ARE-containing reporter mRNA as in Figure 2.4. This reporter has a GFP gene inserted between the IL-3 5' UTR and the ARE-containing 3' UTR of IL-3 (henceforth termed as the GFP-IL3 reporter). In wildtype cells, efficient AMD leads to degradation of reporter mRNA and results in lowered GFP signal intensities in FACS and lesser residual reporter-mRNA in northern blotting experiments.

My goal was to stably over-express HA-BFR1 and HA-BRF2 in SlowC cells. After selecting for survival in presence of the drug, G418, individual clones were isolated and several such clones were screened using FACS for clones showing a GFP signal lower than that in SlowC cells [227]. With regard to BRF2 stable over-expression, FACS analyses identified two clones in which the GFP signal was lower than that in the SlowC cells, hinting at efficient reporter GFP-IL3 mRNA decay. Positive and negative clones each were selected for SlowC cells expressing HA-BRF1 or HA-BRF2. These four clones were fol-

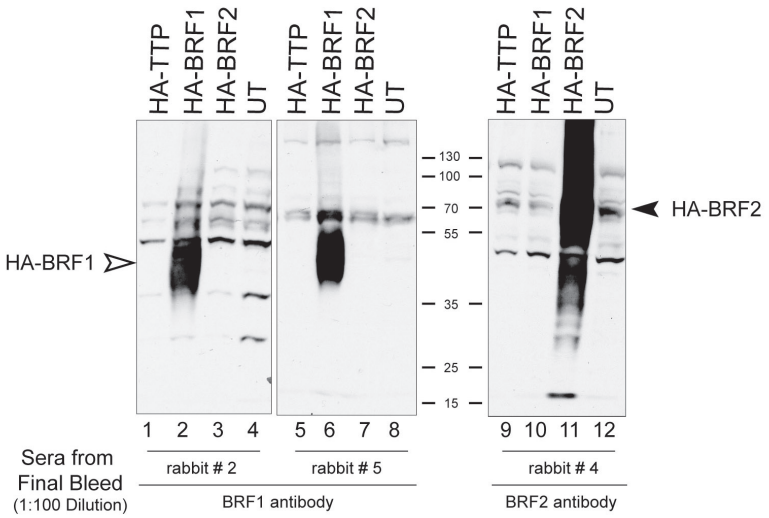

Figure 2.3: Polyclonal antibodies recognize only over-expressed BRF1 and BRF2 proteins. Polyclonal antibodies were raised in rabbits against mutually exclusive regions of BRF1 and BRF2 (two rabbits immunized with GST-BRF1:aa231-288; one rabbit immunized with GST-BRF2:aa1-117). The final sera that was raised against the two antigens did not cross-react with the other TTP family members. They however recognized only the over-expressed forms of BRF1(Lanes 2, 6) or BRF2 (Lane 11). All the three sera fail to recognize endogenous BRF1/BRF2 proteins (Lanes 4, 8, 12).

lowed up with actinomycinD chase experiments to study the degradation of the reporter mRNA. ActinomycinD blocks polymerase II transcription; hence, the 0-hr timepoint depicts steady-state levels of the reporter RNA.

Cell lines used in the assay were: HTwt16 (effective AMD, therefore less reporter mRNA, and less GFP expressed) and SlowC (compromised AMD, therefore more reporter mRNA, and more GFP expressed) as reference standards, positive clone for SlowC-BRF1 (SC-B1-1), negative clone for SlowC-BRF1 (SC-B1-2), first positive clone for SlowC-BRF2-clone I (SC-B2-1), second positive clone for SlowC-BRF2 (SC-B2-2), and a negative clone for SlowC-BRF2 (SC-B2-3). Northern blotting analyses were used to detect the GFP-IL3 reporter mRNA while RPS7 mRNA served as a loading control. FACS was performed of an additional sample withdrawn from all above cell lines at the 0-hr timepoint. FACS analyses showed that the GFP signal in SC-B1-1, SC-B2-1, and SC-B2-2 had decreased, suggesting restored AMD. Northern blotting resulted in an extremely weak signal with a RNA probe specific for the IL-3 3' UTR. These low signal intensities represented low steady-state levels of

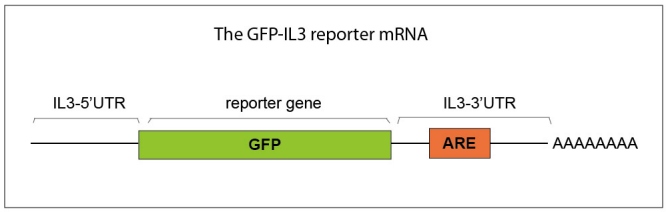

Figure 2.4: The GFP-IL3 reporter mRNA. HTwt16 and SlowC stably express the GFP-IL3 reporter which serves to monitor AMD. Efficient AMD leads to degradation of reporter mRNA and results in lowered GFP signal intensities in FACS and northern blotting experiments. When AMD is compromised, the GFP-IL3 reporter mRNA is not degraded and results in high GFP intensity when estimated by FACS and northern blotting.

the reporter mRNA. This problem was reporter-mRNA specific, since RPS7 mRNA was present in abundant quantities. Low expression could be due to the GFP-IL3 reporter-mRNA transcription being driven by the IL-3 promoter, and not a strong promoter like the CMV promoter. Moreover, efficient AMD decreased the steady-state levels further. Thus, due to the low levels of the GFP-IL3 reporter, it proved difficult to assess the degradation rates of the above clones. Nevertheless, SC-B1-2, SC-B2-1, and SC-B2-2 showed reduced reporter mRNA levels suggesting higher AMD efficiency than in SlowC cells. [FACS and Northern blotting in Figure 2.5].

In order to confirm that these clones in fact over-express HA-BRF2, I carried out western blotting analyses of lysates from different clones, and probed them with an anti-HA antibody to only detect the exogenously expressed BRF1/2 protein Figure 2.6. BRF1 protein is seen at the expected position (Lane 5). Incidentally, lysates from both seemingly BRF2-positive positive clones showed expression of an HA-tagged protein at approximately 35 kDa size [Lanes 7,8]. This protein is much smaller than the full-length BRF2 protein. It may represent the N-terminal portion of BRF2 since the HA tag is detected. This could be due to improper insertion of the transfected plasmid leading to expression of a truncated version of HA-BRF2 or posttranslational proteolytic processing of full-length BRF2 leading to a remainder N-terminal fragment. The single MG132 (proteasome inhibitor) experiment I performed to check for proteolysis of HA-BRF2 via the proteasome did not argue in favour of proteolytic processing, and genomic DNA analyses posed technical problems (data not shown). While it is not clear how the protein fragment of BRF2 was generated, it is interesting to note that the fragment appears to be active in promoting AMD.

I performed a new round of stable transfection, for which the plasmid was linearized with DraIII restriction enzyme. This ensured that prior to transfection,

I started with a linear DNA having the complete HA-BRF2 gene and its auxiliary regions. The second attempt of BRF2 stable transfection in SlowC cells yielded two positive clones, SC-B2-4 and SC-B2-5, which exhibited low levels of GFP by a FACS analysis and SC-B2-6 as a negative control [Figure 2.7:Panel A]. Western blotting shown in Panel B indicated SC-B2-1 expressing full-length HA-BRF2 (Lane 2). Surprisingly, the second clone SC-B2-2 expressed HA-BRF2 of a size around 35 kDa (Panel B, Lane 3). I did not examine this clone further, but continued working with SC-B2-4 which expressed the full-length HA-BRF2

Stable cell clones were expanded and serially passaged over ~4 months. However, after this period of time, the FACS profiles for SC-B2-P appeared to change, displaying higher GFP signal intensities, indicating a gradual loss of AMD capacity [SC-B2-P in Figure 2.8:Panel A]. Western blotting analyses at this point of time indicated a drastic reduction in the level of HA-BRF2 expressed in these stable clones as compared to those in the initial passages [Figure 2.8: Panel B, Lane 3, 2 hrs exposure of film]. This line of work was terminated here, since the effect produced by this mildly-expressed HA-BRF2 would be out of the sensitivity limit of my experiments. Hereon, I switched to a transient-transfection system for studying the role of BRF2 in AMD.

2.3 Transient over-expression of BRF2 destabilizes ARE-containing mRNAs

I used a transient transfection system in HeLa cells where I over-expressed HA-tagged BRF2, the Tet-off transactivator, together with a plasmid encoding an mRNA reporter gene driven by a Tetracycline-sensitive promoter. The reporter consists of a rabbit ß-globin gene with or without the 53 nt-long TNFα ARE in its 3' UTR. The scheme for this reporter is given in [Figure 2.9]. The Tet-off system [240] made it possible to shut off reporter transcription by addition of doxycycline, which determined the 0-hr timepoint for the reporter mRNA decay assay. In such doxycycline-chase assays, samples were collected over a timecourse of 3 hours and total RNA was isolated. Northern blotting was carried out using RNA probes against ß-globin mRNA and nucleolin mRNA as a loading control. In Panel A, where a ß-globin reporter gene devoid of ARE was transfected, no degradation was detected, irrespective of over-expressed HA-BRF2. In Panel B, where samples were transfected with the ß-globin-ARE reporter gene, reporter mRNA decay was accelerated when HA-BRF2 was co-expressed. Calculation of half-lives of the reporter mRNA in all four experimental conditions shows that HA-BRF2 reduces the half-life of the ß-globin-ARE mRNA from 3.8 hrs to 1.1 hrs [Figure 2.9: Panel B]. Thus, BFR2

promotes mRNA degradation in an ARE-specific manner.

2.4 DISCUSSION

BRF2 mRNA shows elevated levels in SlowC cells: BRF1 and BFR2 are homologous proteins belonging to the TTP family of proteins. The absence of a functional BRF1 protein in SlowC cells leads to the loss of AMD activity of the cell. Since limited data is available on both proteins, it is not known if the effects of the two are redundant or additive. Moreover, it is possible that BRF1 regulates BRF2 levels, and viceversa. BRF1 has an established role in AMD as a protein that binds to the ARE and triggers rapid degradation of the bound mRNA [227]. Therefore, it was interesting to investigate whether an AU-rich element exists in the 3' UTR of the BRF2 gene which could make it a target of BRF1. Literature published so far does not acknowledge BRF2 as an ARE-containing gene. Hence, I processed the spliced mRNA sequence of BRF2 (NM_006887.4, NCBI GenBank) using the ARE*Score* algorithm designed by Spasic et al [241]. This algorithm identified five AUUUA pentamers dispersed over the 3' UTR of the BRF2 gene [Figure 2.10]. This makes BRF2 a candidate AMD substrate to potentially undergo AMD in order to regulate its own levels. BRF1 might also control BRF2 at the protein level. However, SlowC cells were generated by random chemical mutagenesis. It is likely that more genes were mutated apart from BRF1, which have not been scored for. Such mutations may favour altered BRF2 regulation. Hence, more detailed experiments need to be performed, e.g., BRF2 protein levels in SlowC and SC-B1-1 (SlowC over-expressing HA-BRF1) should be compared to address any relation between BRF1 and BRF2 at the protein level.

Stable over-expression of BRF2 in SlowC cell lines: Initial passages of SlowC cells over-expressing HA-BRF2 indicated a restored AMD capacity. However, it is possible that the gradual loss of over-expressed BRF2 protein could have contributed to the FACS profiles resembling those of SlowC untransfected cells. Earlier studies on over-expression of BRF2 yielded similar outcomes. BRF2 over-expression was reported to trigger apoptotic-like cell death. When quantified, the percentage of cell death was 10.5% at 24 hrs and 31.9% at 3 days after transfection of BRF2. This was linked to the p53-dependent apoptosis pathway [242]. In an older study, over-expression of TTP, BRF1, and BRF2 had been shown to stimulate the mitochondrial death machinery and induce apoptosis [178]. It is thus a reasonable assumption that in my stable transfection experiments, the cells that originally expressed high levels of HA-BRF2 gradually got eliminated due to apoptosis-like cell death. The remainder could be cells with little expression of HA-BRF2 where apoptosis is not yet triggered. In a transient transfection scenario, cells are allowed to grow only upto 48 hrs after

transfection with BRF2 plasmid before being lysed for experimental purposes. Presumably, this would be a time frame where the cells are not apoptotic.

BRF2 degrades ARE-containing mRNAs: Lai et al. [197] had performed cell-free deadenylation assays to show that TTP, BRF1, and BRF2 are able to deadenylate ARE-containing mRNA reporters. The reactions in this assay were quenched after 60 mins, and the Xenopus ortholog of BRF2, xC3H-3, was used. This demonstrated that deadenylation could be one of the early steps of the human ortholog of BRF2 as well. However, this study did not elaborate on therole of BRF2 in AMD. I chose to study the AMD abilities of BRF2 in a more physiological system as compared to the one in the above study. Since steady state levels for each mRNA are determined by the rates of transcription and degradation, the doxycycline chase assay is an elegant way of uncoupling these two processes and studying only the mRNA decay part. Addition of doxycycline ensures highly-specific shutdown of reporter gene transcription. Therefore, the results seen are solely a readout of mRNA degradation. In the described assay, BRF2 causes degradation of the ARE-containing reporter mRNA, which adds it to the list of proteins that destabilize ARE-containing mRNAs. I had to employ an exogenous over-expression system for BRF2 throughout this study, since the endogenous levels of BRF2 were not sufficient for the kind of experiments I needed to perform (Figure 2.2). Now that the assay to measure mRNA decay was established, regulation of BRF2 activity and players involved therewith were investigated further.

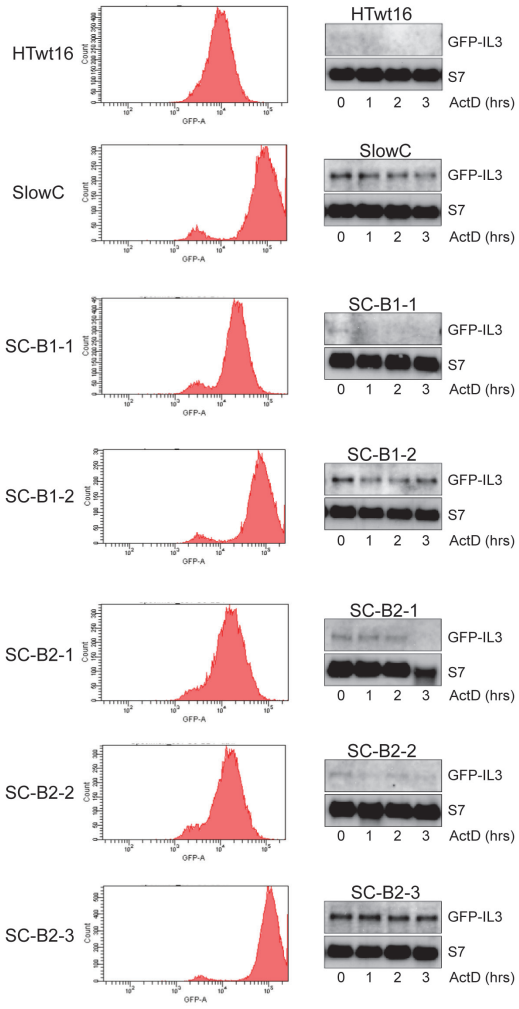

Figure 2.5: FACS and Northern blotting analyses of stable SlowC-BRF1 and SlowC-BRF2 clones: Attempt I. ActinomycinD-chase assays were cerried out over a period of 3 hrs followed by northern blotting experiments. Cell lines used in the assay were: HTwt16 and SlowC (as reference standards), positive clone for SlowC-BRF1 (SC-B1-1), negative clone for SlowC-BRF1 (SC-B1-2), first positive clone for SlowC-BRF2-clone I (SC-B2-1), second positive clone for SlowC-BRF2 (SC-B2-2), and a negative clone for SlowC-BRF2 (SC-B2-3). RNA probes used were specific for IL-3 3'UTR to detect the reporter gene and for RPS7 mRNA as a loading control. FACS was performed with an additional sample withdrawn from all above cell lines at the 0-hr timepoint.

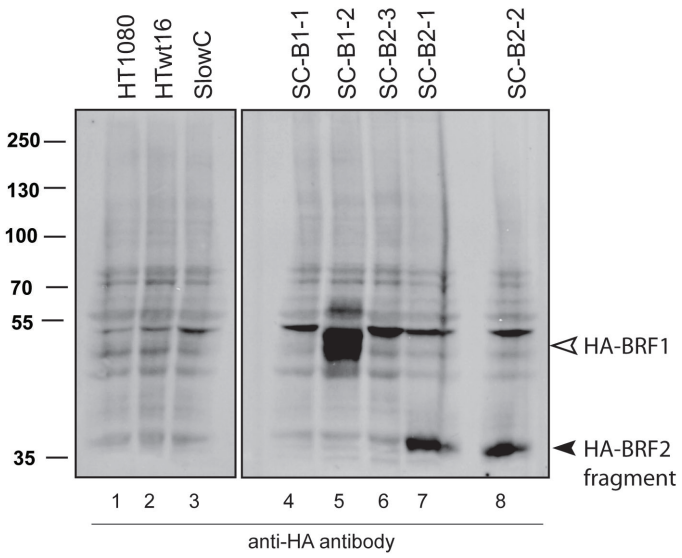

Figure 2.6: Expression of BRF1 or BRF2 protein in respective stable clones. Laemmli lysates of indicated stable cell clones were resolved on 10% polyacrylamide gels, subjected to western blotting, and probed with a mouse monoclonal anti-HA antibody.. Molecular weights are indicated in kDa.

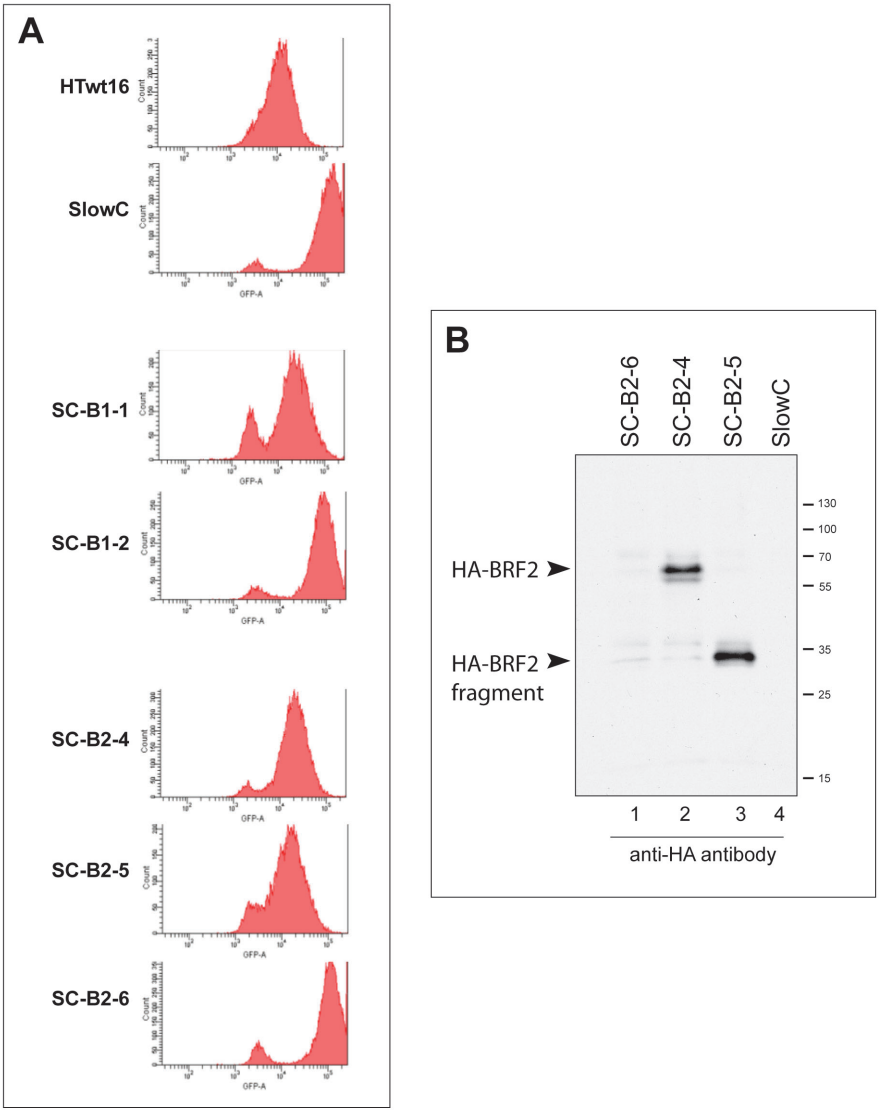

Figure 2.7: FACS profiles and expression of BRF2 protein in stable SlowC-BRF2 clones: Attempt II. Panel **A**: pcDNA-HA-BRF2 plasmid was DraIII-linearized prior to transfection. FACS was performed with samples from cell lines indicated. Panel **B**: Laemmli lysates of indicated stable cell clones were resolved on 10% polyacrylamide gels, subjected to western blotting, and probed with a mouse monoclonal anti-HA antibody. Molecular weights are indicated in kDa.

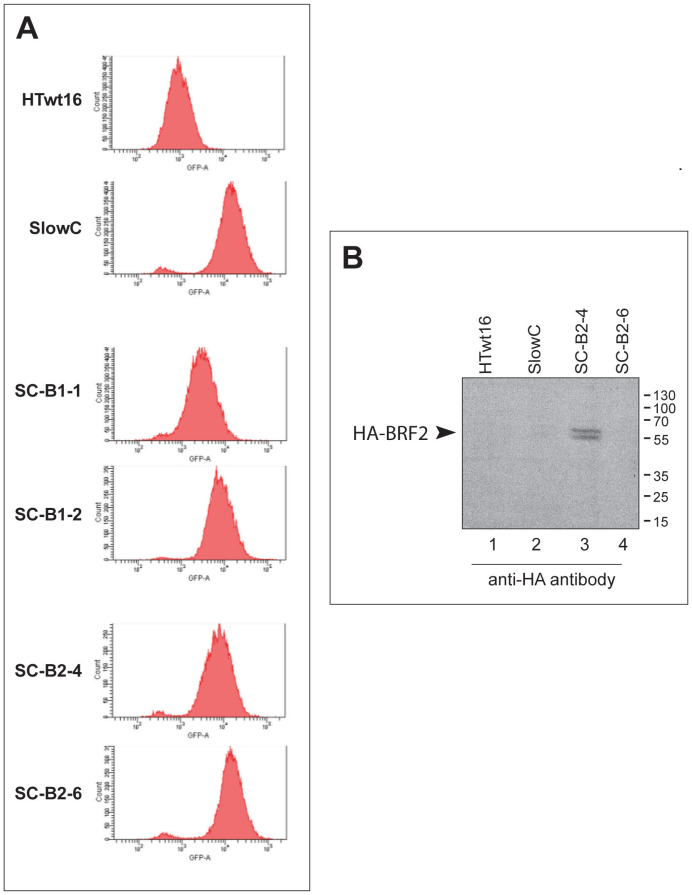

Figure 2.8: FACS profiles and expression of BRF2 protein in stable SlowC-BRF2 clones after serial passages. Stable cell clones were expanded and serially passaged over ~4 months. Panel **A**: FACS was performed with samples from cell lines indicated. Panel **B**: Laemmli lysates of indicated stable cell clones were resolved on 10% polyacrylamide gels, subjected to western blotting, and probed with a mouse monoclonal anti-HA antibody. . Molecular weights are indicated in kDa.

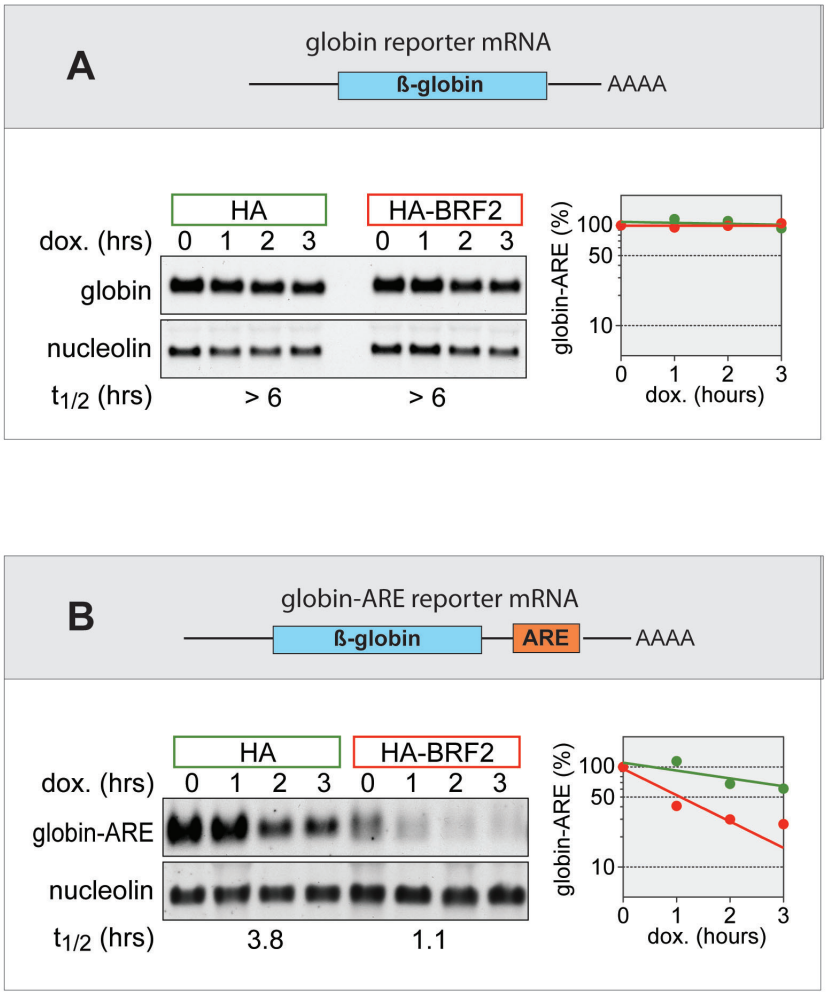

Figure 2.9: BRF2 degrades mRNAs in an ARE-dependent manner. A Tet-off system was employed and HeLa cells were transfected with an empty-vector or with a plasmid encoding HA-BRF2. Transfections in Panel **A** included the ß-globin reporter gene lacking the ARE in the 3' UTR; and those in Panel **B** included the ß-globin-ARE reporter gene. Northern blotting RNA probes used were against ß-globin, reporter gene; and nucleolin, loading control. Reporter mRNA levels were normalized to nucleolin mRNA levels. The 0-hr timepoint is set to 100%. Graphs of reporter mRNA levels vs. time are plotted. Half-lives of the reporter mRNA in each setup is indicated.

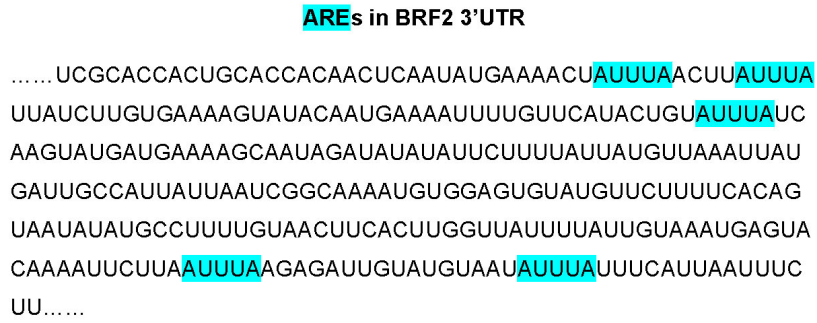

Figure 2.10: Putative AU-rich elements in the 3'UTR of BRF2 as predicted by the ARE*Score* algorithm. The spliced mRNA sequence of BRF2 (NM_006887.4, NCBI GenBank) was analysed using the ARE*Score* algorithm which predicted five AU-rich pentamers at nt positions 3133, 3142, 3190, 3357, and 3378 which are located in the 3'UTR of BRF2 mRNA. Residues (3100-3399) of BRF2 mRNA are given in the figure and the AU-rich pentamers are highlighted.

3 Regulation of BRF2 activity

3.1 BRF2 binds to 14-3-3 protein

3.1.1 BRF2 interaction with 14-3-3 is dependent on phosphorylation

14-3-3 is an abundant adaptor protein that binds to and modulates the activity of various proteins in the cell [243]. Here, I sought to find out if 14-3-3 modulates the AMD activity of BRF2. I performed co-immunoprecipitation experiments to check for possible interaction between BRF2 and 14-3-3. The questions addressed were (a) whether BRF2 interacts with 14-3-3, and if yes, (b) whether this interaction is phosphorylation-dependent.

To answer these, I performed co-immunoprecipitation (co-IP) experiments in HEK293 cells using the GFP-binder beads [Figure 3.1]. The GFP-binder is a bacterially-expressed stable monomer of a 13 kDa binding fragment of the heavy chain antibody of the llama. Recombinant GFP-binder protein is immobilized on NHS-sepharose beads and used in co-IP experiments to pull down GFP tagged proteins.This fragment is known to interact strongly and specifically with GFP [244]. YFP bears high homology with GFP; hence, interacts effiently with the GFP binder. I used YFP-BRF2 as a bait protein. 14-3-3over-expression was not necesary, since the endogenous levels are abundant. Two sets of co-IPs were performed [Figure 3.2]. The first set included phosphatase inhibitors, namely, sodium vanadate, sodium fluoride, and okadaic acid in the lysis buffer. This would preserve the phosphorylation status of proteins and enable possible binding between BRF2 and 14-3-3 in case this interaction depended on covalently linked phosphate groups (Lanes 1,3). The second set included phage lambda phosphatase in the lysis buffer which would dephosphorylate serines and threonines on the proteins after lysis (Lanes 2,4). BRF2 was able to pull down 14-3-3 (Lane 3) in the untreated set. In the set treated with phage lambda phosphatase, only a minimal amount of 14-3-3 was pulled down (Lane 4), which indicates that the interaction was significantly reduced upon loss of phosphorylation. In Lanes 1,2, which represent the empty-vector (YFP-only) control, no 14-3-3 is detected confirming that 14-3-3 does not interact with the YFP tag. This empty-vector control has been used in all further

co-IP experiments. Careful observation reveals two similar molecular weight 14-3-3 bands hinting at a possible heterodimer containing 14-3-3epsilon. With this, I demonstrated that BRF2 interacts with 14-3-3 and that this interaction is dependent on phosphorylation.

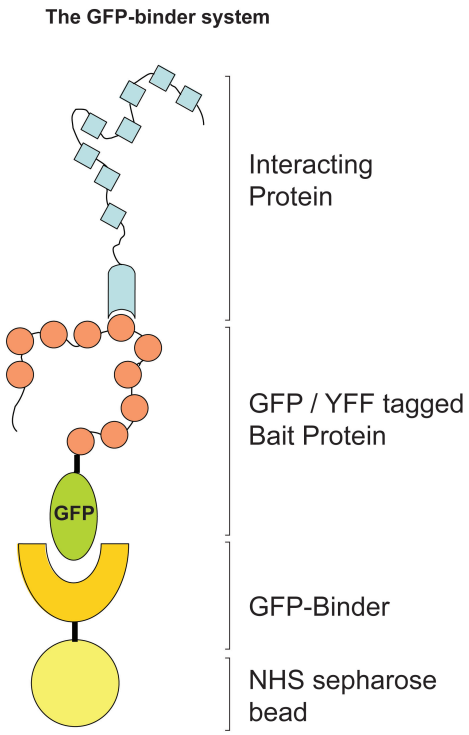

Figure 3.1: The GFP binder system. The GFP-binder is a bacterially-expressed stable monomer of a 13 kDa binding fragment of the heavy chain antibody of the llama. Recombinant GFP-binder protein is immobilized on NHS-sepharose beads and used in co-IP experiments to pull down GFP tagged proteins.

During the standardization phase of the co-IP experiments, I had used HT1080 cells as the SlowC cells are derivatives of HT1080. However, expressing sufficient amounts of BRF2 in these cells proved to be difficult because of the low transfection efficiency and inconsistent expression of BRF2. Thereforth, I used HEK293 cells since they support robust protein expression. Moreover, previously I used HA-BFR2 to pull down 14-3-3. Inadequate amounts of 14-3-3 were pulled down, which made its western blot detection difficult, with rarely-consistent results. Hence, I shifted to using the GFP-binder which has high affinity for YFP. This made the co-IP considerably more efficient and pulled down larger amounts of 14-3-3 in a reproducible manner.

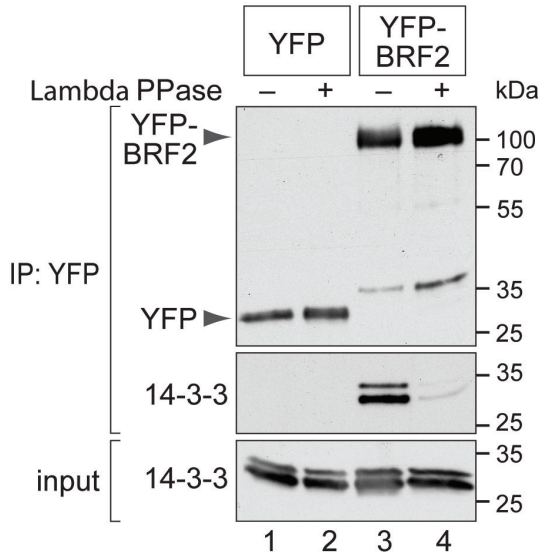

Figure 3.2: BRF2 binds to 14-3-3 in a phosphorylation-dependent manner. HEK293 cells were transiently transfected with plasmids encoding YFP-only or YFP-BRF2. Cytoplasmic lysates were prepared 24 hrs after transfection. The two sets consisted of lysates including phosphatase inhibitors (Lanes 1,3) or lysates including 1 unit/µl of lambda phage phosphatase (lambda PPase) (Lanes 2,4) in the lysis buffers. co-IP experiments were carried out to purify YFP-tagged proteins along with their interacting partners using the GFP-binder beads. Eluted proteins were resolved on 10 % SDS polyacrylamide gels. Western blotting analyses were carried out using an anti-GFP and an anti-14-3-3 antibody.

3.1.2 BRF2 binds to 14-3-3 via serine residues S123 and S257

14-3-3 binding to TTP [245] and BRF1 [232, 211] has already been studied in detail. Keeping the extensive homology between BRF2 and above two proteins in mind, I considered 14-3-3 to be a putative interacting partner of BRF2.

3.1.2.1 BRF2-S123,257A double mutant shows reduced binding to 14-3-3

I wanted to determine the 14-3-3 binding sites of BRF2. Considering the target sequence criteria for 14-3-3 binding [215, 216, 217], the BRF2 protein sequence

was scanned for sequences which bore homology with the optimal sequence motifs recognized by 14-3-3: RSX**pS**XP and RXXX**pS**XP. No sequence with 100% homology could be identified. However, there were multiple sequences that were similar to these motifs. I chose to work on three sequences that were closest to the optimal sequence; RDR**S**FS (S123), KLHH**S**LS (S257), and RLSI**S**DD (S492). The sequences flanking S123 and S257 of BRF2 are conserved among the TTP family of proteins [Figure 3.3].

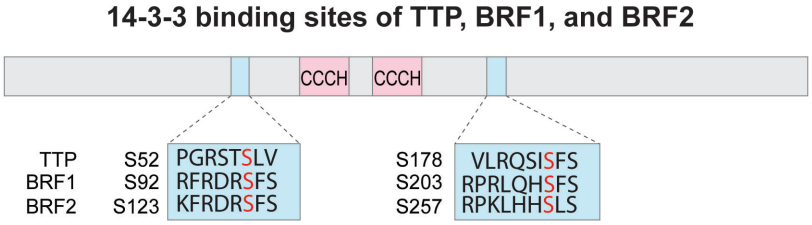

Figure 3.3: 14-3-3 binding sites of TTP, BRF1, and BRF2 bear homology with each other.

I generated three mutants by PCR-based site-directed mutagenesis of BRF2 for the residues S123, S257, and S492, replacing the serines with alanines, thus abolishing putative phosphorylation at these sites [Figure 3.4: Panel A]. Additionally, I created a S123,257A double mutant. co-IP experiments were performed in HEK293 cells using the GFP-binder. BRF2 wildtype or BRF2 mutants were used as a bait to co-IP endogenous 14-3-3. Phosphatase inhibitors were added to all co-IPs to preserve the phosphorylation status of the interacting proteins. Amounts of plasmid DNA was adjusted to achieve equal amounts of expression of all BRF2 constructs. Figure 3.4: Panel B demonstrates that all three single S to A mutants of BRF2 continue to bind to 14-3-3 [Panel B, lanes 3-5]. However, barely-detectable amounts of 14-3-3 were detected for the double mutant BRF2, S123,257A [Panel B, Lane 6]. The input amounts of 14-3-3 were equal in all samples. YFP-only control (Lane 1) shows no interaction with 14-3-3. Taken together, this experiment indicated that the interaction between 14-3-3 and BRF2 is dependent on simultaneous phosphorylation at both residues S123 and S257A of BRF2 and these two sites bear homology with the 14-3-3 binding sites of TTP and BRF1 [Figure 3.3]. At this point, it was interesting to know if artificially increasing the phosphorylation of BRF2 would restore/enhance the 14-3-3 binding capacity of this double mutant.

3.1.2.2 BRF2-S123,257A double mutant shows reduced binding to 14-3-3 on exposure to arsenite-induced oxidative stress

Since the kinase that phosphorylates BRF2 is not known, I followed the approach to non-specifically increase the phosphorylation levels of proteins in the cell. Arsenite causes oxidative stress in the cell, leadnig toa net increase in the phosphorylation status of many proteins due to activation of various kinases. If cells were exposed to arsenite, it is a reasonable assumption that BRF2 phosphorylation would get enhanced. These higher levels of phosphorylation would result in enhanced binding to 14-3-3.

In order to investigate this, co-IP experiments were carried out in transfected HEK293 cells after subjecting the cells to oxidative stress (500 µM arsenite, 45 mins) before final lysis. The binding pattern of BRF2 and its mutants with 14-3-3 on arsenite-induced oxidative stress [Figure 3.4:Panel C] remains similar to that seen in untreated conditions [Figure 3.4: Panel B]. The BRF2-S123,257A double mutant (henceforth termed as BRF2-AA) shows reduced binding to 14-3-3 as compared to wildtype BRF2. The input amounts of 14-3-3 were comparable in all samples. YFP-only control [Panel C, Lane 1] shows no interaction with 14-3-3. This result shows that residues S123 and S257 of BRF2 are responsible for 14-3-3 binding and this fact remains unchanged in conditions of oxidative stress [Figure 3.4:Panel C, Lane 6] .

3.1.2.3 BRF2-S123,257A mutant shows reduced binding to 14-3-3 on exposure to anisomycin-induced oxidative stress

The effects of arsenite on the cell occur mainly via production of reactive oxygen species which has many side-effects apart from activating kinases. I therefore tested anisomycin, a bacterial compound that more specifically activates stress-activated MAPK subtypes. Moreover, serum starvation of cells should downregulate kinase signalling and reduce background activity of other kinases.

In these experiments, binding of 14-3-3 to BRF2 wildtype or the BRF2-AA mutant was checked in presence of anisomycin. The experiment was divided into four sets where transfected HEK293 cells were subjected to favourable growth conditions, serum starvation (DMEM + 0.1% FCS, 2 hrs) or Anisomycin treatment (10 µg/ml, 30 mins) or serum starvation + anisomycin treatment before the final lysis. Figure 3.5 shows that on serum starvation and anisomycin treatments, BRF2-AA can still bind significantly reduced amounts of 14-3-3 (Lanes 3,6,9,12) as compared to the wildtype BRF2 (Lanes 2,5,8,11). Taken together, the experiments involving stress induced by arsenite or anisomycin demonstrate that the kinase responsible for phosphorylating BRF2 and facil-

itating 14-3-3 binding is constitutively expressed and that BRF2 interaction with 14-3-3 is not dependent or affected on stress induction.

3.1.2.4 BRF2-S125,259P mutant shows reduced binding to 14-3-3

As seen in the optimal 14-3-3 binding motifs RSX**pS**XP and RXXX**pS**XP, the presence of a proline at the +2 position was found to enhance 14-3-3 binding [217]. I generated a BRF2-S125,259P (henceforth termed as BRF2-PP) mutant where the +2 positions for both the 14-3-3 binding sites were changed to prolines [Figure 3.6: Panel A].

Subsequently, co-IP experiments were carried out in HEK293 cells to check for the amount of 14-3-3 pulled down by the BRF2-PP mutant. Western blotting shows no increase in 14-3-3 binding by this mutant. On the contrary, 14-3-3 binding was lost in the presence of the two prolines [Figure 3.6: Panel B, Lane 4] as compared to that pulled down by wildtype BRF2 [Figure 3.6: Panel B, Lane 2]. In fact, the phenotype resembles that of the BRF2-AA mutant (Lane 3). Incidentally, in the case of both S123 and S257, the +2 positions are occupied by serines which could serve as alternative phosphorylation sites allowing some residual 14-3-3 binding. Moreover, the sequence including S125 itself conforms to the criteria of an optimal 14-3-3 binding site (RSF**S**EN).

3.2 Regulation of AMD efficiency of BRF2

3.2.1 S123,257A mutations do not alter AMD efficiency of BRF2

14-3-3 is known to modulate activities of its target proteins. It was shown that in conditions of MK2 and PKB activation, 14-3-3 binds to and deactivates TTP and BRF1, and reduces their AMD effiency. In derivatives of TTP and BRF1, where serines in both the 14-3-3 binding sites of TTP and BRF1 were mutated to alanines, 14-3-3 binding this prevented. The two mutants are locked in a constitutively active form seen as enhanced AMD efficiencies. By the above logic and seeing that BRF2 binds to 14-3-3, I hypothesized that 14-3-3 binding might alter the AMD capacity of BRF2 as well.

To test this hypothesis, I performed doxycycline-chase mRNA decay assays in HeLa cells using the ß-globin-ARE reporter mRNA system as was already described in Figure 2.9: Panel B. In the experiment depicted in Figure 3.7, one set consisted of favourable growth conditions (Panel A) and other set included serum starvation (DMEM + 0.1% FCS, 2 hrs) and anisomycin treatment (10

µg/ml, 30 mins) in order to resemble stress conditions in the cell (Panel B). The BRF2-AA mutant did not seem to promote degradation of ß-globin-ARE reporter mRNA significantly differently than BRF2 wildtype. The half-lives were 0.8 hrs for BRF2 wildtype and 1.0 hrs for BRF2-AA in favourable growth conditions (Panel A), and 2.4 hrs for BRF2 wildtype and 1.8 hrs for BRF2-AA in conditions of serum starvation and anisomycin-induced stress (Panel B). To allow for comparison, it was important to confirm that BRF2 wildtype and BRF2-AA were expressed in equal amounts. Therefore, I withdrew an additional sample for protein analysis and confirmed equal levels of expression of both forms of BRF2 by western blotting [Figure 3.7:Panel C]. However, so far the independent biological repeats of this experiment have been difficult to interpret, owing mostly to the inconsistent levels of BRF2 and BRF2-AA expression.

3.2.2 S125,259P mutations do not alter AMD efficiency of BRF2

A similar mRNA decay assay was performed for the BRF2-PP mutant. This mutant degraded reporter mRNA with an efficiency equal to that of BRF2 wildtype. Figure 3.8 shows the ß-globin-ARE reporter mRNA degradation profile of BRF2 wildtype and that of the BRF2-PP. The graph below indicates the quantification of the normalized signals from the northern blots. The ß-globin-ARE reporter mRNA half-life in presence of the BRF2-PP mutant (0.9 hrs) is barely different to that in the presence of wildtype BRF2 (1.1 hrs).

3.3 Cellular localization of 14-3-3 binding site mutants of BRF2

P bodies contain most enzymes for cytoplasmic mRNA degradation and are thought to be sites of RNA decay. They also act as decision centres where the fate of an mRNA is decided regarding decay, return to translation, or storage in stress granules (reviewed in [246, 88]). It is possible that the localization of BRF2 wildtype and its mutants would explain their AMD efficiencies.

To explore the subcellular localization of BRF2, HeLa cells were transfected with HA-tagged versions of BRF2 wildtype, BRF2-AA, or BRF2-PP. Anti-HA antibody was used to detect BRF2 proteins by immunoflorescence (IF). IF microscopy was carried out to gauge three parameters: a) nuclear vs cytoplasmic abundance in presence or absence of stress, b) co-localization with P bodies, and c) co-localization with stress granules. To get a better idea of differences

between the three BRF2 constructs, 100 transfected cells were observed per sample after randomizing the samples. P body and stress granule localizations were quantified as percentage of transfected cells where HA-BRF2 showed co-localization with the Rck and eIF3, respectively.

To check for P-body localization, the cells were left untreated but co-stained for Rck, a P-body marker. P-bodies were counted in the untreated samples based on co-localization of HA-BRF2 with Rck. The results for the co-localization of BRF2 with P-body markers are shown in Figure 3.9. BRF2 showed a uniform cytoplasmic staining. In addition, BRF2 and both its mutants clearly localized to P bodies, determines as co-localization with Rck. As seen in the graphs, BRF2wildtype, BRF2-AA, and BRF2-PP showed co-localization with P bodies in 86%, 92%, and 93% of transfected cells, respectively. Thus, BRF2 wildtype and mutants showed little difference between each other with regard to P-body localization. Unlike TTP [193], a knockdown of Xrn1 was not required to sequester BRF2 in P bodies. However, other studies claimed that Xrn1 knockdown was not required to localize TTP to the P bodies [63, 91].

To check for stress granule localization, the cells were subjected to oxidative stress (500 µM arsenite, 45 mins) prior to fixing and were later co-stained for eIF3, a stress granule marker [Figure 3.10]. Stress granules were counted in the arsenite-treated samples based on co-localization of BRF2 with eIF3. All the three constructs localized to stress granules, but with slightly different efficiencies. Stress granule localization of BRF2 was rather weak, and a careful observation was needed to ensure co-localization with eIF3. As seen in the graphs, BRF2wildtype, BRF2-AA, and BRF2-PP showed co-localization with stress granules in 72%, 85%, and 98% of the transfected cells, respectively.

Finally, for each transfected cell that was analysed, cellular localization was categorized as nuclear (N), cytoplasmic (C), or as nuclear + cytoplasmic (N/C, where traces of HA-BRF2 could be seen in the nucleus, but the overall abundance remained in the cytoplasm). Figure 3.11: Panel A consists of a summarizing graph of the localization studies upon induction of stress or without it. On careful observation and quantification, I noticed a that BRF2-AA and BFR2-PP showed higher nuclear presence, but a majority of the protein continued to remain in the cytoplasm in untreated conditions. In arsenite-induced stress, BRF2 wildtype seemed to show a slight decrease in the nuclear fraction. Such a change was not observed for the mutants. Phillips et al. [182] reported nucleo-cytoplasmic shuttling of BFR2. I extended this study to include the mutants of BFR2 [Figure 3.11: Panel B]. Transfected cells were exposed to Leptomycin B (10 ng/ml, 2 hrs) which is a drug that binds to CRM-1 and prevents proteins with an active nuclear export signal from being exported to the cytoplasm [247]. In the IF experiments performed, I observed a strong nuclear signal excluding the nucleolus for all three constructs of BRF2 with negligible

amounts in the cytoplasm, indicating that BRF2 indeed shuttles between the nucleus and the cytoplasm .

To summarize, there was no significant effect of the mutations on the P-body localization of the BRF2 protein in its nucleo-cytoplasmic shuttling. Stress granule localization appeared to increase in the BRF2 mutants as compared to that in wildtype BRF2. However, this result needs to be treated with caution. Firstly, the mutants seemed to show lesser expression. Secondly, due to a slight increase in the nuclear localization, the cytoplasm could appear more clarified and makes stress granules more easily visible.

3.4 DISCUSSION

BRF2 interacts with 14-3-3: I can confidently conclude from my experiments that BRF2 binds to 14-3-3 protein. Simultaneous S123A and S257A mutations abrogated the interaction between BRF2 and 14-3-3, since the mutated sequences on BRF2 no longer conformed to the consensus binding sequences of 14-3-3 [215, 216, 217]. It should be noted that individual mutations of these sites did not hamper binding of BRF2 with 14-3-3. In many cases 14-3-3 is known to bind as a dimer to two distinct residues of target proteins. Therefore, binding is abrogated when both the binding sites for 14-3-3 in the interacting proteins are simultaneously abolished. This has been exemplified in the TTP family of proteins [194, 211] as well as other interactors of 14-3-3, for example, DAF-16, the forkhead transcription factor [248]. Looking at the story from the side of 14-3-3, it seems probable that 14-3-3 is active as a dimer and each monomer binds to one site in the target protein. To analyse this, Powell et al. [249] carried out a study which proved that 14-3-3 zeta was active only as a dimer. A chemoattractant formyl-methionyl-leucyl-phenylalanine (fMLP) stimulated the p38-MAPK pathway in neutrophils. Upon stimulation, 14-3-3 zeta was found to a target of MK2. MK2 phosphorylates S58 which lies on the dimer-formation interface of 14-3-3 zeta. Phosphorylation of this S58 or a phosphorylation-mimic mutation S58D prevents 14-3-3 dimer formation. The thus-monomeric 14-3-3 is also incapable of binding to Raf-1, a known target of 14-3-3, suggesting that dimer formation could be a pre-requisite for binding to target ligands.

It is known that 14-3-3 isoforms homo-/hetero-dimerize while binding to target proteins. In the co-IP assays of this study, I could see two closely-migrating bands corresponding to 14-3-3. The higher molecular weight form could be 14-3-3 epsilon, although it needs to be proved by using isoform-specific antibodies. This could mean that at least two 14-3-3 isoforms are involved in binding to BRF2. However, this finding needs to be treated with caution. Rittinger

et al. [217] performed elegant *in vitro* experiments which brought to light the fact that isoform-specificity might be possible only in intact cells. They incubated lysates of PC12 and 3T3/L1 cells with GST-tagged baits of seven 14-3-3 isoforms. A-raf, B-raf, c-Raf-1, BAD, and IRS-1 proteins, which exhibit well-defined isoform specificity, were chosen as ligands. It was found that in lysates the ligands lost their specificity towards 14-3-3 isoforms and all the ligands bound to all 14-3-3 isoforms *in vitro*. The sole exception was B-raf which failed to bind to 14-3-3 sigma and tau. This indicates that isoform specificity *in vivo* might depend on cellular localization or transcriptional / translational regulation of the isoforms. Thus, the two types of isoforms pulled down in my experiments could well be a result of isoform non-specificity post lysis of cells.

S123,257A mutations do not affect AMD efficiency of BRF2: In several experiments, I noticed that BRF2-AA was expressed in lower amounts than the wildtype BRF2 inspite of equal amounts of plasmid DNA being transfected. This might indicate that the stability of the BRF2-AA mutant is different. I performed cycloheximide chase assays to analyse this. Cycloheximide inhibits protein synthesis in the cell, thus the 0-hr timepoint is a reflection of the steady-state levels for any protein inside the cell. Time-points collected at 3-hr intervals over the next 9 hrs did not show any distinct difference in the stability of the two proteins (data not shown). Subsequently, I tested various setups in which I transfected a fixed amount of BRF2 wildtype plasmid and compared it to different amounts of BRF2-AA plasmid (data not shown). Based on these experiments, I chose that DNA amounts that gave similar expression levels of BRF2 wildtype and the mutant.

The long-standing idea was that 14-3-3 binds to the TTP family members and inhibits their AMD capacity as was proven for TTP and BRF1. Hence, mutants of TTP and BRF1 to which 14-3-3 failed to bind showed higher AMD activity. However, my results stand in contradiction to this idea. In the given experimental conditions, 14-3-3 binding did not alter AMD efficiency of BRF2. In doxycycline-chase mRNA decay assays, it was seen that BRF2 wildtype and its 14-3-3 binding site mutants degrade ARE-containing reporter mRNA with comparable efficiencies in .

This is similar to the study by Marchese et al. [196] which spoke against involvement of 14-3-3 in controlling TTP-induced deadenylation. The authors carried out *in vitro* deadenaylation assays that included wildtype TTP or its mutant TTP-S52,178A which does not bind to 14-3-3. The results obtained clearly showed that the rates of TTP-induced deadenylation were different for both the constructs of TTP. This difference was dependent on phosphorylation of TTP at S52 and S178; however, independent of 14-3-3 binding. The same was further confirmed by using R18 and dipofein which are high affinity 14-3-3

antagonists that cause nearly complete inhibition of 14-3-3 binding to target proteins. In *in vitro* assays, the deadenylation activity of TTP was unchanged in the presence of these 14-3-3 inhibitors confirming that 14-3-3 did not play a role in inhibition of TTP-induced deadenylation. Eventually the inhibition was attributed to MK2 kinase which phosphorylates TTP and hampers recruitment of the Caf1a deadenylase. However, a caveat is that these data were based on *in vitro* deadenaylation assays carried out over a period of only the initial 30 mins. This approach could miss the later events in the degradation process. Stoecklin et al. [194] had claimed the contrary that 14-3-3 takes an active part in inhibiting AMD activity of TTP and these assays monitored ARE-mRNA decay inside cells. As for BFR1, overexpression of active forms of PKBα kinase [211] and MK2 kinase [233] have been shown to increase 14-3-3 binding and inhibit ARE-mRNA degradation. In conclusion, my study testifies that in the given experimental conditions, AMD activity of BRF2 is regulated differently than the other TTP family members.

Since all experiments in my study are performed in either HEK293 or HeLa cells, they could miss out on some cell-type specific cues. Earlier reports have established that 14-3-3 isoforms can be cell-type specific e.g. 14-3-3 eta forms with two different 5' UTRs which is expressed in hematopoietic cells [250], 14-3-3 sigma which is expressed only on DNA damage in a p53-dependent manner to bring about cell-cycle arrest [251]. Coincidentally, both the above examples cited would be of future interest in this project, since BRF2 is involved in hematopoietic development [235] and over-expression of BRF2 activates the DNA damage response and apoptosis in a p53-dependent manner [252]. The experiments in this study could be repeated in cells of hematopoietic origin.

BRF2 readily localizes to P bodies and to stress granules induced by oxidative stress: For this part of the study, I purposefully chose cells which expressed low to medium levels of transfected BRF2, since the cells expressing high amounts of the protein had a stretched-out appearance resembling apoptotic cells. Moreover, high signal intensities made it difficult to observe co-localization. I noticed a difference between BFR2 and other TTP family members with regard to P-body and stress granule localization. Franks et al. [193] saw that only 13% of cells transfected with TTP showed presence of TTP in P bodies. On knockdown of Xrn1 i.e. when ARE-mRNA degradation is halted midway, presence of TTP in P bodies drastically increased to 90%. This could indicate that TTP localizes to P bodies only transiently. The same study claimed that BRF1 showed a similar effect. My study proved that BRF2 spontaneously localized to P bodies in 86% cells transfected with BRF2. For the 14-3-3 binding mutants of BRF2, these values were >90%. The difference in P-body localization could be attributed to a poly-Q stretch present in the C-terminus of BFR2, something that is absent in both TTP and BRF1. Poly Q/N stretches are a feature common to many P-body proteins, and out of

twenty P-body proteins analysed, all were shown to have significantly above-average Q/N contents. These stretches have been suggested to aid aggregation of these proteins [99]. Whether P-body localization of BRF2 is prompted by the Q-rich domain can be proved by employing a deletion mutant of BRF2 lacking the Q repeats.

As for stress granule localization, Stoeckin et al. demonstrated that MK2-induced TTP:14-3-3 complexes failed to localize to the stress granules. TTP and its 14-3-3 binding mutant were recruited to arsenite-induced stress granules at different efficiencies (TTPwt, 0.5%; TTP-S52,178A, 59%). It was concluded that binding to 14-3-3 prevents localization of TTP to stress granules [194]. Contrary to these observations, I found that BRF2 wildtype and its 14-3-3 binding mutants readily localized to arsenite-induced stress granules. In fact, BRF2-AA and BRF2-PP mutants showed slightly increased localization to oxidative stress-induced stress granules.

14-3-3 affects nucleo-cytoplasmic localization of BRF2 minimally: In my studies, I observed that on exposure to oxidative stress, the slight presence of BRF2 in the nucleus decreased further, indicating export of BRF2 to the cytoplasm. Such a nucleo-cytoplasmic shift was not distinctly seen for BRF2-AA and BRF2-PP. 14-3-3 binding has been shown to alter the cellular localization of target proteins (reviewed in [253]). In a more specific example, 14-3-3 binding causes TTP to shift to the cytoplasm. This is thought to facilitate engaging in AMD which is a cytoplasmic process [213]. In BRF2, now knowing the location of the 14-3-3 binding sites, it is possible that binding to 14-3-3 could mask the NLS which is located in the zinc finger region, and thus promote cytoplasmic localization of the protein. By this logic, mutants that fail to bind to 14-3-3 would have an exposed NLS and hence would show their presence in the nucleus as well, which is seen in my study. On stress induction, increase in 14-3-3 binding to BRF2 possibly causes masking of NLS of BRF2, and 14-3-3 dependent export to the cytoplasm. However, if 14-3-3 binding was the sole determinant of cytoplasmic localization, the mutants which fail to bind to 14-3-3 would show a strong nuclear and minimal cytoplasmic localization which was not observed here. Some more deciding factors for the cytoplasmic localization of BRF2 could be the NES in its C-terminus or interacting proteins of BRF2.

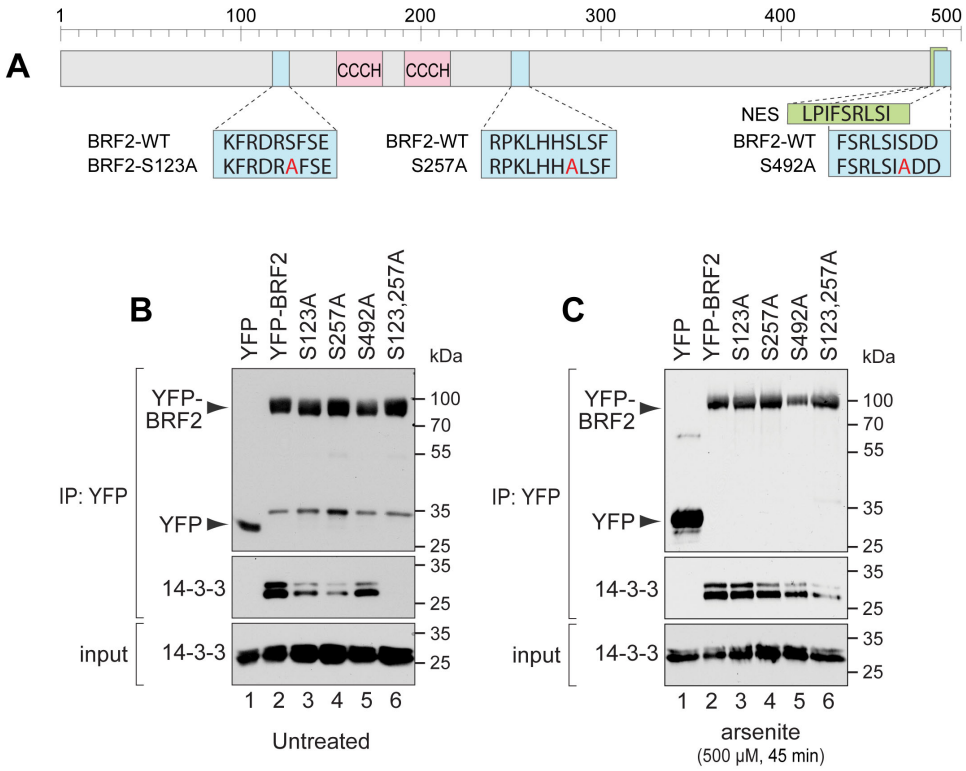

Figure 3.4: BRF2-S123,257A mutant shows reduced binding to 14-3-3. Panel **A**: Summary of mutations affecting putative 14-3-3 binding sites in BRF2 used in this study. Panels **B** and **C**: HEK293 cells were transiently transfected with plasmids expressing YFP-BRF2 wildtype or YFP-tagged 14-3-3 binding site mutants of BRF2. YFP-only is included as a control. Cytoplasmic lysates were prepared 24 hrs after transfection. Panel **B**: Untreated samples. Panel **C**: Transfected cells treated with 500 µM arsenite for 45 mins before final lysis. Lysis buffer included inhibitors to proteases and phosphatases. Co-IP experiments were performed as mentioned previously in Figure 3.2 legend.

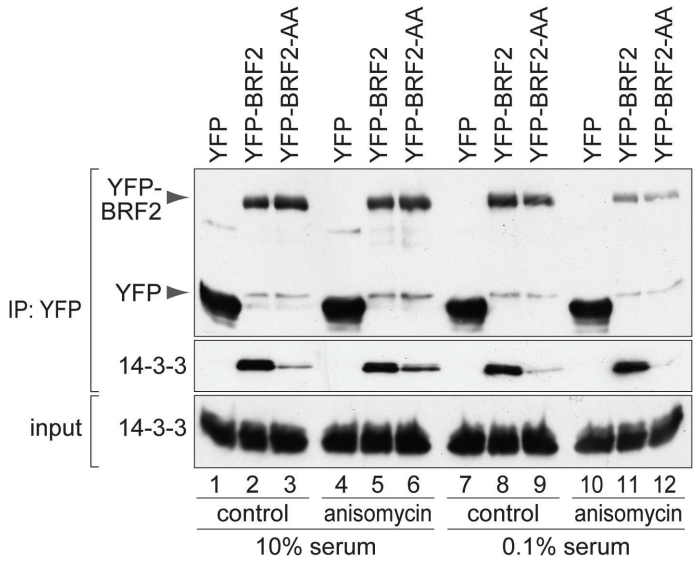

Figure 3.5: BRF2-AA mutant shows reduced binding to 14-3-3 in presence of serum and anisomycin. HEK293 cells were transiently transfected with plasmids encoding YFP-only, YFP-BRF2, or YFP-BRF2-AA as indicated in the figure. Cytoplasmic lysates were prepared 24 hrs after transfection. Before lysis, four combinations of treatments were performed. the treatments were as follows, Lanes 1-3: no serum starvation, no anisomycin; Lanes 4-6: no serum starvation, anisomycin; Lanes 7-9: serum starvation, no anisomycin, and Lanes 10-12: serum starvation, anisomycin. Co-IP experiments were performed as mentioned previously in Figure 3.2 legend.

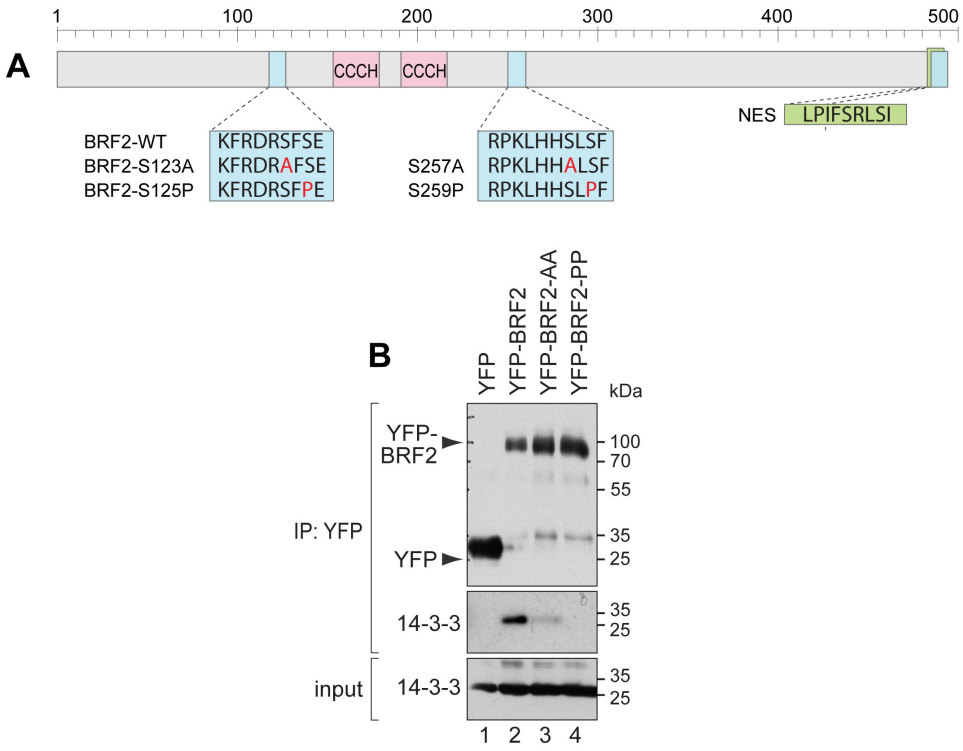

Figure 3.6: BRF2-S125,259P mutant shows reduced binding to 14-3-3. Panel **A**: BRF2-S125,259A mutant. Panel **B**: HEK293 cells were transiently transfected with plasmids encoding YFP-only, YFP-BRF2, YFP-BRF2-AA, or YFP-BRF2-PP, as indicated in the figure. Cytoplasmic lysates were prepared 24 hrs after transfection. Co-IP experiments were performed as mentioned previously in Figure 3.2 legend.

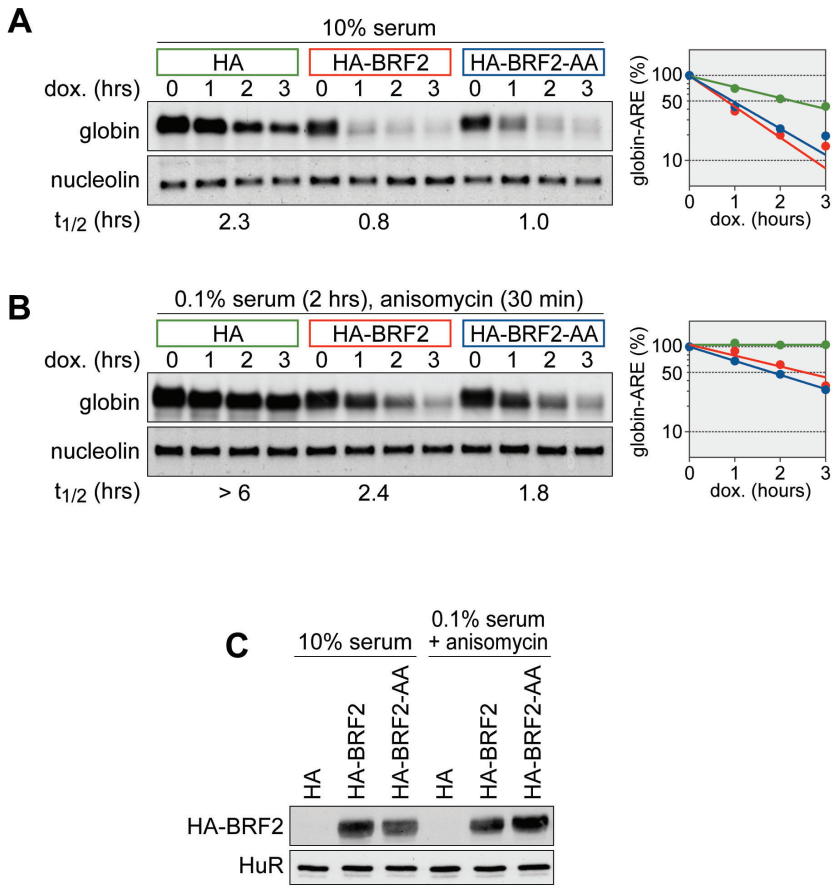

Figure 3.7: AMD efficiency of BRF2-AA mutant as compared to BRF2 wild-type. A Tet-off system was employed. HeLa cells were transfected with empty-vector, or plasmids encoding HA-BRF2, or HA-BRF2-AA as indicated in the figure. Panel **A**: Favourable growth conditions (DMEM + 10% FCS). Panel **B**: serum starvation (DMEM + 0.1% FCS, 2 hrs) and anisomycin treatment (10 µg/ml, 30 mins) before the 0-hr time-points of the doxycycline -chase mRNA decay assays which were performed over a period of 3 hrs. Northern blotting RNA probes used were specific for ß-globin reporter gene and nucleolin as loading control. Reporter mRNA levels were normalized to nucleolin mRNA levels. 0-hr timepoint which represents steady state levels of reporter mRNA was set to 100% and the other values were compared to that. mRNA levels plotted on the graph and the half-lives are a mean ± s.e.m. of three independent biological repeats. Panel **C**: Samples of transfected cells were processed by western blotting and probed with mouse monoclonal anti-HA antibody to detect BRF2 protein.

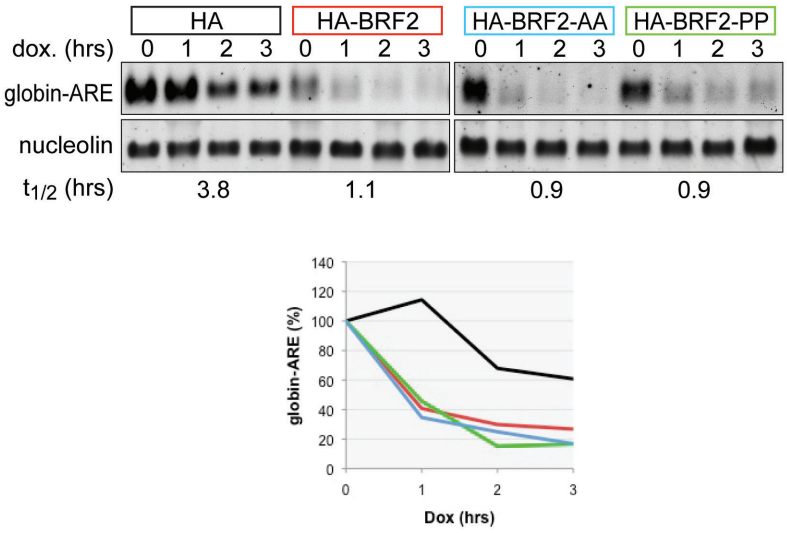

Figure 3.8: BRF2-PP mutant degrades ARE-containing mRNAs with equal efficiency as wildtype BRF2. A Tet-off system was employed. HeLa cells were transfected with empty-vector, or plasmids encoding HA-BRF2, HA-BRF2-AA, or HA-BRF2-PP as indicated in the figure. doxycycline -chase mRNA decay assays were performed over a period of 3 hrs. Northern blotting was carried out as mentioned in Figure 3.7 legend.

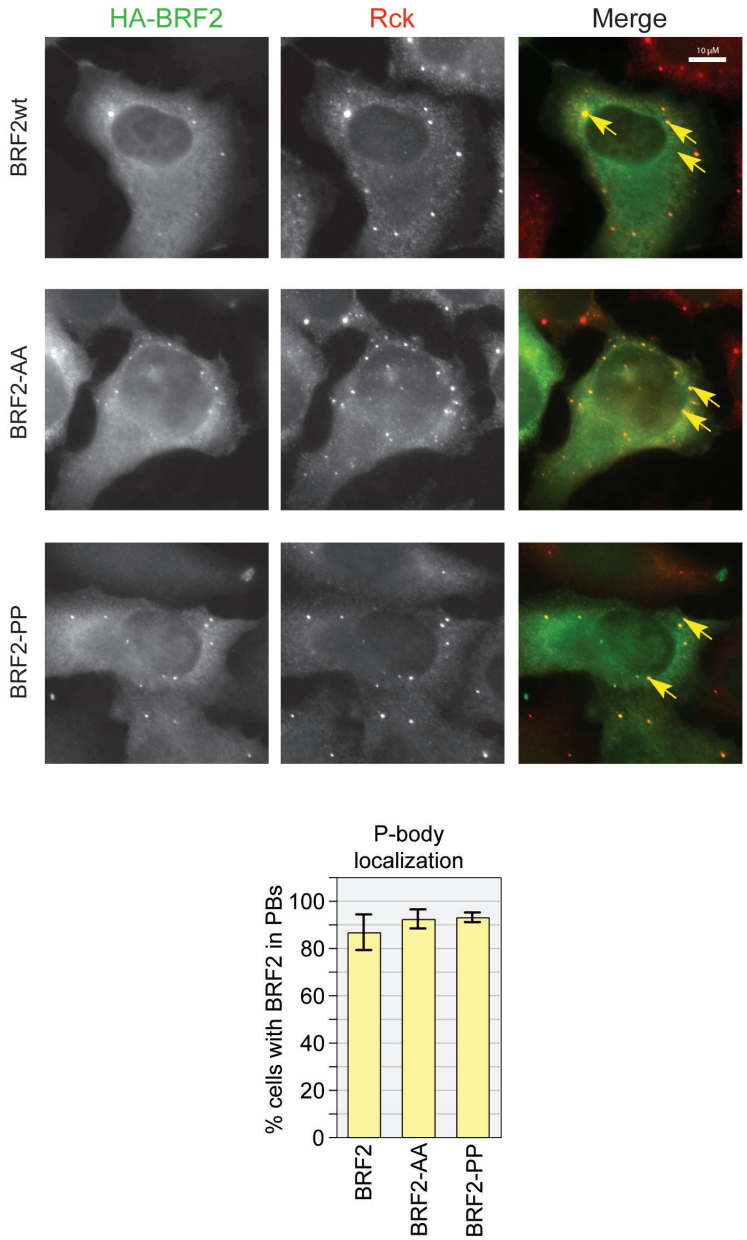

Figure 3.9: BRF2 wildtype and its 14-3-3 binding site mutants localize to P bodies at comparable efficiencies. HeLa cells were transfected with plasmids encoding HA-BRF2 wildtype, HA-BRF2-AA, or HA-BRF2-PP. Cells were stained with mouse monoclonal anti-HA antibody to visualise BRF2 protein, and were co-stained for Rck protein, a P body marker. The graph depicts percentage of transfected cells in which BRF2 and its mutants were recruited to P bodies.

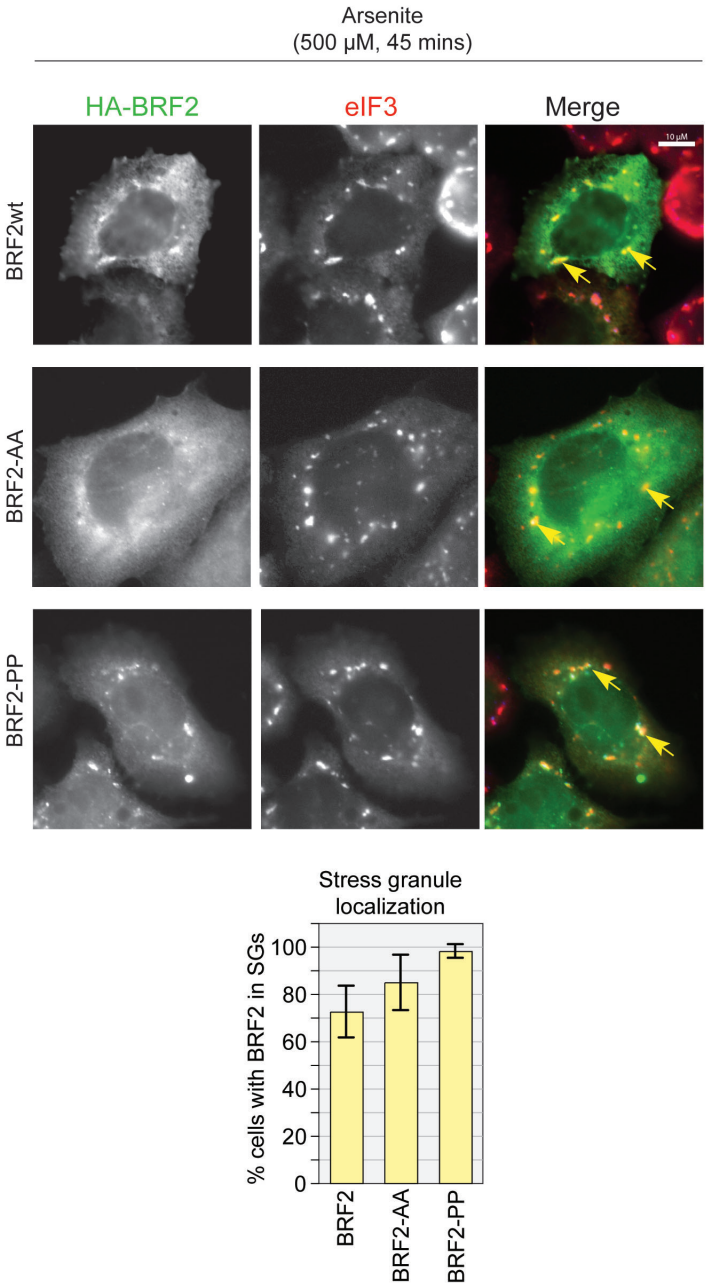

Figure 3.10: BRF2 wildtype and its 14-3-3 binding site mutants localize to oxidative stress-induced stress granules at varying efficiencies. HeLa cells were transfected with plasmids encoding HA-BRF2 wildtype, HA-BRF2-AA, or HA-BRF2-PP. Cells were exposed to oxidative stess (500 µM arsenite, 45 mins) prior to fixing, stained with mouse monoclonal anti-HA antibody to visualise BRF2 protein, and co-stained for eIF3 protein, a marker for oxidative stress-induced stress granules. The graph depicts percentage of transfected cells in which BRF2 and its mutants were recruited to stress granules.

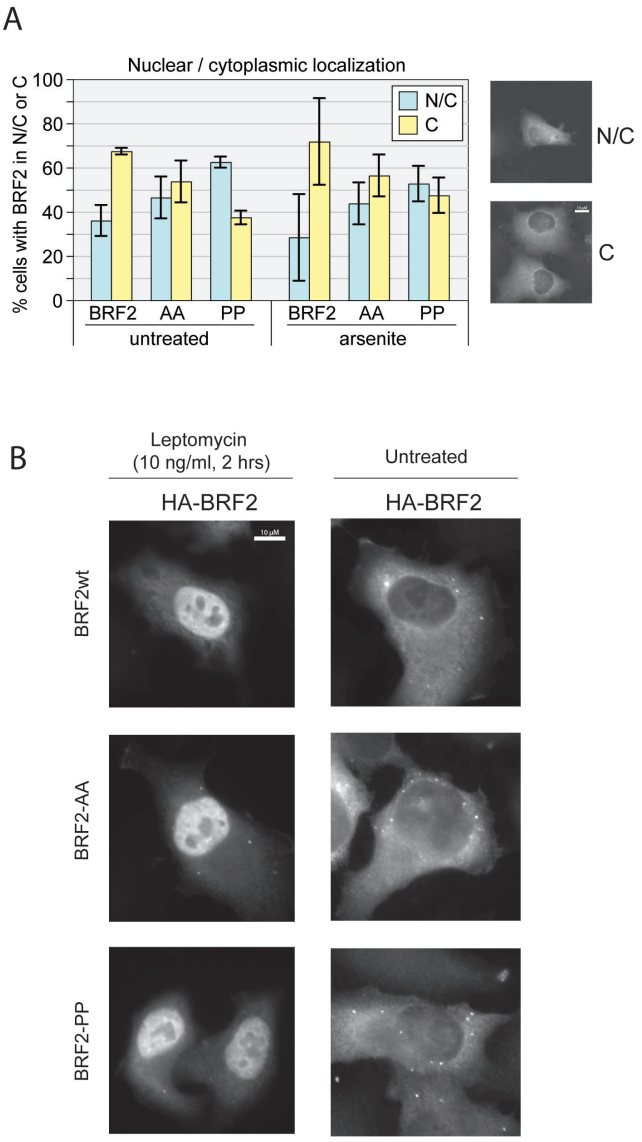

Figure 3.11: Cellular localization of BRF2 wildtype and its 14-3-3 binding site mutants. HeLa cells were transfected with plasmids encoding HA-BRF2 wildtype, HA-BRF2-AA, or HA-BRF2-PP. Cells were stained with mouse monoclonal anti-HA antibody to visualise BRF2 protein in samples in all the panels below. Panel **A**: For each transfected cell that was observed, cellular localization was categorized as nuclear (N), cytoplasmic (C), or as nuclear + cytoplasmic (N/C, where traces of protein could be seen in the nucleus, but overall abundance remained in the cytoplasm). Graph depicts percentage of transfected cells showing BRF2 localization as N or N/C in untreated or arsenite-treated samples. IF images of examples of C and N/C localization are included for reference. Panel **B**: Cells were exposed to Leptomycin B (10 ng/ml, 2 hrs) prior to fixing. Images from corresponding untreated cells are reproduced from Figure 3.9.

4 Kinase(s) involved in phosphorylating BRF2

In the previous co-IP experiments, I demonstrated that the phosphorylation status at S123 and S257 of BRF2 determines its binding to 14-3-3. The kinase(s) involved in BRF2 phosphorylation are as yet unknown. The results of the previous experiments indicated that I should screen kinases which would target phospho-serines in the BRF2 sequence. I analysed the BRF2 protein sequence (P47974 from UniProtKB/Swiss-Prot database) using the Phospho-Motif Finder database published in [254]. The sequence was queried against the known substrate sequence motifs for various protein serine/threonine kinases which led to a list of >300 substrate sequence motifs in BRF2. These results included a significant number of redundant hits. I next used the PhosphoNET database (PhosphoNET is an online open-access resource developed by Kinexus Bioinformatics Corporation, Canada) which still predicted >30 possible phosphoserines in BRF2 and multiple kinases corresponding to each serine-containing sequence stretch.

4.1 PKBα and MK2 kinases may affect BRF2 binding to 14-3-3

Since the number of prospective kinases was overwhelming, I decided to follow an approach of analogy between BRF2 and other members of the TTP family of proteins, namely, BRF1 and TTP. It is known from the literature that 14-3-3 binding sites of TTP are phosphorylated by MK2 kinase [194] and those of BRF1 by the kinases PKBα [232] and MK2 [233]. With this, I proceeded with checking the effect of these two enzymes first. Constitutively-active forms and inactive forms of PKBα and MK2 kinases were co-transfected during co-IP experiments. The idea was to alter the levels of phosphorylation of over-expressed BRF2 proteins by co-overexpressing active/inactive forms of the kinases. If these kinases were involved in the process, active forms of the kinase should enhance BRF2 phosphorylation and 14-3-3 binding. The inactive forms should compete with their endogenous active counterparts and

reduce BRF2 phosphorylation and 14-3-3 binding. If the kinases were not involved, the extent of 14-3-3 binding would remain unaltered. The modified co-IP protocol included serum starvation (DMEM + 0.1% FCS, different durations ranging from 6-24 hrs were tried). Serum starvation was used to ensure downregulation of kinase signalling to bring down the steady-state phosphorylation levels inside the cell. The activity of the studied kinases would thus be monitored without interference from other kinases. No difference in BRF2:14-3-3 binding was observed between normal growth conditions and conditions of serum starvation.

As seen in Figure 4.1, YFP-BRF2 is over-expressed in all sets except the empty-vector control. Co-IP experiments were carried out using GFP-binder beads as described before. Additionally, input fractions were probed with anti-MK2 antibody to ensure that equal amounts of active and inactive MK2 was expressed. When compared with the levels of 14-3-3 pulled down by YFP-BRF2 alone (Lane 2), the following observations were made. a) Lane 3: YFP-BRF2 + MK2-T205,317E (constitutively active mutant of MK2, henceforth termed as MK2-EE) pulls down more 14-3-3, b) Lane 4 : YFP-BRF2 + MK2-K76R (kinase-dead mutant of MK2, henceforth termed as MK2-KR) pulled down reduced amounts 14-3-3, c) Lane 6: YFP-BRF2 + m/p PKBα (constitutively active mutant of PKBα, henceforth termed as PKB) pulled down less 14-3-3, and d) Lane 7 : YFP-BRF2 + PKBα-K179A (inactive mutant of PKBα, henceforth termed as PKBα-KA) pulls down reduced amounts 14-3-3. These data suggest that MK2 is involved in phosphorylating BRF2, hence the inactive kinase reduces BRF2 phosphorylation and impedes its binding with 14-3-3. In the case of active PKBα, lesser 14-3-3 appears to be pulled down; however, the amount of precipitated YFP-BRF2 is also lower than in other lanes. Thus the effect of PKBα on BRF2 was not conclusive. Lanes 5 and 8 involved chemical inhibitors of the p38 and PI3K pathways, respectively, and will be discussed in the next section.

4.2 Effect of inhibitors of the PKB and MK2 kinase pathways

In the previous experiment, I saw that PKB and MK2 both might be involved in phosphorylating BRF2. This strategy was prone to artifacts of over-expression. An alternative test would be to suppress the activity of these kinases by addition of specific chemical inhibitors. I made use of inhibitors to kinases that are upstream to MK2 and PKBα. I hence attempted to inhibit PKB using Wortmanin which inhibits the upstream PI-3Kinase [255], and MK2 using SB202190 which inhibits the upstream p38 kinase [256].

Preliminary experiments involving these inhibitors were performed in normal growth conditions or under serum starvation and showed no difference in 14-3-3 binding to BRF2 [Figure 4.1: Lanes 4,8, and data not shown]. Henceforth, I treated the cells with anisomycin to additionally activate the stress response, increase the requirement for stress-responsive kinases, so that the cells would respond to the inhibitors more drastically. If the PKBα or MK2 kinase was essential for BRF2 phosphorylation, the corresponding inhibitor would cause a reduction in BRF2 phosphorylation and reduce 14-3-3 binding to BRF2. In this experiment, I also included a set where I used both inhibitors together to achieve a tighter inhibition of BRF2 phosphorylation in case both the kinases were redundant in action.

Figure 4.2 depicts the effect of the inhibitors in combination with anisomycin treatment. The presence of inhibitors did not cause any reduction in BRF2 binding to 14-3-3 (Lane 3 for p38 inhibitor, Lane 4 for PI3-K inhibitor, Lane 5 for both inhibitors in unison). Here it was important to confirm whether the inhibitors had worked. The levels of active PKB were checked by using antibodies against phospho-PKB kinase, which did not work due to technical problems in western blotting experiments. I checked for levels of active MK2 by probing the input fractions with a anti-phosphoT334-MK2 antibody. All the lanes, including the ones with SB202190 inhibitor, had the same levels of active MK2 kinase, shown by phosphorylation of T334 residue of MK2, which is a site phosphorylated by p38 kinase. This suggests that either the inhibitor to p38 kinase had not worked hence the MK2 kinase was still being phosphorylated or the inhibitor was not being taken up by the cells. I decided to follow the more direct and specific siRNA approach to silence the kinases.

4.3 Effect of siRNA-mediated knockdown of MK2

Co-expression of both active and inactive forms of PKBα kinase disturbed the expression of BRF2 and BRF2 levels were mostly decreased compared to those in the other sets. This made interpretation of the experiments very difficult. In the experiments hereforth, I focussed first on MK2 kinase. I used a siRNA against MK2 kinase, as mentioned in [214]. As seen in Figure 4.3: Panel B, I transfected siRNA-MK2 twice over a period of four days. siRNA-D0 was included in the experiment as a control. siRNA-MK2 effectively reduced the levels of MK2 to 22.4 % (Panel B, Lane 2). However, samples in all lanes had the almost equal levels of activated MK2, shown by phosphorylation of T334 residue of MK2, which is a site phosphorylated by p38 kinase Figure 4.3: Lanes 1-4.

The downregulation of MK2 failed to cause any alteration in 14-3-3 binding to BRF2 (Panel A, Lane 2) compared to that in presence of control siRNA-D0

(Panel A, Lane 4). One reason for this could be that the remaining level of MK2 is sufficient for phosphorylating the BRF2 present in the cell. Moreover, downregulation of MK2 kinase might be compensated by other kinases in the cell. In conclusion, the inhibitor studies and the siRNA knockdown of MK2 failed to confirm that MK2 kinase plays a role in BRF2 phosphorylation.

4.4 MK2 does not alter AMD-efficiency of BRF2

The final goal of studying involvement of MK2 in phosphorylating BRF2 was to know if BRF2 phosphorylation and binding to 14-3-3 alters the AMD efficiency of BRF2. I hence performed mRNA decay assays using globin-ARE reporter mRNA in the presence of BRF2 and co-expressed MK2-EE or MK2-KR. Serum starvation conditions (DMEM + 0.1% FCS, 12 hrs) were used to downregulate basal kinases activity and ensure that the effect seen, if any, was due to the over-expressed MK2 kinase versions.

I performed two sets of doxycycline -chase mRNA decay experiments as seen in Figure 4.4. Sets seen in Panel A were performed under normal growth conditions, and those in Panel B under serum starvation conditions. In each set, globin-ARE mRNA decay in the presence of BRF2 plus empty vector was taken as a reference. I found that there was no detectable effect of over-expression of MK2 kinase active or inactive forms on AMD brought about by BRF2, since the reporter mRNA half-lives in presence of BFR2 + MK2-EE or BFR2 + MK2-KR were similar to those in presence of BRF2 alone. Values from three independent biological repeats of this experiment were compiled and plotted in the graphs beside the northern blots and the half-lives are given as mean ± s.e.m. Panel C shows a western blot to ensure equal expression of the two MK2 forms.

4.5 DISCUSSION

p38 MAP kinase and activated downstream kinases have been shown to antagonize AMD and stabilize ARE-containing mRNA. mRNAs of IL-6 and IL-8 are stabilized by MEKK-1, and that of IL-8 by MK2 [257]. MK2 controls TNFα and IL-6 biosynthesis albeit by different mechanisms [203, 204]. Kinases affect stability of mRNAs indirectly via control of RNA binding proteins. PKB [211] and MK2 [233] are known to independently control AMD efficiency of BRF1. MK2 also determines the stability of TNFα mRNA via modulation of the expression and activity of TTP [202].

I could consistently see in co-IP experiments that co-expressing MK2-KR reduced binding of 14-3-3 to BRF2, while co-expressing MK2-EE showed more

or less equal levels of 14-3-3 binding to BRF2 in comparison to the BRF2-only transfected controls [Figure 4.1]. Drawing analogy with other TTP family members, I hypothesized that MK2-EE over-expression would hyper-phosphorylate BRF2, enhance 14-3-3 binding, and cause a concommitant decrease in the AMD efficiency of BRF2. To this end, I checked if over-expression of the MK2 active or inactive forms affected the ability of BRF2 to accelerate ß-globin-ARE reporter mRNA degradation. I could see no significant difference in the RNA decay patterns in presence and absence of MK2. This implies that in the given experimental conditions MK2 did not modulate AMD efficiency of BRF2. This was rather contradictory to regulation of other TTP family members by MK2, but nevertheless an important finding of this study.

It is possibile that phosphorylation of a substrate by MK2 may not produce any discernible change in the function of the substrate. One such example is that of a structural protein, Vimentin, which is involved in intermediate filament assembly [258]. Vimentin is a substrate for multiple kinases and in most cases phosphorylation causes structural changes. However, it was shown that MK2 phosphorylated recombinant Vimentin protein on residues S38, S50, S55, and S82 but this did not produce any drastic structural changes. Vimentin maintained its filament-forming activity despite being phosphorylated by MK2, while phosphorylation by protein kinase A (PKA) caused a loss of filament structure [259].

One more observation was that the MK2 active and inactive mutants produced the same effect with regard to ß-globin-ARE mRNA degradation. The mutants of MK2 used are the constitutively active mutant, MK2-T205,317E; and the kinase-dead mutant, MK2-K76R. In the active MK2 form, the two given threonines are mutated to glutamate to mimic the negative charge of phosphates otherwise needed to activate MK2 [260]. The inactive form, MK2-K76R, involves a mutation of the conserved lysine in the ATP-binding subdomain II to arginine. This confers upon it the qualities of a kinase-dead negative interfering mutant [257]. In the ideal situation, the mutant lacking kinase activity should translate into some difference in activity between the two MK2 forms. The reasons for both the mutants behaving in a similar fashion with regard to ß-globin-ARE mRNA degradation could be: a) 14-3-3 acts as a scaffold protein between BRF2 and MK2, and MK2 acts merely as a platform onto which further complexes load/are prevented from loading, b) formation of BRF2/14-3-3/MK2 complex does not hinder downstream mRNA degradation processes, e.g. blocking of Caf1a recruitment, as shown for TTP in [196] because binding regions for different complexes are mutually exclusive. Both of the above could need only the physical presence of MK2, irrespective of its catalytic activity. Alternatively, c) MK2 may not play any role in regulating BRF2-mediated AMD, but BRF2 phosphorylation might be brought about by a constitutive kinase which performs its function despite the presence of over-expressed MK2

active or inactive forms.

In my study, the only parameter I have questioned so far was AMD efficiency of BRF2. The change brought about in the cell due to BRF2:14-3-3 complex formation might manifest in alternate ways, e.g., MK2 controls TNFα [203] and BRF1 controls VEGF [229] at the level of translation. On the basis of these studies, it could be possible that MK2 action on BRF2 may alter the translation rate of ARE-containing target mRNA.

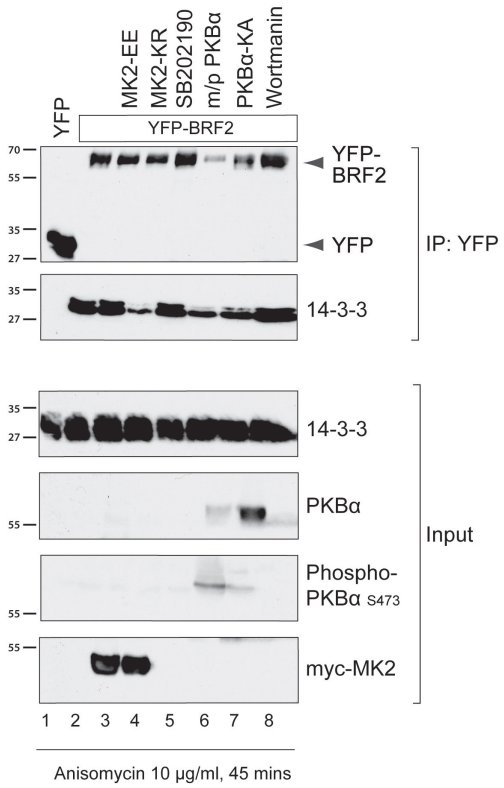

Figure 4.1: MK2 and PKBα kinases may affect 14-3-3 binding to BRF2. HEK293 cells were transiently transfected with plasmids encoding YFP-only, YFP-BRF2, YFP-BRF2+MK2-EE (active), YFP-BRF2+MK2-KR (inactive), YFP-BRF2+m/pPKBα (active), or YFP-BRF2+PKBα-KA (inactive) as indicated in the figure. Cytoplasmic lysates were prepared 24 hrs after transfection. Co-IP experiments were performed as mentioned previously in Figure 3.2 legend. Additionally, the input fractions were probed with anti-myc (MK2) and anti-PKBα antibodies to ensure expression of equal amounts of kinases. Information on inhibitors to kinases in the later section.

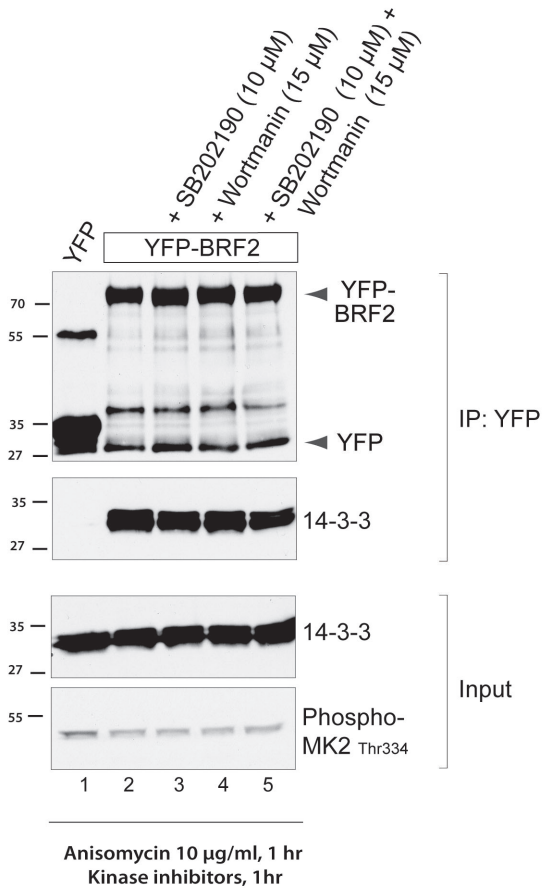

Figure 4.2: Effect of chemical inhibitors to MK2 and PKBα kinase pathways on 14-3-3 binding to BRF2. HEK293 cells were transiently transfected with plasmid encoding YFP-BRF2. 1 hr before lysis, 10 µg/ml anisomycin was added to the medium in combination with inhibitors to MK2 or PKBα kinases: 10 µM SB202190 (p38 MAPK inhibitor) against MK2, 15 µM Wortmanin (PI3-Kinase inhibitor) against PKBα. YFP-only was indcluded as a control. Cytoplasmic lysates were prepared 24 hrs after transfection. Co-IP experiments were performed as mentioned previously in Figure 3.2 legend. Additionally, the input fractions were probed with anti-phosphoMK2-T334, a residue phosphorylated by p38 kinase, to check for the effect of SB202190 inhibitor.

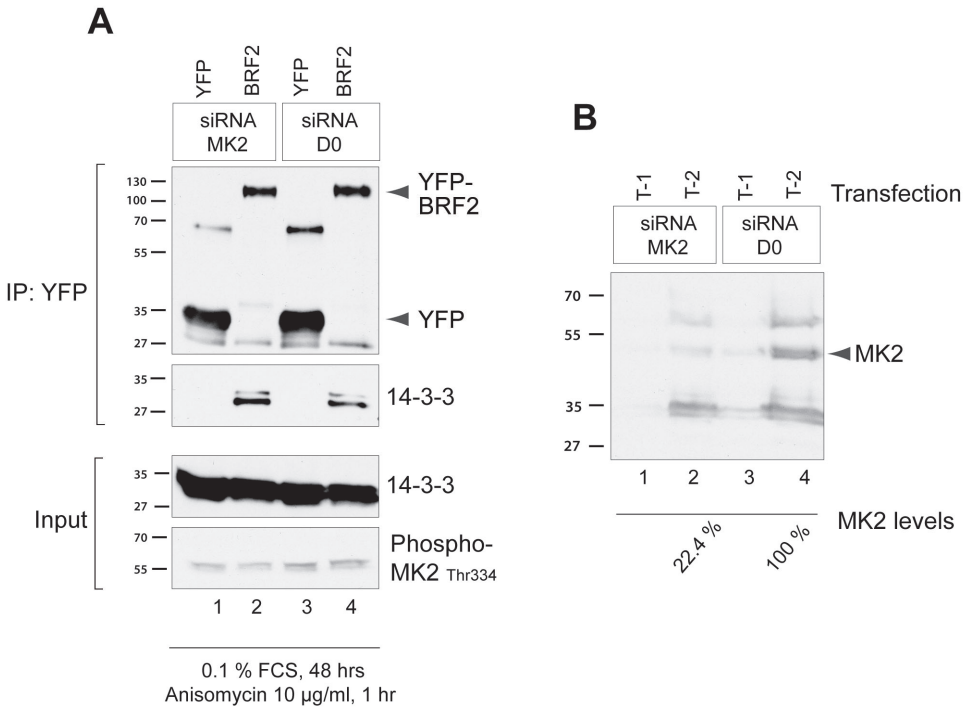

Figure 4.3: siRNA knockdown of MK2 does not have any effect on 14-3-3 binding to BRF2. Panel **A**: Co-IP experiments were carried out after transfecting siRNA-MK2 or siRNA-D0 twice over a period of 4 days. Plasmids encoding YFP-BRF2 or YFP-only control siRNA-MK2 were included in the second transfection. co-IP experiments were performed as mentioned previously. Co-IP experiments were performed as mentioned previously in Figure 3.2 legend. Additionally, the input fractions were probed with anti-phospho MK2-T334 to check for the remainder active form of MK2. Panel **B**: Samples were withdrawn 24 hrs after the first transfection, i.e. Day-2 (T-1), and 24 hrs after the second transfection, i.e. Day 4 (T-2), and subjected to western blotting to determine the efficiency of MK2 knockdown. MK2 levels from the western blot after the second transfection from samples treated with siRNA-MK2 or siRNA-D0 were normalized to an unidentified band each from the ponceau staining.

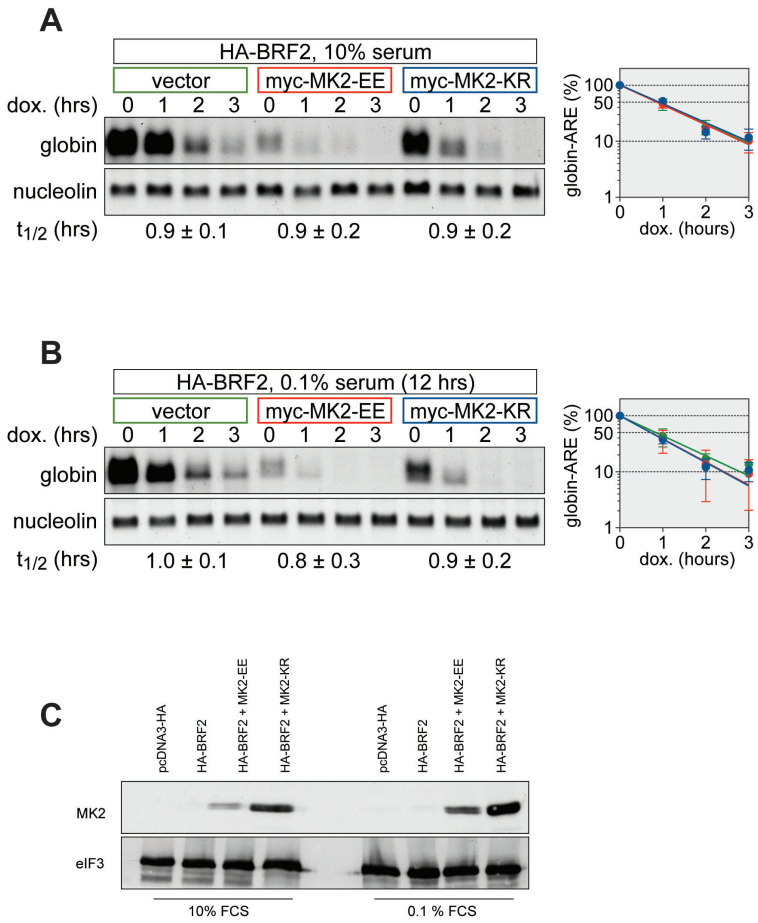

Figure 4.4: MK2 does not modulate AMD efficiency of BRF2. A Tet-off system was employed. HeLa cells were transfected with empty-vector, or plasmids encoding HA-BRF2, HA-BRF2+MK2-EE (active), or HA-BRF2+MK2-KR (inactive) as indicated in the figure. Panel **A**, untreated cells; Panel **B**, cells subjected to serum starvation (DMEM + 0.1% FCS, 12 hrs) before final lysis. doxycycline -chase mRNA decay assays were performed over a period of 3 hrs. Northern blotting and quantification of results was carried out as mentioned in Figure 3.7 legend. Panel **C**: Samples of transfected cells were subjected to western blotting and probed with anti-MK2 antibody.

5 BRF2 interacts with the deadenylation machinery

5.1 BRF2 interacts with Not1 and Caf1a

Having established that phosphorylation of BRF2 and the consequent 14-3-3 binding does not affect the functionality of BRF2 regarding AMD, I decided to explore for additional interactors of BRF2 to reveal other layers of regulation. Previous studies have unearthed links between the deadenylation apparatus and the TTP family members. TTP interacts with Not1, Caf1a via Not1 [198], and Ccr4 [179]. BRF1 was also shown to interact with Not1 (unpublished observation, Heike Sandler) and Ccr4 [179]. Moreover, Lai et al. [197] provided evidence that BRF2 was capable of initiating mRNA deadenylation. Keeping in mind the above findings, I decided to check if BRF2 physically interacts with members of the deadenylation apparatus in the cell.

To this effect, I performed co-IP experiments in HEK293 cells where HA-BRF2 was co-expressed with Not1 or Caf1a. Not1 protein spans 2376 amino acids and has been known to pose problems with regard to over-expression. Having experienced this difficulty myself in the initial experiments, I chose to work with YFP-Not1(aa1330-1601), a fragment of Not1 which is known to interact efficiently with TTP [198]. YFP-tagged versions of the deadenylation machinery components were used as a bait and HA-BRF2 was pulled down employing the GFP-binder approach. As seen in Figure 5.1, HA-BRF2 interacts with Not1 (Lane 2) and Caf1a (Lane 3). This strongly hints at interactions between BRF2 and the deadenylation apparatus.

5.2 DISCUSSION

PolyA tails have enjoyed an important role in AMD. TTP, and to a certain extent BRF1, have been previously studied in terms of their abilities to interact with the cellular deadenylation machinery [201, 179, 261, 198]. The deadenylase PARN has already been shown to play a role in deadenylation of ARE-containing mRNAs in presence of BRF2 [197]. In my study, I tried to

see if BRF2 also interacts with the CCR4-Not complex, the major cytoplasmic deadenylation complex in metazoans. In this multi-component machinery (reviewed in [262, 23]), Not1 is the scaffold protein that holds together multiple components of the deadenylation complex. Not1 interacts with the C-terminus of TTP. Caf1a is recruited to TTP indirectly via Not1 [198]. The domain of interaction in BRF1 is as yet unmapped. A functional TTP-deadenylation complex thus forms which progressively shortens the polyA tail, wherein TTP provides mRNA selectivity. Figure 5.1 shows that BRF2 interacts with the Not1 fragment and Caf1a. Unless the remaining portion of the Not1 acts inhibitory in any way, it seems possible that BRF2 could be the link between the deadenylation machinery and the ARE-containing mRNA which is destined for degradation. This finding needs to be confirmed with more repeats, with full-length Not1, and if possible with the endogenous deadenylating proteins. Moreover, it remains to be determined whether these interactions are direct.

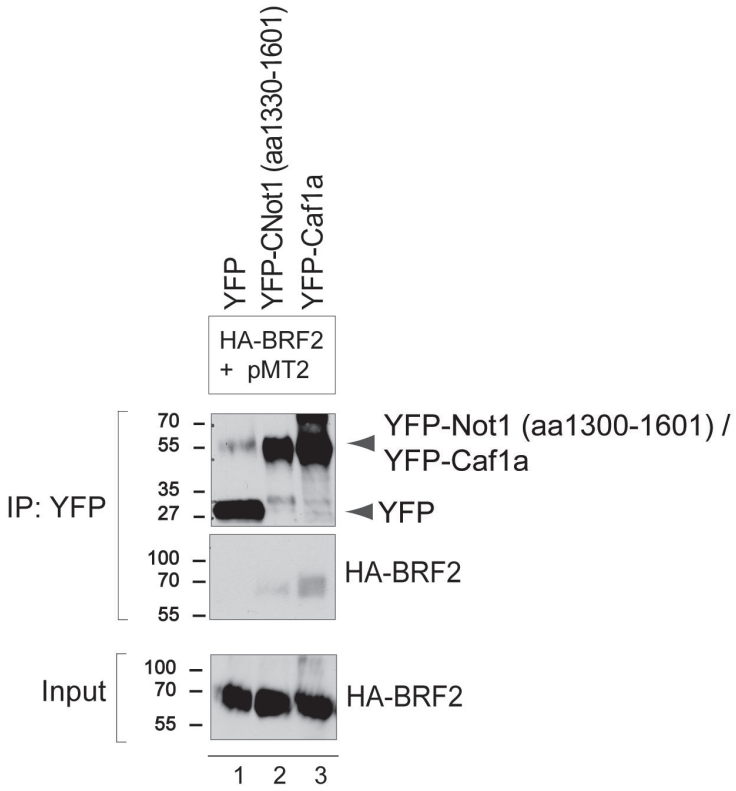

Figure 5.1: BRF2 interacts with the deadenylation machinery. Co-IP experiments were carried out using HEK293 cells where plasmids encoding YFP-Not1 or YFP-Caf1a were transfected along with HA-BRF2. Plasmid pMT2 was co-transfected to improve expression especially of Not1. Cytoplasmic lysates were prepared 24 hrs after transfection. Co-IP experiments were performed as mentioned previously in Figure 3.2 legend. Western blotting analyses were carried out using an anti-GFP antibody to detect the YFP-Not1 and YFP-Caf1a, and a mouse monoclonal anti-HA antibody to detect BRF2.

6 Truncation mutants of BRF2

BRF2 is a relatively new player on the AMD scene and little is known about its functions and domain structure. That BRF2 possesses two C3H-type zinc fingers is well-established [263]. My study suggested the presence of at least two 14-3-3 binding sites. Bioinformatical approaches to predict the domain structure of BRF2 reveal rather limited information. Hence, I created truncation mutants of BRF2 [Figure 6.1] in order to find the minimal active region of BRF2 with regard to AMD and the contribution of other regions in regulating this activity.

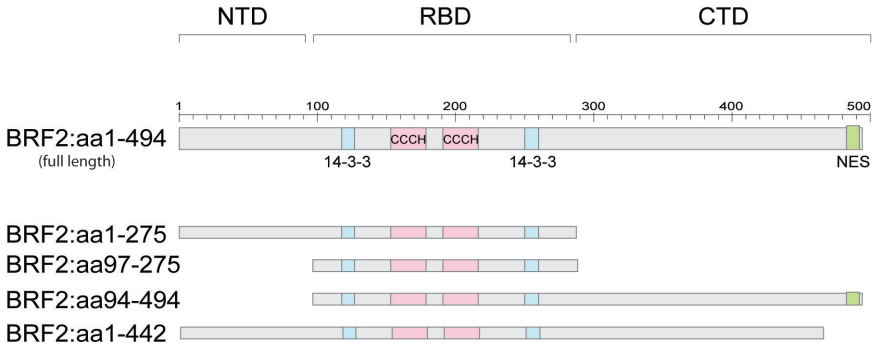

Figure 6.1: Schematic representation of truncation mutants of BRF2. PCR-based cloning was carried out to generate the following truncation mutants: 1) aa1-275 (NTD+RBD), 2) BRF2:aa97-275 (RBD), 3) BRF2:aa97-494 (RBD+CTD), and 4) BRF2:aa97-442 (RBD+CTD lacking the Nuclear export signal, NES).

BRF2 protein can be divided into three domains: 1) the N-terminal domain (NTD), 2) the central domain which consisted of the two 14-3-3 binding sites (this study) and the two $C_8C_5C_3H$ zinc-finger motifs (RBD, RNA-binding domain), and 3) the C-terminal domain (CTD). PCR-based cloning was carried out to generate the following truncation mutants: aa1-275 (NTD+RBD), aa97-275 (RBD), aa97-494 (RBD+CTD), and aa97-442 (RBD+CTD lacking the Nuclear export signal, NES). Of these four clonings, the first two were successful and the remainder two are in progress.

6.1 Cellular localization of truncated versions of BRF2

Immunoflorescence experiments were carried out to check the cellular localization of HA-tagged NTD+RBD and RBD alone. Two sets of cells were processed and the results are as seen in Figure 6.2. The first set of cells (Panel A) were co-stained for the Rck protein, a marker for P bodies. BRF2:aa1-275 bears a predominantly-nuclear localization with low amounts seen in the cytoplasm, whereas BRF2:aa97-275 shows an even stronger nuclear signal with only minimal amounts seen in the cytoplasm. Both forms of BRF2 were recruited to P bodies seen as co-localization with Rck; BRF2:aa97-275 was recruited at a lesser frequency which could be because of the already less amounts present in the cytoplasm. Leptomycin treatment (10 ng/ml, 2 hrs) confined the protein to the nucleus in cases of both the constructs. Cells seen in Panel B were exposed to oxidative stress (500 µM arsenite, 45 mins) to induce stress-granule formation, and co-stained for eIF3 which is a stress granule marker. Under these conditions, BRF2:aa1-275 displayed a striking change in cellular localization. In all the transfected cells observed, the protein shifted from a predominantly-nuclear to a strongly-cytoplasmic localization. Interestingly, BRF2:aa97-275 remained mostly nuclear and there appeared to be a faint signal from the cytoplasm as against full-length BRF2 which is predominantly cytoplasmic. Both these forms of BRF2 were recruited to stress granules seen as co-localization with eIF3. Co-localization with stress granules was more readily visualized in these truncation mutants as compared to that in wildtype due to the highly-clarified cytoplasm. For the sake of comparison, Panel A and B include BRF2 wildtype controls reproduced from Figure 3.9 and Figure 3.10, respectively.

6.2 AMD-efficiency of truncated mutants of BRF2

doxycycline -chase RNA decay assays were performed with the truncated proteins as described in the previous sections. Figure 6.3: Panel A shows the results of the single RNA decay experiment performed till date employing the constructs, BRF2:aa1-275 and BRF2:aa97-275. Similar to the full-length protein, both the constructs were found be capable of accelerating ARE-containing reporter mRNA degradation as seen from the half-lives of the ß-globin-ARE reporter mRNA. Panel B is a graphical representation of northern blots and Panel C is to ensure comparable levels of expression of the constructs.

6.3 DISCUSSION

BRF2:aa1-275 and BRF2:aa97-275 show a predominantly-nuclear localization, as against a cytoplasmic localization for BRF2 wildtype. This could be because both these truncation constructs are devoid of the NES in the C-terminus of the full-length protein, but still bear the NLS which is in the zinc finger domain (Figure 3.4). The NLS, which is embedded in the two zinc fingers could render the truncated proteins nuclear [182]. Previous studies by Phillips et al. showed that deletion or substitution mutants of TTP and BRF1 NES sequences led to nuclear localization [182]. A I373fsX91 frameshift mutation in BRF2 was observed in a patient suffering from acute myeloid leukemia that caused loss of the C-terminus of BRF2 and thus loss of the known NES. However, this mutant BRF2 protein localized to the cytoplasm [236].

Both the BRF2 truncation constructs are capable of promoting ß-globin-ARE reporter mRNA degradation, and both are present in P bodies. However, since the RBD alone (aa97-275) is sufficient to bring about RNA decay, this could mean that the NTD and the CTD have more of a regulatory role with regard to RNA decay activity. In cells subjected to arsenite-induced oxidative stress, both constructs show presence in stress granules. BRF2:aa97-275 retains its nuclear localization after arsenite treatment. BRF2:aa1-275, however, adopts a strong cytoplasmic localization following stress. This behaviour of BRF2:aa1-275 on arsenite treatment can be explained in the following ways. a) it interacts with some factor which either masks the existing NLS or promotes passive export out of the nucleus. b) it loses an interactor or changes its conformation such that a second NES somewhere in the N-terminus is exposed. I scanned the N-terminal region of BRF2 for any sequence which could fulfill the criteria of an NES. Indeed there appears to be a sequence in the N-terminal which contains multiple leucines, one of the characteristics of a NES (approximately BRF2 aa5-25) [Figure 6.4]. If this sequence acts as a NES, BRF2:aa97-275 probably fails to exit the nucleus upon arsenite treatment because it lacks this region. The nature of this export signal is worth further investigation because it appears to be activated under conditions of oxidative stress.

The results obtained with truncated BRF2 protein are also intriguing since both truncations show a strong nuclear localization and potently induce AMD. To date, AMD has not been reported to take place in the nucleus. This could mean that a) the negligible amount left in the cytoplasm is sufficient to promote AMD, b) there is active nucleo-cytoplasmic shuttling and AMD nevertheless takes place in the cytoplasm, and c) that AMD could actually also be nucleus-associated.

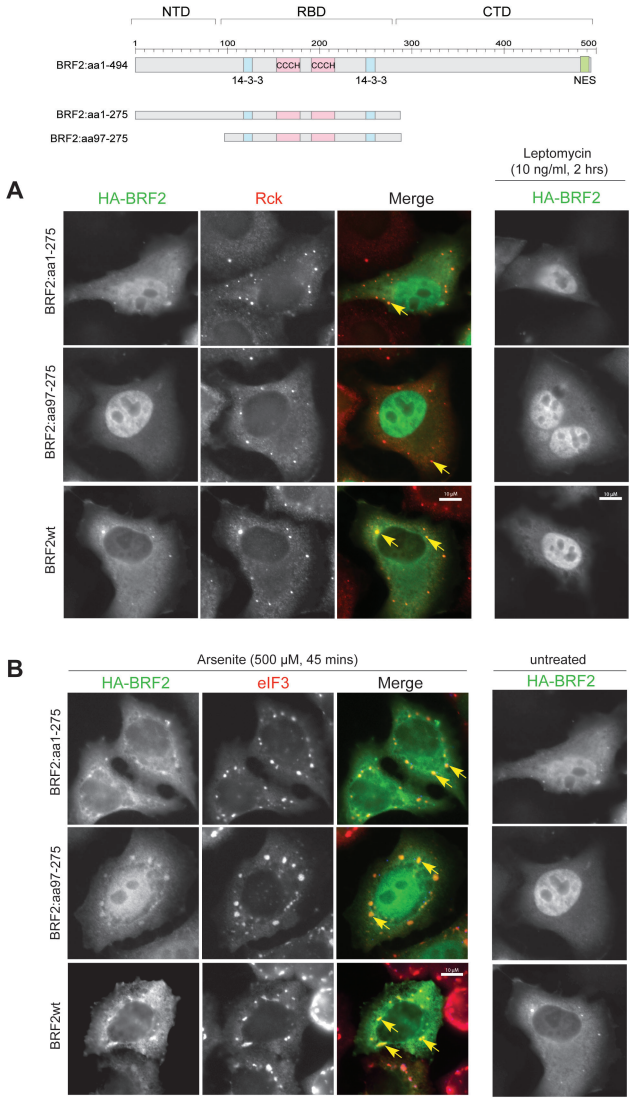

Figure 6.2: BRF2 truncation mutants show nuclear localization and co-localize with P bodies and oxidative stress-induced stress granules. On exposure to oxidative stress, BRF2:aa1-275 shifts to cytoplasm from the nucleus. Panel **A**, **B**: HeLa cells were transfected with HA-BRF2 wildtype, HA-BRF2:aa1-275, or HA-BRF2:aa97-275. Cells were stained with mouse monoclonal anti-HA antibody to visualise BRF2 protein in samples in all the panels below. Panel **A**: Cells were co-stained for Rck protein, a P body marker. Cells from the panel to the extreme right were exposed to Leptomycin B (10 ng/ml, 2 hrs) prior to fixing and stained as above to visualize BRF2 protein. Panel **B**: Cells were exposed to oxidative stess (500 µM arsenite, 45 mins) prior to fixing and co-stained for eIF3 protein, a marker for oxidative stress-induced stress granules.

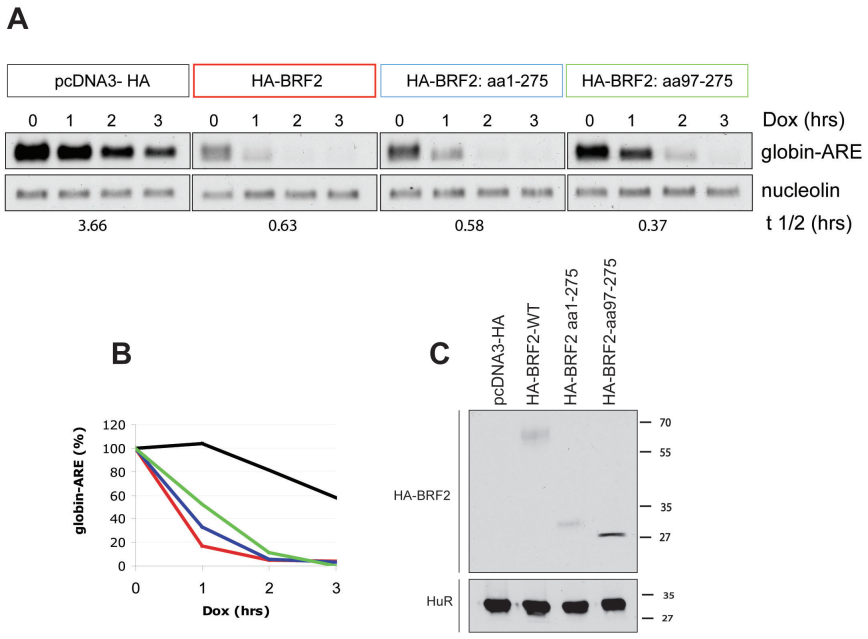

Figure 6.3: Truncated mutants of BRF2 are capable of degrading ß-globin-ARE reporter mRNA. A Tet-off system was employed. HeLa cells were transfected with the empty-vector, or plasmids encoding HA-BRF2 wildtype, HA-BRF2:aa1-275, or HA-BRF2:aa97-275 as indicated in the figure. doxycycline -chase mRNA decay assays were performed over a period of 3 hrs. Northern blotting was carried out as mentioned in Figure 3.7 legend. Panel **C**: Samples of transfected cells were processed by western blotting and probed with mouse monoclonal anti-HA antibody to detect BRF2 protein levels.

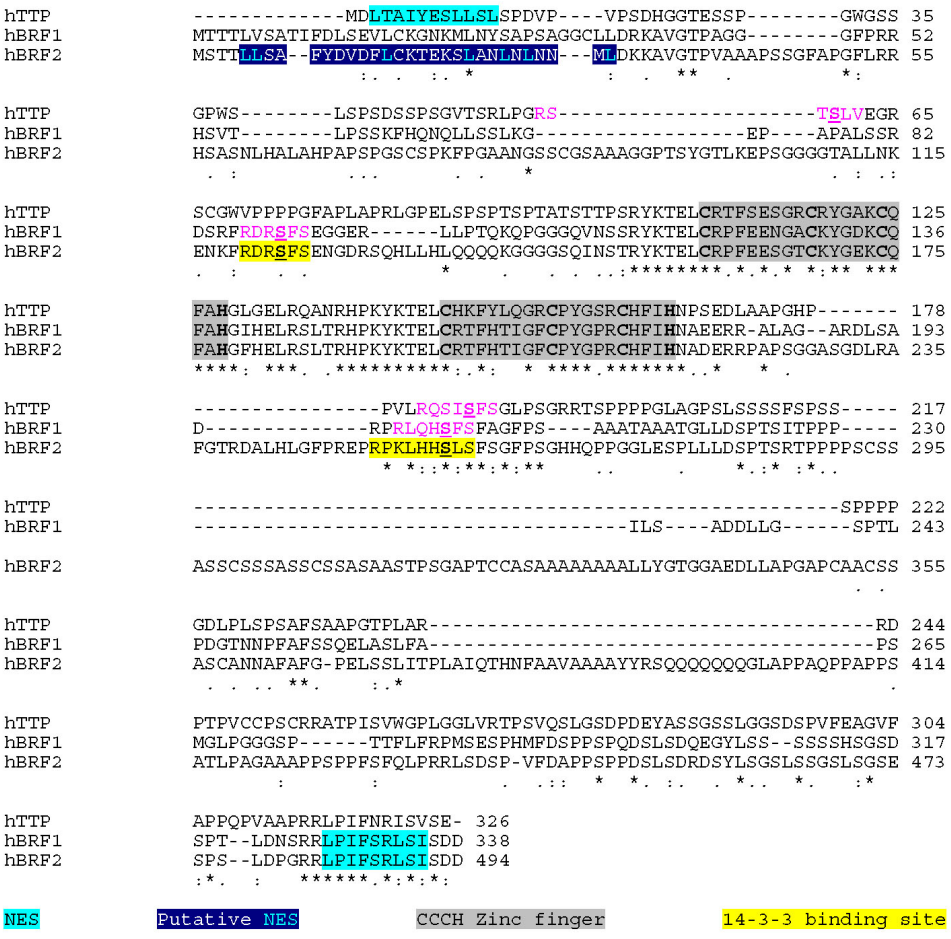

Figure 6.4: Putative NES in N-terminus of BRF2. N-terminus of BRF2 was scanned for presence of hydrophobic amino acids, especially Leucine, which optimally constitute an NES. A putative NES in the N-terminus is highlighted in dark blue.

7 Outlook and future directions

7.1 Summary

In my study, I performed experiments which led me to the following conclusions:

1) BFR2 degrades mRNA in an ARE-dependent manner.

2) BRF2 binds to 14-3-3 in a phosphorylation-dependent manner. I studied to greater detail the binding characteristics of BRF2 with 14-3-3 as a possible means of regulation of the AMD activity of BRF2. I could establish that S123 and S257 together form the binding site for 14-3-3 on BRF2. This has been similar to the 14-3-3 binding characteristics of TTP and BRF1 which have been studied in detail before. There is a possibility that more than one species of 14-3-3 interact with BRF2.

3) In analogy with TTP and BRF1, 14-3-3 binding to BRF2 was expected to alter the AMD efficiency of BRF2. However, in my experiments performed so far, it has been difficult to conclude anything to that effect. More experiments are underway. BRF2-PP mutant behaved unlike the TTP-S54,180P mutant, since instead of an expected increase in binding of BRF2-PP to 14-3-3, the binding actually reduced.

4) Similar to BRF1 (and TTP regarding only MK2), MK2 and PKBα kinases seemed to affect phosphorylation of BRF2 and 14-3-3 binding. 14-3-3 binding appeared reduced when inactive forms of MK2 or PKBα kinases were co-expressed along with BRF2. However, unlike observed in TTP and BRF1, MK2 did not appear to alter AMD efficiency of BRF2 in the given experimental conditions. This puts in question the role of MK2 with regard to modulating the AMD efficiency of BRF2.

5) Nucleo-cytoplasmic localization, and co-localization to P bodies and to oxidative stress-induced stress granules was quantified for BRF2 wildtype, BRF2-AA, and BRF2-PP. Both the 14-3-3 binding mutants showed a slightly more nuclear presence than the BRF2 wildtype which remained predominantly cytoplasmic. On exposure to arsenite stress, a part of the nuclear fraction of the BRF2 wildtype protein seemed to shift to the cytoplasm. All the three BRF2

constructs spontaneously localized to P bodies equally efficiently, to arsenite-induced stress granules with slightly varying efficiencies, and showed positive nucleo-cytoplasmic shuttling.

6) In preliminary co-IP experiments, BRF2 interacted with Not1 (aa1300-1601) and with Caf1a, indicating that BRF2 is associated with the mRNA deadenylation machinery.

7) In preliminary experiments, BRF2:aa1-275 and BRF2:aa97-275 were seen to localize to the nucleus. This could be because of lack of the NES present in the C-terminal. Interestingly, BRF2:aa1-275 shifted to the cytoplasm on exposure oxidative stress, which could indicate presence of an additional NES in the N-terminal. Moreover, it was seen that the central RBD region consisting of the two 14-3-3 sites and two zinc fingers was sufficient to promote AMD of ß-globin-ARE reporter mRNA.

7.2 Future directions:

Second NES in BRF2 ?

A plasmid construct encoding BRF2:aa1-96 + NLS + GFP could be transfected into the cells to check if the presence of BRF2:aa1-96 causes export of the nuclear GFP. Additionally, the interactors to this portion could be studied by mass spectrometry to know what contributes to export to cytoplasm on oxidative stress.

Do different domains of BRF2 have different regulatory roles ?

A simplified view of the BRF2 partial [234] and complete [235] knockout mice studies might indicate that BRF2:aa30-494 could be sufficient to bring about hematopoiesis, while BRF2:aa1-29 could be necessary for fertility. This could mean that different regions of BRF2 are involved in distinct functions and could involve diverse sets of interacting partners depending on the stage of life. Study of proteins interacting with individual domains of BRF2 by mass spectrometry could possibly reveal the role of BRF2 in embryonic development and possible housekeeping functions.

Is PKB involved in regulating BRF2 activity ? A future direction and a hypothesis.

BRF2, on over-expression, triggered apoptosis in a p53-dependent manner [242] and activated pro-apoptotic factors like caspase-3 and poly ADP-ribose polymerase (PARP) [236]. Over-expressed BRF2 triggered an S-phase checkpoint response in HeLa cells, and caused growth inhibition. Taken together, this suggests that under favourable growth conditions, BRF2 could play a role

in regulating cell cycle/growth. Incidentally, arsenite-induced oxidative stress is known to result in mitotic arrest of the cells [264]. It could be possible that such a cell-cycle arrest is achieved via BRF2. If so, then under conditions of stress, functional BRF2 protein would be required to achieve the cell-cycle arrest, and this could possibly justify why BRF2 may not be deactivated by a stress-induced kinase like MK2. Moreover, ARE-binding proteins, e.g. HuR, have already been implicated in effectuating hypoxic stress response [165, 166].

If BRF2 inhibits cell cycle progression, in favourable growth conditions when growth is to be facilitated, BRF2 activity might have to be supressed possibly via some kinase. PKB kinase could serve as an example of such a kinase. PKB is known to phosphorylate and deactivate components of apoptotic machinery, thus promoting survival. In conditions of DNA damage, PKB is deactivated by binding to homodimers of 14-3-3 sigma, curbing its proliferative effect (reviewed in [265]).

For further studies, the effect of PKB on BRF2 could be examined. PKB is a pro-proliferative kinase [266] and BRF2 is an anti-proliferative protein, therefore seemingly opposite in function, and a fine balance needs to exist between these pro- and anti-proliferative mechanisms for steady growth to occur. In conclusion, it would be interesting to check whether PKB modulates BRF2 activity, and viceversa. Probing deeper into these networks might expose new targets for anti-cancer therapies.

Acronyms

Acronym	Expanded form
ADAR-1	adenosine deaminase acting on RNA-1
Ago	Argonaute
AMD	adenylate/uridylate-rich element-mediated mRNA decay
AMP	adenosine mono phosphate
ARE	adenylate/uridylate-rich element
AUBP	AU-rich element binding protein
BRF1	Butyrate response factor 1
Ccr4	catabolite repressor protein 4
co-IP	co-immunoprecipitation
CTD	C-terminal domain
Dcp	decapping protein
DMEM	Dulbecco's modified eagle's medium
ELAV	embryonic-lethal abnormal vision
EMSA	electrophoretic mobility shift assay
FACS	fluorescence activated cell sorting
FCS	fetal calf serum
FGF	fibroblast growth factor
GFP	green fluorescent protein
GM-CSF	Granulocyte macrophage colony stimulating factor
HA	hemaglutinin
HDAC6	histone deacetylase 6
HSC	hematopoietic stem cells
HuR	human antigen R
IL	interleukin
IRES	internal ribosomal entry sites
JNK	c-jun-N-terminal kinase
kDa	kilo dalton
LPS	lipopolysaccharide
MAPK	mitogen-activated protein kinase
miRNA	microRNA
MK2	MAPK-activated protein kinase-2
mRNP	messenger ribonucleoprotein
NES	nuclear export signal
NGD	No-go mRNA decay
NLS	nuclear localization signal
NMD	Nonsense-mediated decay

Acronym	Expanded form
Not1	negative on TATA
NSD	Nonstop mRNA decay
NTD	N-terminal domain
P body	processing body
PABP	polyA binding protein
PAN	polyAnuclease
PARN	polyA ribonuclease
PARP	and poly ADP-ribose polymerase
PCR	polymerase chain reaction
PDGF	platelet derived growth factor
PI-3	phosphoinositide-3
PKBα	Protein kinase Bα
polyA	poly adenosine
PTC	premature stop codon
RBD	RNA-binding domain
RNA	Ribonucleic acid
SG	stress granule
TNFα	Tumor necrosis factor α
TTP	tristetraprolin
UTR	untranslated regions
UV	ultraviolet
VEGF	vascular endothelial growth factor
VHL	von Hippel Lindau protein
YFP	yellow florescent protein

8 Materials and methods

Plasmid construction:

pcDNA3 was obtained from Invitrogen and pTet-off was obtained from Clonetech. The construction of the following plasmids has been previously described: pcDNA3-HA (p2003) and pcDNA-YFP (p2168) [67], pcDNA3-myc-MK2-EE (p2064), pcDNA3-myc-MK2-K76R (p2065) [257], pcDNA3-7B (p2308), and pTet-7B-ARE (p2260) [194], pCMV5-m/pPKBα (p2070) , and pCMV5- PKBα-K179R (p2071) [211].

Plasmid pcDNA3-HA-BRF2 (p2114) was constructed by amplifying the coding region of human BRF2 gene using human cDNA as template and primers G1179 / G1034 and was cloned into the BamHI and XbaI sites of pcDNA3-HA. The XbaI site in pcDNA3-HA-BRF2 (p2114) gets methylated due to the formation of a GATC sequence at the XbaI site. This makes if resistant to XbaI digestion. In primer G1390, an additional G was added between the gene sequence and the XbaI restriction site to disrupt the GATC formation, thus reviving the functionality of the XbaI site. BRF2 coding region from p2114 was amplified using primers G1389 / G1390 and the product was digested with BamHI and XbaI and ligated into pcDNA3-YFP backbone digested with BamHI and XbaI to generate pcDNA-YFP-BRF2 (p2769).

Site-directed mutagenesis was performed to create BRF2 phosphorylation-site mutants, namely, pcDNA3-YFP-BRF2-S123A (p2727), pcDNA3-YFP-BRF2-S257A (p2913), pcDNA3-YFP-BRF2-S492A (p2728), pcDNA3-YFP-BRF2-S123,257A (p2870). DNA stretches 5' and 3' to the desired mutations were amplified individually as two overlapping fragments, with the overlapping regions containing the desired mutation. The following primers were used for the same; primers G1389 / G1391 (5' fragment) and G1392 / G1390 (3' fragment) for BRF2-S123A and primers G1389 / G1396 (5' fragment) and G1397 / G1390 (3' fragment) for BRF2-S257A. The above 5' and 3' fragments were aligned and were subjected to one more round of amplification using primers G1389 and G1390 to yield full-length coding regions of BRF2 harbouring respective mutations. Primers G1389 and mutation-containing G1395 were used to construct pcDNA3-YFP-BRF2-S492A. The above products were then digested with BamHI and XbaI and cloned into the same sites of pcDNA-YFP. For creating pcDNA-YFP-BRF2-S123,257A double mutant, the 5' region of BRF2-S123A existing between BamHI and XhoI sites was swapped with the

corresponding unmutated 5' region of BRF2 in pcDNA-YFP-BRF2-S257A. pcDNA-YFP-BRF2-S125,259P double mutant (p3080) was created using long primers G2536 / G2637 wherein each primer harbours one desired mutation. The PCR-amplified product was digested with restriction enzymes AflII and XhoI and this product was swapped with the corresponding region of the wildtype BRF2 from the plasmid pcDNA3-YFP-BRF2. The BRF2 coding sequences corresponding to the two double mutants were excised from the pcDNA-YFP backbones by digestion with BamHI and XbaI and subcloned into the same sites of pcDNA3-HA to give pcDNA3-HA-BRF2-S123,257A (p2870) and pcDNA-HA-BRF2-S125,259P (p3018).

pcDNA-HA-BRF2:aa1-275 (p3077) was generated by digesting pcDNA-YFP-BRF2 (p2769) with enzymes BamHI and XhoI and was subcloned between the same sites of pcDNA3-HA. To generate pcDNA-HA-BRF2:aa97-275, primers G2693 / G2694 and pcDNA-YFP-BRF2 (p2769) as template were used, the amplified product was digested with EcoRI and XbaI, and subsequently cloned into the same sites of pcDNA3-HA.

The PCR program used to amplify full-length BRF2 is listed in Table 8.1. Durations of the elongation step are modified depending on the length of expected product.

Table 8.1: PCR program for amplification of full length BRF2. Annealing times reduced depending on the length of amplified product.

Temperature (°C)	Duration (mins)	Cycles
94	3	1
94	1	5
50	1	
72	1.5	
94	1	35
57	1	
72	1.5	
72	10	1
4		

Cell culture and transfection:

The cell lines used in this study are listed in Table 8.2.

All cell lines used in this study are adherent cells and grow as monolayer cultures. Cells lines were maintained at 37°C, 5% CO_2, in Dulbecco's modified Eagle's medium (DMEM; Sigma) with additions of 10 % fetal calf serum (FCS; Biochrom AG), 2mM L-Glutamine, 100 U/ml penicillin and 0.1 mg/ml

Table 8.2: Cell lines used in this study.

Cell line	Remarks
HEK293	Hypotriploid human embryonic kidney cell line (CRL-1573)
HeLa	Human cervical epithelial adenocarcinoma cell line (CCL-2)
HT1080	Human connective tissue fibrosarcoma cell line (CCL-121)
HTwt16	Derivative of HT1080 cell line, stably expressing GFP-IL3 reporter
SlowC	Derived by chemical mutagenesis of HTwt16, both alleles of BRF1 dysfunctional
SC-B1-1	SlowC stably expressing full-length HA-BRF1
SC-B1-2	SlowC stably transfected with, but not expressing HA-BRF1
SC-B2-1	SlowC stably expressing HA-BRF2 fragment
SC-B2-2	SlowC stably expressing HA-BRF2 fragment
SC-B2-3	SlowC stably transfected with, but not expressing HA-BRF2
SC-B2-4	SlowC stably expressing full-length HA-BRF2
SC-B2-5	SlowC stably expressing HA-BRF2 fragment
SC-B2-6	SlowC stably transfected with, but not expressing HA-BRF2

streptomycin (all from PAN biotech). Cells were trypsinized using trypsin-EDTA (PAN biotech), and subcultivation ratio was 1:10 to 1:16 depending on individual growth rates.

For transient transfections for co-immunoprecipitation experiments, DNA was transfected using polyethylineimine (PEI; Polysciences Inc.) with a ratio of DNA:PEI equalling 1: 2.5 in serum-free DMEM devoid of antibiotics. After 4 hrs of incubation, medium was changed to regular medium that included serum and antibiotics. For immunoflorescence experiments, Fugene HD transfection reagent (Promega) was used for transfections according to manufacturer's protocol.

100 nM siRNAs were transfected using Lipofectamine 2000 twice over a period of 5 days. Serum starvation treatment involved incubating cells with DMEM containing 0.1 % FCS for indicated durations, arsenite treatment included exposure of cells to 500 µM arsenite for 45 mins, anisomycin treatment included exposure to 10 µg/ml anisomycin for 30 mins. Kinase inhibitors SB202190 and wortmanin were used at working concentrations of 10µM and 15µM, respectively, for a duration of 1 hr. Durations of treatments were calculated keeping as reference the time of final lysis of cells for co-IP experiments or that of commencement of RNA decay assays.

Stable transfections:

Htwt16 and SlowC cells were generated as mentioned in [227]. SlowC cell lines were stably transfected with plasmids encoding HA-tagged versions of BRF1 or BRF2 after prior linearization of the plasmids with DraIII restriction en-

zyme. 48 hrs after transfection, G418 (1 mg/ml) was added to the medium to eliminate untransfected cells, and the remainder cells were allowed to grow further till they formed visible colonies. Samples of cells were dislodged gently from the centre of each selected transformant colony, aspirated directly from the colony using a micropipette, while visualising under the microscope, and inoculated into individual wells of a 24-well plate pre-containing 500 µl growth medium per well. Each individual clone was expanded using growth medium + G418 drug and tested by FACS to guage the GFP signal intensity of the clones. Positive clones were expected to have an increased AMD efficiency, degrade GFP-IL3 mRNA more efficiently, leading to lower GFP protein signal intensity lower, all of the above when compared to SlowC cells. All clones showing reduced GFP signal intensity were expanded individually. One clone per transfection was chosen in which the GFP signal intensity remained unchanged, i.e. showed GFP signal intensity similar to SlowC cells; this clone would serve as a negative control for later experiments.

Immunoprecipitation and Western blotting:

4 X 10^6 HEK293 cells were seeded per 10-cm dish, transfected the next day, and incubated for 24 hrs before the time of lysis. Cells from each such dish were lysed in 400 µl RNP lysis buffer (50 mM Tris-HCl ppH 8.0, 150 mM NaCl, 1 mM MgCl2, 1% NP-40, 10% glycerol, 1 mM DTT, Complete EDTA-free protease inhibitor cocktail (Roche) and the following phosphatase inhibitors; 1mM NaVO3, 50 mM NaF, 40 nM Okadaic acid). For the phosphatase treated samples, Lambda phage phosphatase (NEB) was included in the lysis buffer at the concentration of 1 unit/µl and phosphatase inhibitors were excluded. YFP-tagged proteins were purified as mentioned in [244]. GFP-binder beads with protein complexes attached to them were washed 6 times with above RNP lysis buffer, excluding phosphatase inhibitors, and later boiled with 2X Laemmli buffer. Inputs and eluted complexes were resolved on 10% SDS-polyacrylamide gels and transferred onto nitrocellulose membranes with pore-size of 0.2 µM (Peqlab) for western blotting. The blots were developed using Western Lightening chemiluminiscence substrate (Perkin Elmer) and medical X-ray films (Fujifilm).

RNA decay assays and Northern blotting:

For RNA decay experiments using stable lines, 8 X 10^6 cells per cell line were seeded on Day I. On Day II, cells were trypsinized and split into 4 equal aliquots and were incubated with 5 µg/ml ActinomycinD for indicated time intervals. 11 µg of total RNA per sample was processed further. RNA probes to be used were generated by PCR amplification using primers G293/G294 against IL3-I and primers G078/G1008 against human RPS7 (loading control).

For RNA decay experiments using the Tet-off transient transfection system, 4 X 10^6 HeLa cells were seeded on Day I, transfected on Day II with pTet-

off plasmid (Clonetech), pTet-7B-ARE (globin-ARE) reporter plasmid, and the experimental plasmid DNA as indicated. On Day III, cells belonging to each transfection were trypsinized and split into 5 equal aliquots. Cells from one aliquot were subjected to western blotting to estimate level of protein expression. The remainder 4 aliquots were incubated with 1 µg/ml doxycycline (Sigma) for indicated time intervals. Following this, total RNA was isolated using Genematrix RNA purification kit (Eurx. Roboklon). 7 µg of total RNA per sample was processed further. RNA probes to be used were generated by PCR amplification using primers G1000/G1001 against exons 1 and 2 of rabbit ß-globin and primers G83/G1009 against human nucleolin (loading control).

In cases of both ActinomycinD- and doxycycline -chase assays, total RNA was resolved by electrophoresis on 1.1% agarose/2% formaldehyde/ MOPS gel. The thus-resolved RNA was blotted overnight in 8X saline-sodium citrate (SSC) onto Hybond-N+ membranes (GE healthcare). Membranes were hybridized overnight at 55°C and probed with aforementioned digoxygenin-labelled RNA probes that were synthesized in vitro using SP6 polymerase (Fermentas). Membranes with the blotted RNA were washed at 65°C twice with 2X SSC/0.1 % SDS for 5 mins each and twice with 0.5X SSC/0.1 % SDS for 20 mins each. Alkaline phosphatase-coupled anti-digoxygenin Fab fragment and CDP-Star substrate (both from Roche) were used according to the manufacturers protocol for the detection of the probes.

RT-qPCR:

cDNA was synthesized from 2 µg of total RNA by reverse transcription using random hexamers (Fermantas) and Transcriptor reverse transcriptase (Roche). The reaction mixture contained the following: 2µg total RNA, 4 µl 5X transcription buffer (Promega), 2 µl 10 mM dNTPs (dATP, dTTP, dGTP, dCTP), 0.01 µg random hexamer primers, 0.5 µl RNase inhibitor (Promega), 10 U transcriptor reverse transcriptase (Roche). Reaction mixture was incubated for 30 mins at 55°C for cDNA synthesis after which the enzyme was inactivated at 85°C for 5 mins. cDNA thus generated was diluted 1:5 using PCR-grade water.

Real-time PCRs were carried out using 2.5 µl diluted cDNA as a template and 200 nM target specific forward and reverse primers. The following primers were used for the PCR reaction: G2057 / G2059 for BRF1-Set I, G 2058 / G 2060 for BRF1-Set II, G 2061 / G 2063 for BRF2-Set I, G2062 / G2064 for BRF2-Set II, and G1576 / G1577 for human nucleolin as internal control. 10 µl reactions were set using SYBR green Mastermix (Roche) and were processed using a Lightcycler 480 (Roche). The quantitative real time PCR program was as seen in Table 8.3

Immunoflorescence:

HeLa cells were seeded in wells of a 6-well plate and transfected with plasmid DNA. Transfection mix was substituted with regular medium after 4 hrs

Table 8.3: Quantitative real time PCR program.

Program	Target (°C)	Acquisition mode	Hold	Ramp rate
Pre-Incubation	95	none	5 min	4.4
Amplification	95	none	10 sec	4.4
	55	none	15 sec	2.5
	72	single	25 sec	4.8
Melting curve	95	none	5 sec	4.8
	60	none	1 min	2.5
	97	single	-	0.11
Cooling	40	none	10 sec	2

and cells were incubated further for 2 hrs. Cells from each well were then trypsinized and split into 5-8 wells (depending on the cell density) of a 24-well plate and allowed to grow overnight. Cells to be visualised for stress granules were treated with 500 µM arsenite for 45 mins. Leptomycin treatment involved incubating cells with 10 ng/ml leptomycin for 2 hrs. Subsequently, cells were fixed with 5% para formaldehyde (PFA) and then with 20% chilled methanol. As per requirement, cells were stained with anti-HA antibody to visualize over-expressed HA-BRF2, anti-Rck antibody to stain P bodies, anti-eIF3 antibody to stain SGs. To quantify the cellular localization of BRF2 and its association with P bodies or SGs, 100 transfected cells were observed under the microscope and localization of BRF2 was noted down. Three independent transfections were analyzed to calculate average percentages and standard errors of the mean (s.e.m.).

Antibodies used in this study:

Sr. No.	Antibody	Remark	Dilution	Company
A003	14-3-3 beta (K-19) (Lot # D1808)	polyclonal	1:1000	Santa Cruz sc-630
A007	c-myc (9E10)	monoclonal	1:1000	Covance MMS-150P
A024	GFP (ab290)	polyclonal	1:10000	Abcam ab290
A026	HA.11	monoclonal	1:1000	Covance Innovative Antibodies MMS-101P
A029	HuR (3A2)	monoclonal	1:1000	Santa Cruz sc-5261
A040	RCK (Dhh1)	polyclonal	1:1000	bethyl A300-461A
A050	BRF1+2	polyclonal	1:1000	Ch.Moroni, Basel
A096	Phospho-PKBα (Ser473)	monoclonal	1:1000	Cell Signaling(NEB)#4051

Sr. No.	Antibody	Remark	Dilution	Company
A097	PKBα	polyclonal	1:1000	Cell Signaling(NEB) #9272
A102	eIF3eta	polyclonal	1:1000	Santa Cruz sc-16377
A134	MAPKAPK-2	polyclonal	1:1000	Cell Signaling(NEB) #3042
A135	Phospho-MAPKAPK-2 (Thr334)	polyclonal	1:1000	Cell SignallingNEB) #3041
	Secondary antibodies:			
	donkey anti-mouse IgG	HRP-coupled	1:5000	Jackson ImmunoResearch
	donkey anti-rabbit IgG	HRP-coupled	1:5000	Jackson ImmunoResearch
	Cy2 donkey anti-mouse		1:1000	Jackson ImmunoResearch
	Cy3 donkey anti-goat		1:1000	Jackson ImmunoResearch
	Cy2 donkey anti-rabbit		1:1000	Jackson ImmunoResearch

DNA oligonucleotides:

Name:	DNA oligonucleotide sequence:
G 83	TTACAAAGTCACTCAGGATG
G 1000	GTGCATCTGTCCAGTG
G 1001	GCCGATTTAGGTGACACTATAGAAT ACCCTGAAGTTCTC
G 1009	GCCGATTTAGGTGACACTATAGAAT ACTTAGCGTCTTCG
G 1034	AATTCTCGAGGTTCTCCTTGTTG
G 1179	ATATGGATCCCCCTCCTGCTCTTC
G 1389	ATATGGATCCTCGACCACACTT
G 1390	ATATTCTAGAGTCAGTCGTCGGA
G 1391	CAAATTCCGGGACCGCGCGTTTAGCGAG
G 1392	CTCGCTAAACGCGCGGTCCCGGAATTTG
G 1395	CGCCTGTCCGACGCGCCCGTGTTCGAC
G 1396	GTCGAACACGGGCGCGTCGGACAGGCG

Name:	DNA oligonucleotide sequence:
G 1397	ATATTCTAGAGTCAGTCGTCGGCGATGGAGAGGC
G 1576	GTTGCACCACGCCCTCAGCTTC
G 1577	GAAGCTGAGGGCGTGGTGCAAC
G 2057	GTCTGCCACCATCTTCGAC
G 2058	CCACCATCTTCGACTTGAGC
G 2059	GGGCAGGGTGACTGAGTG
G 2060	CTGGGCAGGGTGACTGAG
G 2061	TTCTGTCCGCCTTCTACGATG
G 2062	CTGTCCGCCTTCTACGATGTC
G 2063	GAGTGCCGTCGGAGGAATC
G 2064	AGTGCCGTCGGAGGAATC
G 2536	CCCTTAAGGAGCCGTCGGGGGGCGGCGGCACA GCCCTGCTCAACAAGGAGAACAAATTCCGGGA CCGCTCGTTTCCGGAGAACGGCGAT
G 2537	CGACTCGAGGCCGCCCGGGGGCTGATGGTGGC CCGACGGGAAGCCCGAGAACGGGAGGCTGTGGTG
G 2693	CAGTGAATCCCCTACGGCACCCTTAAGG
G 2694	CAGTAGATCTCGGGCGAGTCGGACAGGC

Northern probes:

Sr. No.	Oligonucleotide sequence	Remark
G1000	GTGCATCTGTCCAGTG	Bex12 probe_forward
G1001	GCCGATTTAGGTGACACTAT AGAATACCCTGAAGTTCTC	Bex12 probe Sp6_reverse
G083	TTACAAAGTCACTCAGGATG	hNCL probe_forward
G1009	GCCGATTTAGGTGACACTATA GAATACTTAGCGTCTTCG	hNCL probe SP6_reverse
G293	AACAGCAGGCAGAGCAC	IL3-I probe_forward
G294	GCCGATTTAGGTGACACTAT AGAATACAGGAACATAATTAG	Sp6-IL3-I probe_reverse
G078	GGTGGTCGGAAAGCTATC	hRPS7 probe_forward
G1008	GCCGATTTAGGTGACACTAT AGAATACTATAGACACCAG	hRPS7 probe SP6_reverse

siRNAs used in this study:

Sr.No.	siRNA	Sequence
S002	D0 (Non-specific)	GCAUUCACUUGGAUAGUAA

Sr.No.	siRNA	Sequence
S057	siRNA-MK2	UCACCGAGUUUAUGAACCA

Disposable materials and kits:

Material / Kit	Company
1.5 ml, 2 ml Reaction Tubes	Eppendorf
15 ml, 50 ml Falcon Tubes	Falcon, Greiner, Nunc
2 ml Cryotubes	Nunc
Filter tips	StarLab
Filter paper Whatman 3MM	Whatman
Cellscraper CoStar	Corning Inc.
CellStar Tissue culture flasks (T75, T25)	Greiner Bio-One
CellStar Tissue culture dishes (6, 10, 15cm)	Greiner Bio-One
CellStar Cell culture plates (6-well, 12-well, 24-well)	Greiner Bio-One
DIG labelling Kit	Ambion
Gloves	Meditrade
Pipette tips Steinbrenner,	Starlab
PureLink HiPure Plasmid Midiprep Kit	Invitrogen
PureLink HiPure Plasmid Maxiprep Kit	Invitrogen
QIAquick Gel Extraction Kit	QIAgen
QIAprep Spin Miniprep Kit	QIAgen
QIAquick PCR Purification Kit	QIAgen
QIAquick Nucleotide Removal Kit	QIAgen
Rapid DNA Ligation Kit	Fermentas
RNA Isolation Kit EURx,	Roboklon
Transcriptor First Strand cDNA Synthesis Kit	Roche

Chemicals used in this study:

Chemical	Company
10x Taq Polymerase Buffer	QIAgen
2-Mercaptoethanol (2-ME)	Sigma
5x Transcription Buffer	Promega
Acetic Acid	Fluka
Actinomycin D	AppliChem
Agarose	Biozym Scientific GmbH

Chemical	**Company**
Ammoniumpersulfate	AppliChem
Ampicillin	Applichem
Bromphenol blue	Applichem
Calf Intestine Phosphatase (CIP)	New England Biolabs
Chloroform	VWR
Complete Protease Inhibitor Cocktail Tablets, EDTA-free	Roche
Coomassie Brillant Blue R250	ROTH
Coomassie Brillant Blue R250	AppliChem
Desoxyadenosine triphosphate (dATP)	Fermentas
Desoxycytidine triphosphate (dCTP)	Fermentas
Desoxyguanosine triphosphate (dGTP)	Fermentas
Desoxythymidine triphosphate (dTTP)	Fermentas
DH5alpha competent E. coli cells	Invitrogen
DIG labelling mix	Roche
Dimethylsulfoxid (DMSO)	Serva Electrophoresis
Disodiumhydrogenphosphate	Roth
Dithiothreitol (DTT)	Applichem
doxycycline e	AppliChem
Ethanol	Riedel-de-Haen
Ethidium bromide (EtBr)	Applichem
Ethylenediaminetetraacetic acid (EDTA)	Roth
Formaldehyde	Merck
Formamide	AppliChem
Gene Ruler 1kb Ladder Plus	Fermentas
Glycerol	Roth
Glycine	Gerbu
HEPES	Roth
Isopropanol	Sigma-Aldrich
Kanamycinesulfate	Roth
L-glutamine	PAN
Lipofectamine 2000	Invitrogen
Magnesium chloride	Merck
Maleic acid	Fluka
Methanol	Fluka
Milk powder	Roth
MOPS	Roth
Nonidet P-40 (NP-40)	US Biological
O'GeneRuler 100bp Plus DNA Ladder	Fermentas
Ocadaic acid	Sigma-Aldrich

Chemical	Company
PageRuler Prestained Protein Ladder	Fermentas
Paraformaldehyde	AppliChem
Penicillin-streptomycin	PAN
Polyethyleneimine (PEI)	Polysciences Europe
Ponceau S	MD
Potassiumacetate	Roth
Potassiumchloride	Roth
Random hexamers	Fermentas
Restriction Enzymes	New England Biolabs
RNase inhibitor RNasin	Promega
Rotiphorese Acrylamide Solution	Roth
RQ1 DNase	Promega
Sodium arsenite	Fluka
Sodium azide	AppliChem
Sodium chloride	Sigma-Aldrich
Sodium dodecyl sulphate (SDS)	Gerbu
Sodium hydroxide pellets	Riedel-de-Haen
Sodiumfluoride	Sigma-Aldrich
Sodiumvanadate	Sigma-Aldrich
SP6 polymerase	Fermentas
T4 DNA Ligase	Fermentas
TEMED	AppliChem
Thermo polymerase buffer	New England Biolabs
Transcriptor reverse transcriptase	Roche
Transcriptor reverse transcriptase 5x reaction buffer	Roche
Trisodiumcitrate	VWR
Triton-X-100	Applichem
Trizma base	Sigma-Aldrich
Trypsin/EDTA	PAN
Tween-20	Sigma-Aldrich
Vent DNA Polymerase	New England Biolabs
Xylenecyanol	Applichem
Yeast tRNA	Ambion

Equipment:

Equipment / instrumentation	Company
Freezer -20°C	Liebherr
Freezer -80°C x	Liebherr

Equipment / instrumentation	**Company**
Fridge 4°C	Liebherr
Cell Culture Incubator	Hera cell
Centrifuge (5417R)	Eppendorf
Centrifuge (J2-MC, rotor JA-17)	Beckman
Centrifuge (Labofuge M)	Heraeus Sepatech
Centrifuge (Multifuge 1S)	Thermo
Centrifuge (Pico17)	Thermo
Film Development Apparatus (HyperProcessor)	Amersham
GeneAmp PCR System 9700	Applied Biosystems
Heating Block (neoBlock 1)	NeoLab
Intelli-mixer	NeoLab
Laminar Flow Cabinet	Hera cell
Magnetic Stirrer (MR3001)	NeoLab
Micropipettes	Gilson
Microwave	Privileg
Mini Protean 3 Cell	BIORAD
Mini Trans Blot Cell	BIORAD
Nanodrop ND 1000	PeQLab
pH Meter (766 Calimetic)	Knick
Poly-Prep column	Biorad
Power Supply (powerpack300)	Biorad
Scale (440-47N)	Kern
Shaker (DOS-20S)	NeoLab
Shaker (PMR-30)	Grant-bio
Sorvall Discovery 90SE	Thermo Scientific
Speedvac	Eppendorf Concentrator
TurboBlotter (northern blotting)	Whatman
UV Gel Documentation System	Raytest IDA
UV Table (TVL-312A)	Specktroline
Vortex	NeoLab
Waterbath	GFL

Acknowledgements

I take this opportunity to thank.....

....**Dr. Georg Stoecklin** for allowing me to be a part of his group, for being an extremely patient mentor, for good scientific education, for ensuring an atmosphere of trust and co-operation in the lab, for the encouragement and motivation, for constructive criticizm.

....**Prof. Ingrid Grummt** and **Dr. Brian Luke** for providing me with guidance and direction through my Ph.D.

....**Dr. Ulrike Engel** and **Dr. Christian Ackermann** from Nikon Imaging Center for helping me with microscopy.

....**Milan** for lending a listening ear when necessary and always providing reasons to laugh !....**Heike** for helping me out in my initial days in the lab, for all the positive thinking, for the gossips, giggles, and extra-curriculars, for the spontaneous German lessons !....**Sevim** for being a great neighbour in the office, for sharing protocols, for always being up for creative pursuits, for providing delicious Turkish food recepies !....**Sarah** for the delicious cakes, for always being so enthusiastic, for running around for me in difficult times treating my problems as your own, for lending your German language skills when I needed them the most !....**Kathrin** for extra-curricular scientific chats, for the movie-nights, for the delicious muffins, for the rides to EMBL !....**Johanna** for the informative chats on history, for constructive scientific discussions, and for introducing me to my wonderful niece, "the" Lieschen ! ....**Sahil** for the being helpful, for the silent pranks, for not making me miss speaking Hindi !....**Sonya** for car rides and laughs in the lab....**Jochen** for helping me a lot with laborious experiments, for introducing me to the "reset" button (have had to use that often in my Ph.D.), for the interesting self-made thriller movies (which really kept the suspense on, sometimes even after the movie was over), for the enojyable barbeques every summer, for teaching me sentences in German language which I should not use anywhere !

....all my transiently-localized lab collegues**: Freddy, Janine, Ines, Aravindan, Nicole, Gizem, Moritz, Bogdan, Ivana**, et al.,....it was wonderful knowing you.

....**Mithun B**. for tutoring me on LyX software.....all my **friends** who provided me with reprints at a short notice and ones who proofread my thesis.

....last but not the least, my **Notebook**, which stood by me all throughout my doctoral studies and made thesis writing easier.

I dedicate this work to my **family members**, who have been a source of inspiration and unconditional support in every given situation. I am because they are.

Bibliography

[1] Philipp Kapranov, Aarron T. Willingham, and Thomas R. Gingeras. Genome-wide transcription and the implications for genomic organization. *Nat Rev Genet*, 8(6):413–423, Jun 2007.

[2] E. N. C. O. D. E Project Consortium , Ewan Birney, John A. Stamatoyannopoulos, Anindya Dutta, Roderic Guigó, Thomas R. Gingeras, Elliott H. Margulies, Zhiping Weng, Michael Snyder, Emmanouil T. Dermitzakis, Robert E. Thurman, Michael S. Kuehn, Christopher M. Taylor, Shane Neph, Christoph M. Koch, Saurabh Asthana, Ankit Malhotra, Ivan Adzhubei, Jason A. Greenbaum, Robert M. Andrews, Paul Flicek, Patrick J. Boyle, Hua Cao, Nigel P. Carter, Gayle K. Clelland, Sean Davis, Nathan Day, Pawandeep Dhami, Shane C. Dillon, Michael O. Dorschner, Heike Fiegler, Paul G. Giresi, Jeff Goldy, Michael Hawrylycz, Andrew Haydock, Richard Humbert, Keith D. James, Brett E. Johnson, Ericka M. Johnson, Tristan T. Frum, Elizabeth R. Rosenzweig, Neerja Karnani, Kirsten Lee, Gregory C. Lefebvre, Patrick A. Navas, Fidencio Neri, Stephen C J. Parker, Peter J. Sabo, Richard Sandstrom, Anthony Shafer, David Vetrie, Molly Weaver, Sarah Wilcox, Man Yu, Francis S. Collins, Job Dekker, Jason D. Lieb, Thomas D. Tullius, Gregory E. Crawford, Shamil Sunyaev, William S. Noble, Ian Dunham, France Denoeud, Alexandre Reymond, Philipp Kapranov, Joel Rozowsky, Deyou Zheng, Robert Castelo, Adam Frankish, Jennifer Harrow, Srinka Ghosh, Albin Sandelin, Ivo L. Hofacker, Robert Baertsch, Damian Keefe, Sujit Dike, Jill Cheng, Heather A. Hirsch, Edward A. Sekinger, Julien Lagarde, Josep F. Abril, Atif Shahab, Christoph Flamm, Claudia Fried, Jörg Hackermüller, Jana Hertel, Manja Lindemeyer, Kristin Missal, Andrea Tanzer, Stefan Washietl, Jan Korbel, Olof Emanuelsson, Jakob S. Pedersen, Nancy Holroyd, Ruth Taylor, David Swarbreck, Nicholas Matthews, Mark C. Dickson, Daryl J. Thomas, Matthew T. Weirauch, James Gilbert, Jorg Drenkow, Ian Bell, XiaoDong Zhao, K. G. Srinivasan, Wing-Kin Sung, Hong Sain Ooi, Kuo Ping Chiu, Sylvain Foissac, Tyler Alioto, Michael Brent, Lior Pachter, Michael L. Tress, Alfonso Valencia, Siew Woh Choo, Chiou Yu Choo, Catherine Ucla, Caroline Manzano, Carine Wyss, Evelyn Cheung, Taane G. Clark, James B. Brown, Madhavan Ganesh, Sandeep Patel, Hari Tammana, Jacqueline

Chrast, Charlotte N. Henrichsen, Chikatoshi Kai, Jun Kawai, Ugrappa Nagalakshmi, Jiaqian Wu, Zheng Lian, Jin Lian, Peter Newburger, Xueqing Zhang, Peter Bickel, John S. Mattick, Piero Carninci, Yoshihide Hayashizaki, Sherman Weissman, Tim Hubbard, Richard M. Myers, Jane Rogers, Peter F. Stadler, Todd M. Lowe, Chia-Lin Wei, Yijun Ruan, Kevin Struhl, Mark Gerstein, Stylianos E. Antonarakis, Yutao Fu, Eric D. Green, Ula? Karaöz, Adam Siepel, James Taylor, Laura A. Liefer, Kris A. Wetterstrand, Peter J. Good, Elise A. Feingold, Mark S. Guyer, Gregory M. Cooper, George Asimenos, Colin N. Dewey, Minmei Hou, Sergey Nikolaev, Juan I. Montoya-Burgos, Ari Löytynoja, Simon Whelan, Fabio Pardi, Tim Massingham, Haiyan Huang, Nancy R. Zhang, Ian Holmes, James C. Mullikin, Abel Ureta-Vidal, Benedict Paten, Michael Seringhaus, Deanna Church, Kate Rosenbloom, W James Kent, Eric A. Stone, N. I. S. C Comparative Sequencing Program , Baylor College of Medicine Human Genome Sequencing Center , Washington University Genome Sequencing Center , Broad Institute , Children's Hospital Oakland Research Institute , Serafim Batzoglou, Nick Goldman, Ross C. Hardison, David Haussler, Webb Miller, Arend Sidow, Nathan D. Trinklein, Zhengdong D. Zhang, Leah Barrera, Rhona Stuart, David C. King, Adam Ameur, Stefan Enroth, Mark C. Bieda, Jonghwan Kim, Akshay A. Bhinge, Nan Jiang, Jun Liu, Fei Yao, Vinsensius B. Vega, Charlie W H. Lee, Patrick Ng, Atif Shahab, Annie Yang, Zarmik Moqtaderi, Zhou Zhu, Xiaoqin Xu, Sharon Squazzo, Matthew J. Oberley, David Inman, Michael A. Singer, Todd A. Richmond, Kyle J. Munn, Alvaro Rada-Iglesias, Ola Wallerman, Jan Komorowski, Joanna C. Fowler, Phillippe Couttet, Alexander W. Bruce, Oliver M. Dovey, Peter D. Ellis, Cordelia F. Langford, David A. Nix, Ghia Euskirchen, Stephen Hartman, Alexander E. Urban, Peter Kraus, Sara Van Calcar, Nate Heintzman, Tae Hoon Kim, Kun Wang, Chunxu Qu, Gary Hon, Rosa Luna, Christopher K. Glass, M Geoff Rosenfeld, Shelley Force Aldred, Sara J. Cooper, Anason Halees, Jane M. Lin, Hennady P. Shulha, Xiaoling Zhang, Mousheng Xu, Jaafar N S. Haidar, Yong Yu, Yijun Ruan, Vishwanath R. Iyer, Roland D. Green, Claes Wadelius, Peggy J. Farnham, Bing Ren, Rachel A. Harte, Angie S. Hinrichs, Heather Trumbower, Hiram Clawson, Jennifer Hillman-Jackson, Ann S. Zweig, Kayla Smith, Archana Thakkapallayil, Galt Barber, Robert M. Kuhn, Donna Karolchik, Lluis Armengol, Christine P. Bird, Paul I W. de Bakker, Andrew D. Kern, Nuria Lopez-Bigas, Joel D. Martin, Barbara E. Stranger, Abigail Woodroffe, Eugene Davydov, Antigone Dimas, Eduardo Eyras, Ingileif B. Hallgrímsdóttir, Julian Huppert, Michael C. Zody, Gonçalo R. Abecasis, Xavier Estivill, Gerard G. Bouffard, Xiaobin Guan, Nancy F. Hansen, Jacquelyn R. Idol, Valerie V B. Maduro, Baishali Maskeri, Jen-

nifer C. McDowell, Morgan Park, Pamela J. Thomas, Alice C. Young, Robert W. Blakesley, Donna M. Muzny, Er. Identification and analysis of functional elements in 1genome by the encode pilot project. *Nature*, 447(7146):799–816, Jun 2007.

[3] S. W. Peltz, G. Brewer, P. Bernstein, P. A. Hart, and J. Ross. Regulation of mrna turnover in eukaryotic cells. *Crit Rev Eukaryot Gene Expr*, 1(2):99–126, 1991.

[4] Olaf Isken and Lynne E. Maquat. Quality control of eukaryotic mrna: safeguarding cells from abnormal mrna function. *Genes Dev*, 21(15):1833–1856, Aug 2007.

[5] C. J. Decker and R. Parker. A turnover pathway for both stable and unstable mrnas in yeast: evidence for a requirement for deadenylation. *Genes Dev*, 7(8):1632–1643, Aug 1993.

[6] Roy Parker and Ujwal Sheth. P bodies and the control of mrna translation and degradation. *Mol Cell*, 25(5):635–646, Mar 2007.

[7] Paul Anderson and Nancy Kedersha. Stress granules: the tao of rna triage. *Trends Biochem Sci*, 33(3):141–150, Mar 2008.

[8] Akio Yamashita, Tsung-Cheng Chang, Yukiko Yamashita, Wenmiao Zhu, Zhenping Zhong, Chyi-Ying A. Chen, and Ann-Bin Shyu. Concerted action of poly(a) nucleases and decapping enzyme in mammalian mrna turnover. *Nat Struct Mol Biol*, 12(12):1054–1063, Dec 2005.

[9] C. G. Körner and E. Wahle. Poly(a) tail shortening by a mammalian poly(a)-specific 3'-exoribonuclease. *J Biol Chem*, 272(16):10448–10456, Apr 1997.

[10] Niklas Henriksson, Per Nilsson, Mousheng Wu, Haiwei Song, and Anders Virtanen. Recognition of adenosine residues by the active site of poly(a)-specific ribonuclease. *J Biol Chem*, 285(1):163–170, Jan 2010.

[11] Jae Eun Kwak and Marvin Wickens. A family of poly(u) polymerases. *RNA*, 13(6):860–867, Jun 2007.

[12] Nicole L. Garneau, Jeffrey Wilusz, and Carol J. Wilusz. The highways and byways of mrna decay. *Nat Rev Mol Cell Biol*, 8(2):113–126, Feb 2007.

[13] Nikolaos A A. Balatsos, Per Nilsson, Catherine Mazza, Stephen Cusack, and Anders Virtanen. Inhibition of mrna deadenylation by the nuclear cap binding complex (cbc). *J Biol Chem*, 281(7):4517–4522, Feb 2006.

[14] Murat A. Cevher, Xiaokan Zhang, Sully Fernandez, Sergey Kim, Jorge Baquero, Per Nilsson, Sean Lee, Anders Virtanen, and Frida E. Kleiman. Nuclear deadenylation/polyadenylation factors regulate 3' processing in response to dna damage. *EMBO J*, 29(10):1674–1687, May 2010.

[15] Wi S. Lai, Elizabeth A. Kennington, and Perry J. Blackshear. Tristetraprolin and its family members can promote the cell-free deadenylation of au-rich element-containing mrnas by poly(a) ribonuclease. *Mol Cell Biol*, 23(11):3798–3812, Jun 2003.

[16] Karen C M. Moraes, Carol J. Wilusz, and Jeffrey Wilusz. Cug-bp binds to rna substrates and recruits parn deadenylase. *RNA*, 12(6):1084–1091, Jun 2006.

[17] Frank Bollig, Reinhard Winzen, Michael Kracht, Beniam Ghebremedhin, Birgit Ritter, Arno Wilhelm, Klaus Resch, and Helmut Holtmann. Evidence for general stabilization of mrnas in response to uv light. *Eur J Biochem*, 269(23):5830–5839, Dec 2002.

[18] Gayatri Gowrishankar, Reinhard Winzen, Frank Bollig, Beniam Ghebremedhin, Natalie Redich, Birgit Ritter, Klaus Resch, Michael Kracht, and Helmut Holtmann. Inhibition of mrna deadenylation and degradation by ultraviolet light. *Biol Chem*, 386(12):1287–1293, Dec 2005.

[19] C. Blattner, P. Kannouche, M. Litfin, K. Bender, H. J. Rahmsdorf, J. F. Angulo, and P. Herrlich. Uv-induced stabilization of c-fos and other short-lived mrnas. *Mol Cell Biol*, 20(10):3616–3625, May 2000.

[20] R. Boeck, S Tarun, Jr, M. Rieger, J. A. Deardorff, S. Müller-Auer, and A. B. Sachs. The yeast pan2 protein is required for poly(a)-binding protein-stimulated poly(a)-nuclease activity. *J Biol Chem*, 271(1):432–438, Jan 1996.

[21] C. E. Brown, SZ Tarun, Jr, R. Boeck, and A. B. Sachs. Pan3 encodes a subunit of the pab1p-dependent poly(a) nuclease in saccharomyces cerevisiae. *Mol Cell Biol*, 16(10):5744–5753, Oct 1996.

[22] J. E. Lowell, D. Z. Rudner, and A. B. Sachs. 3'-utr-dependent deadenylation by the yeast poly(a) nuclease. *Genes Dev*, 6(11):2088–2099, Nov 1992.

[23] Martine A. Collart and H Th Marc Timmers. The eukaryotic ccr4-not complex: a regulatory platform integrating mrna metabolism with cellular signaling pathways? *Prog Nucleic Acid Res Mol Biol*, 77:289–322, 2004.

[24] Olesya Panasenko, Emilie Landrieux, Marc Feuermann, Andrija Finka, Nicole Paquet, and Martine A. Collart. The yeast ccr4-not complex controls ubiquitination of the nascent-associated polypeptide (nac-egd) complex. *J Biol Chem*, 281(42):31389–31398, Oct 2006.

[25] Angela Schwede, Louise Ellis, Julia Luther, Mark Carrington, Georg Stoecklin, and Christine Clayton. A role for caf1 in mrna deadenyla-

tion and decay in trypanosomes and human cells. *Nucleic Acids Res*, 36(10):3374–3388, Jun 2008.

[26] D. Muhlrad, C. J. Decker, and R. Parker. Deadenylation of the unstable mrna encoded by the yeast mfa2 gene leads to decapping followed by 5'–>3' digestion of the transcript. *Genes Dev*, 8(7):855–866, Apr 1994.

[27] Michelle Steiger, Anne Carr-Schmid, David C. Schwartz, Megerditch Kiledjian, and Roy Parker. Analysis of recombinant yeast decapping enzyme. *RNA*, 9(2):231–238, Feb 2003.

[28] Katharina Rzeczkowski, Knut Beuerlein, Helmut Müller, Oliver Dittrich-Breiholz, Heike Schneider, Daniela Kettner-Buhrow, Helmut Holtmann, and Michael Kracht. c-jun n-terminal kinase phosphorylates dcp1a to control formation of p bodies. *J Cell Biol*, 194(4):581–596, Aug 2011.

[29] Je-Hyun Yoon, Eui-Ju Choi, and Roy Parker. Dcp2 phosphorylation by ste20 modulates stress granule assembly and mrna decay in saccharomyces cerevisiae. *J Cell Biol*, 189(5):813–827, May 2010.

[30] A. Stevens and T. L. Poole. 5'-exonuclease-2 of saccharomyces cerevisiae. purification and features of ribonuclease activity with comparison to 5'-exonuclease-1. *J Biol Chem*, 270(27):16063–16069, Jul 1995.

[31] Olivier Pellegrini, Nathalie Mathy, Ciarán Condon, and Lionel Bénard. In vitro assays of 5' to 3'-exoribonuclease activity. *Methods Enzymol*, 448:167–183, 2008.

[32] A. Stevens. 5'-exoribonuclease 1: Xrn1. *Methods Enzymol*, 342:251–259, 2001.

[33] Meenakshi K. Doma and Roy Parker. Endonucleolytic cleavage of eukaryotic mrnas with stalls in translation elongation. *Nature*, 440(7083):561–564, Mar 2006.

[34] Andrea B. Eberle, Søren Lykke-Andersen, Oliver Mühlemann, and Torben Heick Jensen. Smg6 promotes endonucleolytic cleavage of nonsense mrna in human cells. *Nat Struct Mol Biol*, 16(1):49–55, Jan 2009.

[35] David Gatfield and Elisa Izaurralde. Nonsense-mediated messenger rna decay is initiated by endonucleolytic cleavage in drosophila. *Nature*, 429(6991):575–578, Jun 2004.

[36] Eric Huntzinger, Isao Kashima, Maria Fauser, Jérôme Saulière, and Elisa Izaurralde. Smg6 is the catalytic endonuclease that cleaves mrnas containing nonsense codons in metazoan. *RNA*, 14(12):2609–2617, Dec 2008.

[37] Jidong Liu, Michelle A. Carmell, Fabiola V. Rivas, Carolyn G. Marsden, J Michael Thomson, Ji-Joon Song, Scott M. Hammond, Leemor Joshua-Tor, and Gregory J. Hannon. Argonaute2 is the catalytic engine of mammalian rnai. *Science*, 305(5689):1437–1441, Sep 2004.

[38] Javier Martinez and Thomas Tuschl. Risc is a 5' phosphomonoester-producing rna endonuclease. *Genes Dev*, 18(9):975–980, May 2004.

[39] Dianne S. Schwarz, Yukihide Tomari, and Phillip D. Zamore. The rna-induced silencing complex is a mg2+-dependent endonuclease. *Curr Biol*, 14(9):787–791, May 2004.

[40] C Y Chen, R Gherzi, S E Ong, E L Chan, R Raijmakers, G J Pruijn, G Stoecklin, C Moroni, M Mann, and M Karin. AU binding proteins recruit the exosome to degrade ARE-containing mRNAs. *Cell*, 107(4):451–64, November 2001.

[41] Wei-Jye Lin, Aaron Duffy, and Ching-Yi Chen. Localization of au-rich element-containing mrna in cytoplasmic granules containing exosome subunits. *J Biol Chem*, 282(27):19958–19968, Jul 2007.

[42] Fabrice Lejeune, Xiaojie Li, and Lynne E. Maquat. Nonsense-mediated mrna decay in mammalian cells involves decapping, deadenylating, and exonucleolytic activities. *Mol Cell*, 12(3):675–687, Sep 2003.

[43] Dinghai Zheng, Nader Ezzeddine, Chyi-Ying A. Chen, Wenmiao Zhu, Xiangwei He, and Ann-Bin Shyu. Deadenylation is prerequisite for p-body formation and mrna decay in mammalian cells. *J Cell Biol*, 182(1):89–101, Jul 2008.

[44] M. Tucker, M. A. Valencia-Sanchez, R. R. Staples, J. Chen, C. L. Denis, and R. Parker. The transcription factor associated ccr4 and caf1 proteins are components of the major cytoplasmic mrna deadenylase in saccharomyces cerevisiae. *Cell*, 104(3):377–386, Feb 2001.

[45] Nicolas Cougot, Sylvie Babajko, and Bertrand Séraphin. Cytoplasmic foci are sites of mrna decay in human cells. *J Cell Biol*, 165(1):31–40, Apr 2004.

[46] Claudia Temme, Sophie Zaessinger, Sylke Meyer, Martine Simonelig, and Elmar Wahle. A complex containing the ccr4 and caf1 proteins is involved in mrna deadenylation in drosophila. *EMBO J*, 23(14):2862–2871, Jul 2004.

[47] Claudia Temme, Lianbing Zhang, Elisabeth Kremmer, Christian Ihling, Aymeric Chartier, Andrea Sinz, Martine Simonelig, and Elmar Wahle. Subunits of the drosophila ccr4-not complex and their roles in mrna deadenylation. *RNA*, 16(7):1356–1370, Jul 2010.

[48] Denise Muhlrad and Roy Parker. The yeast edc1 mrna undergoes deadenylation-independent decapping stimulated by not2p, not4p, and not5p. *EMBO J*, 24(5):1033–1045, Mar 2005.

[49] Thomas K. Albert, Hiroyuki Hanzawa, Yvonne I A. Legtenberg, Marjolein J. de Ruwe, Fiona A J. van den Heuvel, Martine A. Collart,

Rolf Boelens, and H Th Marc Timmers. Identification of a ubiquitin-protein ligase subunit within the ccr4-not transcription repressor complex. *EMBO J*, 21(3):355–364, Feb 2002.

[50] Nader Ezzeddine, Tsung-Cheng Chang, Wenmiao Zhu, Akio Yamashita, Chyi-Ying A. Chen, Zhenping Zhong, Yukiko Yamashita, Dinghai Zheng, and Ann-Bin Shyu. Human tob, an antiproliferative transcription factor, is a poly(a)-binding protein-dependent positive regulator of cytoplasmic mrna deadenylation. *Mol Cell Biol*, 27(22):7791–7801, Nov 2007.

[51] C. G. Körner, M. Wormington, M. Muckenthaler, S. Schneider, E. Dehlin, and E. Wahle. The deadenylating nuclease (dan) is involved in poly(a) tail removal during the meiotic maturation of xenopus oocytes. *EMBO J*, 17(18):5427–5437, Sep 1998.

[52] Julie E. Baggs and Carla B. Green. Nocturnin, a deadenylase in xenopus laevis retina: a mechanism for posttranscriptional control of circadian-related mrna. *Curr Biol*, 13(3):189–198, Feb 2003.

[53] Zuoren Wang, Xinfu Jiao, Anne Carr-Schmid, and Megerditch Kiledjian. The hdcp2 protein is a mammalian mrna decapping enzyme. *Proc Natl Acad Sci U S A*, 99(20):12663–12668, Oct 2002.

[54] Dierk Ingelfinger, Donna J. Arndt-Jovin, Reinhard Lührmann, and Tilmann Achsel. The human lsm1-7 proteins colocalize with the mrna-degrading enzymes dcp1/2 and xrnl in distinct cytoplasmic foci. *RNA*, 8(12):1489–1501, Dec 2002.

[55] Erwin van Dijk, Nicolas Cougot, Sylke Meyer, Sylvie Babajko, Elmar Wahle, and Bertrand Séraphin. Human dcp2: a catalytically active mrna decapping enzyme located in specific cytoplasmic structures. *EMBO J*, 21(24):6915–6924, Dec 2002.

[56] Ujwal Sheth and Roy Parker. Decapping and decay of messenger rna occur in cytoplasmic processing bodies. *Science*, 300(5620):805–808, May 2003.

[57] Chia-ying Chu and Tariq M. Rana. Translation repression in human cells by microrna-induced gene silencing requires rck/p54. *PLoS Biol*, 4(7):e210, Jul 2006.

[58] Ana Eulalio, Isabelle Behm-Ansmant, Daniel Schweizer, and Elisa Izaurralde. P-body formation is a consequence, not the cause, of rna-mediated gene silencing. *Mol Cell Biol*, 27(11):3970–3981, Jun 2007.

[59] Anjon Audhya, Francie Hyndman, Ian X. McLeod, Amy S. Maddox, John R Yates, 3rd, Arshad Desai, and Karen Oegema. A complex containing the sm protein car-1 and the rna helicase cgh-1 is required for

embryonic cytokinesis in caenorhabditis elegans. *J Cell Biol*, 171(2):267–279, Oct 2005.

[60] Martin Fenger-Grøn, Christy Fillman, Bodil Norrild, and Jens Lykke-Andersen. Multiple processing body factors and the are binding protein ttp activate mrna decapping. *Mol Cell*, 20(6):905–915, Dec 2005.

[61] Carolyn J. Decker, Daniela Teixeira, and Roy Parker. Edc3p and a glutamine/asparagine-rich domain of lsm4p function in processing body assembly in saccharomyces cerevisiae. *J Cell Biol*, 179(3):437–449, Nov 2007.

[62] Jiang Hong Yu, Wei-Hong Yang, Tod Gulick, Kenneth D. Bloch, and Donald B. Bloch. Ge-1 is a central component of the mammalian cytoplasmic mrna processing body. *RNA*, 11(12):1795–1802, Dec 2005.

[63] Nancy Kedersha, Georg Stoecklin, Maranatha Ayodele, Patrick Yacono, Jens Lykke-Andersen, Marvin J Fritzler, Donalyn Scheuner, Randal J Kaufman, David E Golan, and Paul Anderson. Stress granules and processing bodies are dynamically linked sites of mRNP remodeling. *The Journal of cell biology*, 169(6):871–84, June 2005.

[64] Georg Stoecklin, Thomas Mayo, and Paul Anderson. Are-mrna degradation requires the 5'-3' decay pathway. *EMBO Rep*, 7(1):72–77, Jan 2006.

[65] Nicoletta Scheller, Patricia Resa-Infante, Susana de la Luna, Rui Pedro Galao, Mario Albrecht, Lars Kaestner, Peter Lipp, Thomas Lengauer, Andreas Meyerhans, and Juana Díez. Identification of patl1, a human homolog to yeast p body component pat1. *Biochim Biophys Acta*, 1773(12):1786–1792, Dec 2007.

[66] Gabrielle Haas, Joerg E. Braun, Cátia Igreja, Felix Tritschler, Tadashi Nishihara, and Elisa Izaurralde. Hpat provides a link between deadenylation and decapping in metazoa. *J Cell Biol*, 189(2):289–302, Apr 2010.

[67] Sevim Ozgur, Marina Chekulaeva, and Georg Stoecklin. Human pat1b connects deadenylation with mrna decapping and controls the assembly of processing bodies. *Mol Cell Biol*, 30(17):4308–4323, Sep 2010.

[68] Joerg E. Braun, Felix Tritschler, Gabrielle Haas, Cátia Igreja, Vincent Truffault, Oliver Weichenrieder, and Elisa Izaurralde. The c-terminal alpha-alpha superhelix of pat is required for mrna decapping in metazoa. *EMBO J*, 29(14):2368–2380, Jul 2010.

[69] Tadanori Yamochi, Kei Ohnuma, Osamu Hosono, Hirotoshi Tanaka, Yoshiyuki Kanai, and Chikao Morimoto. Ssa/ro52 autoantigen inter-

acts with dcp2 to enhance its decapping activity. *Biochem Biophys Res Commun*, 370(1):195–199, May 2008.

[70] Man-Gen Song, You Li, and Megerditch Kiledjian. Multiple mrna decapping enzymes in mammalian cells. *Mol Cell*, 40(3):423–432, Nov 2010.

[71] Brenda A. Peculis, Kristen Reynolds, and Megan Cleland. Metal determines efficiency and substrate specificity of the nuclear nudix decapping proteins x29 and h29k (nudt16). *J Biol Chem*, 282(34):24792–24805, Aug 2007.

[72] V. I. Bashkirov, H. Scherthan, J. A. Solinger, J. M. Buerstedde, and W. D. Heyer. A mouse cytoplasmic exoribonuclease (mxrn1p) with preference for g4 tetraplex substrates. *J Cell Biol*, 136(4):761–773, Feb 1997.

[73] Maria V. Zabolotskaya, Dominic P. Grima, Ming-Der Lin, Tze-Bin Chou, and Sarah F. Newbury. The 5'-3' exoribonuclease pacman is required for normal male fertility and is dynamically localized in cytoplasmic particles in drosophila testis cells. *Biochem J*, 416(3):327–335, Dec 2008.

[74] Steven West, Natalia Gromak, and Nick J. Proudfoot. Human 5' –> 3' exonuclease xrn2 promotes transcription termination at co-transcriptional cleavage sites. *Nature*, 432(7016):522–525, Nov 2004.

[75] Minshi Wang and Dimitri G. Pestov. 5'-end surveillance by xrn2 acts as a shared mechanism for mammalian pre-rrna maturation and decay. *Nucleic Acids Res*, 39(5):1811–1822, Mar 2011.

[76] Claudia Schneider, Eileen Leung, Jeremy Brown, and David Tollervey. The n-terminal pin domain of the exosome subunit rrp44 harbors endonuclease activity and tethers rrp44 to the yeast core exosome. *Nucleic Acids Res*, 37(4):1127–1140, Mar 2009.

[77] Alice Lebreton, Rafal Tomecki, Andrzej Dziembowski, and Bertrand Séraphin. Endonucleolytic rna cleavage by a eukaryotic exosome. *Nature*, 456(7224):993–996, Dec 2008.

[78] P. Mitchell, E. Petfalski, A. Shevchenko, M. Mann, and D. Tollervey. The exosome: a conserved eukaryotic rna processing complex containing multiple 3'–>5' exoribonucleases. *Cell*, 91(4):457–466, Nov 1997.

[79] Raymond H J. Staals, Alfred W. Bronkhorst, Geurt Schilders, Shimyn Slomovic, Gadi Schuster, Albert J R. Heck, Reinout Raijmakers, and Ger J M. Pruijn. Dis3-like 1: a novel exoribonuclease associated with the human exosome. *EMBO J*, 29(14):2358–2367, Jul 2010.

[80] Amy C. Graham, Daniel L. Kiss, and Erik D. Andrulis. Differential distribution of exosome subunits at the nuclear lamina and in cytoplasmic foci. *Mol Biol Cell*, 17(3):1399–1409, Mar 2006.

[81] Jidong Liu, Marco Antonio Valencia-Sanchez, Gregory J. Hannon, and Roy Parker. Microrna-dependent localization of targeted mrnas to mammalian p-bodies. *Nat Cell Biol*, 7(7):719–723, Jul 2005.

[82] George L. Sen and Helen M. Blau. Argonaute 2/risc resides in sites of mammalian mrna decay known as cytoplasmic bodies. *Nat Cell Biol*, 7(6):633–636, Jun 2005.

[83] Justin M. Pare, Nasser Tahbaz, Joaquín López-Orozco, Paul LaPointe, Paul Lasko, and Tom C. Hobman. Hsp90 regulates the function of argonaute 2 and its recruitment to stress granules and p-bodies. *Mol Biol Cell*, 20(14):3273–3284, Jul 2009.

[84] Anthony K L. Leung, J Mauro Calabrese, and Phillip A. Sharp. Quantitative analysis of argonaute protein reveals microrna-dependent localization to stress granules. *Proc Natl Acad Sci U S A*, 103(48):18125–18130, Nov 2006.

[85] P. D. Zamore, T. Tuschl, P. A. Sharp, and D. P. Bartel. Rnai: double-stranded rna directs the atp-dependent cleavage of mrna at 21 to 23 nucleotide intervals. *Cell*, 101(1):25–33, Mar 2000.

[86] Sébastien Durand, Nicolas Cougot, Florence Mahuteau-Betzer, Chi-Hung Nguyen, David S. Grierson, Edouard Bertrand, Jamal Tazi, and Fabrice Lejeune. Inhibition of nonsense-mediated mrna decay (nmd) by a new chemical molecule reveals the dynamic of nmd factors in p-bodies. *J Cell Biol*, 178(7):1145–1160, Sep 2007.

[87] Kazufumi Matsushita, Osamu Takeuchi, Daron M. Standley, Yutaro Kumagai, Tatsukata Kawagoe, Tohru Miyake, Takashi Satoh, Hiroki Kato, Tohru Tsujimura, Haruki Nakamura, and Shizuo Akira. Zc3h12a is an rnase essential for controlling immune responses by regulating mrna decay. *Nature*, 458(7242):1185–1190, Apr 2009.

[88] J Ross Buchan and Roy Parker. Eukaryotic Stress Granules : The Ins and Out of Translation What are Stress Granules ? *Molecular and Cellular Biology*, 36(6), 2009.

[89] Ujwal Sheth and Roy Parker. Targeting of aberrant mrnas to cytoplasmic processing bodies. *Cell*, 125(6):1095–1109, Jun 2006.

[90] Leonie Unterholzner and Elisa Izaurralde. Smg7 acts as a molecular link between mrna surveillance and mrna decay. *Mol Cell*, 16(4):587–596, Nov 2004.

[91] Georg Stoecklin and Paul Anderson. In a tight spot: Are-mrnas at processing bodies. *Genes Dev*, 21(6):627–631, Mar 2007.

[92] Jacob Blumenthal and Irith Ginzburg. Zinc as a translation regulator in neurons: implications for p-body aggregation. *J Cell Sci*, 121(Pt 19):3253–3260, Oct 2008.

[93] Theophany Eystathioy, Andrew Jakymiw, Edward K L. Chan, Bertrand Séraphin, Nicolas Cougot, and Marvin J. Fritzler. The gw182 protein colocalizes with mrna degradation associated proteins hdcp1 and hlsm4 in cytoplasmic gw bodies. *RNA*, 9(10):1171–1173, Oct 2003.

[94] Gunter Meister, Markus Landthaler, Lasse Peters, Po Yu Chen, Henning Urlaub, Reinhard Lührmann, and Thomas Tuschl. Identification of novel argonaute-associated proteins. *Curr Biol*, 15(23):2149–2155, Dec 2005.

[95] Lukas Stalder and Oliver Mühlemann. Processing bodies are not required for mammalian nonsense-mediated mrna decay. *RNA*, 15(7):1265–1273, Jul 2009.

[96] Muriel Brengues, Daniela Teixeira, and Roy Parker. Movement of eukaryotic mrnas between polysomes and cytoplasmic processing bodies. *Science*, 310(5747):486–489, Oct 2005.

[97] Jong-Hwan Jung and Jinmi Kim. Accumulation of p-bodies in candida albicans under different stress and filamentous growth conditions. *Fungal Genet Biol*, 48(12):1116–1123, Dec 2011.

[98] Guy R. Pilkington and Roy Parker. Pat1 contains distinct functional domains that promote p-body assembly and activation of decapping. *Mol Cell Biol*, 28(4):1298–1312, Feb 2008.

[99] Martin A M. Reijns, Ross D. Alexander, Michael P. Spiller, and Jean D. Beggs. A role for q/n-rich aggregation-prone regions in p-body localization. *J Cell Sci*, 121(Pt 15):2463–2472, Aug 2008.

[100] Jonathan D. Dougherty, James P. White, and Richard E. Lloyd. Poliovirus-mediated disruption of cytoplasmic processing bodies. *J Virol*, 85(1):64–75, Jan 2011.

[101] Adva Aizer, Yehuda Brody, Lian Wee Ler, Nahum Sonenberg, Robert H. Singer, and Yaron Shav-Tal. The dynamics of mammalian p body transport, assembly, and disassembly in vivo. *Mol Biol Cell*, 19(10):4154–4166, Oct 2008.

[102] Paul Anderson and Nancy Kedersha. Rna granules: post-transcriptional and epigenetic modulators of gene expression. *Nat Rev Mol Cell Biol*, 10(6):430–436, Jun 2009.

[103] G. Laroia, R. Cuesta, G. Brewer, and R. J. Schneider. Control of mrna decay by heat shock-ubiquitin-proteasome pathway. *Science*, 284(5413):499–502, Apr 1999.

[104] Valérie Hilgers, Daniela Teixeira, and Roy Parker. Translation-independent inhibition of mrna deadenylation during stress in saccharomyces cerevisiae. *RNA*, 12(10):1835–1845, Oct 2006.

[105] Gayatri Gowrishankar, Reinhard Winzen, Oliver Dittrich-Breiholz, Natalie Redich, Michael Kracht, and Helmut Holtmann. Inhibition of mrna deadenylation and degradation by different types of cell stress. *Biol Chem*, 387(3):323–327, Mar 2006.

[106] N. Kedersha and P. Anderson. Stress granules: sites of mrna triage that regulate mrna stability and translatability. *Biochem Soc Trans*, 30(Pt 6):963–969, Nov 2002.

[107] Rammohan Narayanaswamy, Matthew Levy, Mark Tsechansky, Gwendolyn M. Stovall, Jeremy D. O'Connell, Jennifer Mirrielees, Andrew D. Ellington, and Edward M. Marcotte. Widespread reorganization of metabolic enzymes into reversible assemblies upon nutrient starvation. *Proc Natl Acad Sci U S A*, 106(25):10147–10152, Jun 2009.

[108] Mong-Hong Lee and Guillermina Lozano. Regulation of the p53-mdm2 pathway by 14-3-3 sigma and other proteins. *Semin Cancer Biol*, 16(3):225–234, Jun 2006.

[109] Ken Fujimura, Fumi Kano, and Masayuki Murata. Identification of pcbp2, a facilitator of ires-mediated translation, as a novel constituent of stress granules and processing bodies. *RNA*, 14(3):425–431, Mar 2008.

[110] Sophie Bonnal, Frédéric Pileur, Cécile Orsini, Fabienne Parker, Françoise Pujol, Anne-Catherine Prats, and Stéphan Vagner. Heterogeneous nuclear ribonucleoprotein a1 is a novel internal ribosome entry site trans-acting factor that modulates alternative initiation of translation of the fibroblast growth factor 2 mrna. *J Biol Chem*, 280(6):4144–4153, Feb 2005.

[111] Kristin M. Bedard, Brandon L. Walter, and Bert L. Semler. Multimerization of poly(rc) binding protein 2 is required for translation initiation mediated by a viral ires. *RNA*, 10(8):1266–1276, Aug 2004.

[112] Kyoko Arimoto, Hiroyuki Fukuda, Shinobu Imajoh-Ohmi, Haruo Saito, and Mutsuhiro Takekawa. Formation of stress granules inhibits apoptosis by suppressing stress-responsive mapk pathways. *Nat Cell Biol*, 10(11):1324–1332, Nov 2008.

[113] Rebekka Weissbach and A D J. Scadden. Tudor-sn and adar1 are components of cytoplasmic stress granules. *RNA*, 18(3):462–471, Mar 2012.

[114] R. C. Wek, H-Y. Jiang, and T. G. Anthony. Coping with stress: eif2 kinases and translational control. *Biochem Soc Trans*, 34(Pt 1):7–11, Feb 2006.

[115] Georg Stoecklin, Tiffany Stubbs, Nancy Kedersha, Stephen Wax, William F C. Rigby, T Keith Blackwell, and Paul Anderson. Mk2-induced tristetraprolin:14-3-3 complexes prevent stress granule association and are-mrna decay. *EMBO J*, 23(6):1313–1324, Mar 2004.

[116] Martin Schmidlin, Min Lu, Sabrina A. Leuenberger, Georg Stoecklin, Michel Mallaun, Brigitte Gross, Roberto Gherzi, Daniel Hess, Brian A. Hemmings, and Christoph Moroni. The are-dependent mrna-destabilizing activity of brf1 is regulated by protein kinase b. *EMBO J*, 23(24):4760–4769, Dec 2004.

[117] I. E. Gallouzi, F. Parker, K. Chebli, F. Maurier, E. Labourier, I. Barlat, J. P. Capony, B. Tocque, and J. Tazi. A novel phosphorylation-dependent rnase activity of gap-sh3 binding protein: a potential link between signal transduction and rna stability. *Mol Cell Biol*, 18(7):3956–3965, Jul 1998.

[118] H. Tourrière, I. E. Gallouzi, K. Chebli, J. P. Capony, J. Mouaikel, P. van der Geer, and J. Tazi. Rasgap-associated endoribonuclease g3bp: selective rna degradation and phosphorylation-dependent localization. *Mol Cell Biol*, 21(22):7747–7760, Nov 2001.

[119] Helene Tourrière, Karim Chebli, Latifa Zekri, Brice Courselaud, Jean Marie Blanchard, Edouard Bertrand, and Jamal Tazi. The rasgap-associated endoribonuclease g3bp assembles stress granules. *J Cell Biol*, 160(6):823–831, Mar 2003.

[120] Takbum Ohn, Nancy Kedersha, Tyler Hickman, Sarah Tisdale, and Paul Anderson. A functional rnai screen links o-glcnac modification of ribosomal proteins to stress granule and processing body assembly. *Nat Cell Biol*, 10(10):1224–1231, Oct 2008.

[121] Sohee Kwon, Yu Zhang, and Patrick Matthias. The deacetylase hdac6 is a novel critical component of stress granules involved in the stress response. *Genes Dev*, 21(24):3381–3394, Dec 2007.

[122] Frederic De Leeuw, Tong Zhang, Corinne Wauquier, Georges Huez, Véronique Kruys, and Cyril Gueydan. The cold-inducible rna-binding protein migrates from the nucleus to cytoplasmic stress granules by a methylation-dependent mechanism and acts as a translational repressor. *Exp Cell Res*, 313(20):4130–4144, Dec 2007.

[123] Isabelle Goulet, Sophie Boisvenue, Sophie Mokas, Rachid Mazroui, and Jocelyn Côté. Tdrd3, a novel tudor domain-containing protein, localizes to cytoplasmic stress granules. *Hum Mol Genet*, 17(19):3055–3074, Oct 2008.

[124] Wen Xie and Robert B. Denman. Protein methylation and stress granules: posttranslational remodeler or innocent bystander? *Mol Biol Int*, 2011:137459, 2011.

[125] Natalie Gilks, Nancy Kedersha, Maranatha Ayodele, Lily Shen, Georg Stoecklin, Laura M. Dember, and Paul Anderson. Stress granule assembly is mediated by prion-like aggregation of tia-1. *Mol Biol Cell*, 15(12):5383–5398, Dec 2004.

[126] Eugene G. Rikhvanov, Nina V. Romanova, and Yury O. Chernoff. Chaperone effects on prion and nonprion aggregates. *Prion*, 1(4):217–222, 2007.

[127] Pavel A. Ivanov, Elena M. Chudinova, and Elena S. Nadezhdina. Disruption of microtubules inhibits cytoplasmic ribonucleoprotein stress granule formation. *Exp Cell Res*, 290(2):227–233, Nov 2003.

[128] Elena Kolobova, Andrey Efimov, Irina Kaverina, Arun K. Rishi, John W. Schrader, Amy-Joan Ham, M Cecilia Larocca, and James R. Goldenring. Microtubule-dependent association of akap350a and ccar1 with rna stress granules. *Exp Cell Res*, 315(3):542–555, Feb 2009.

[129] Ken Fujimura, Jun Katahira, Fumi Kano, Yoshihiro Yoneda, and Masayuki Murata. Microscopic dissection of the process of stress granule assembly. *Biochim Biophys Acta*, 1793(11):1728–1737, Nov 2009.

[130] Mariela Loschi, Claudia C. Leishman, Neda Berardone, and Graciela L. Boccaccio. Dynein and kinesin regulate stress-granule and p-body dynamics. *J Cell Sci*, 122(Pt 21):3973–3982, Nov 2009.

[131] Rachid Mazroui, Sergio Di Marco, Randal J. Kaufman, and Imed-Eddine Gallouzi. Inhibition of the ubiquitin-proteasome system induces stress granule formation. *Mol Biol Cell*, 18(7):2603–2618, Jul 2007.

[132] María Gabriela Thomas, Leandro J. Martinez Tosar, María Andrea Desbats, Claudia C. Leishman, and Graciela L. Boccaccio. Mammalian staufen 1 is recruited to stress granules and impairs their assembly. *J Cell Sci*, 122(Pt 4):563–573, Feb 2009.

[133] Nien-Pei Tsai, Ping-Chih Ho, and Li-Na Wei. Regulation of stress granule dynamics by grb7 and fak signalling pathway. *EMBO J*, 27(5):715–726, Mar 2008.

[134] Daniel Nilsson and Per Sunnerhagen. Cellular stress induces cytoplasmic rna granules in fission yeast. *RNA*, 17(1):120–133, Jan 2011.

[135] J Ross Buchan, Denise Muhlrad, and Roy Parker. P bodies promote stress granule assembly in saccharomyces cerevisiae. *J Cell Biol*, 183(3):441–455, Nov 2008.

[136] Anason S. Halees, Rashad El-Badrawi, and Khalid S A. Khabar. Ared organism: expansion of ared reveals au-rich element cluster variations between human and mouse. *Nucleic Acids Res*, 36(Database issue):D137–D140, Jan 2008.

[137] C. Y. Chen and A. B. Shyu. Au-rich elements: characterization and importance in mrna degradation. *Trends Biochem Sci*, 20(11):465–470, Nov 1995.

[138] C. A. Lagnado, C. Y. Brown, and G. J. Goodall. Auuua is not sufficient to promote poly(a) shortening and degradation of an mrna: the functional sequence within au-rich elements may be uuauuua(u/a)(u/a). *Mol Cell Biol*, 14(12):7984–7995, Dec 1994.

[139] T. Lewis, C. Gueydan, G. Huez, J. J. Toulmé, and V. Kruys. Mapping of a minimal au-rich sequence required for lipopolysaccharide-induced binding of a 55-kda protein on tumor necrosis factor-alpha mrna. *J Biol Chem*, 273(22):13781–13786, May 1998.

[140] A. M. Zubiaga, J. G. Belasco, and M. E. Greenberg. The nonamer uuauuuauu is the key au-rich sequence motif that mediates mrna degradation. *Mol Cell Biol*, 15(4):2219–2230, Apr 1995.

[141] Wi S. Lai, Danielle M. Carrick, and Perry J. Blackshear. Influence of nonameric au-rich tristetraprolin-binding sites on mrna deadenylation and turnover. *J Biol Chem*, 280(40):34365–34377, Oct 2005.

[142] T. Bakheet, M. Frevel, B. R. Williams, W. Greer, and K. S. Khabar. Ared: human au-rich element-containing mrna database reveals an unexpectedly diverse functional repertoire of encoded proteins. *Nucleic Acids Res*, 29(1):246–254, Jan 2001.

[143] Perry J. Blackshear, Wi S. Lai, Elizabeth A. Kennington, Gary Brewer, Gerald M. Wilson, Xiaoju Guan, and Pei Zhou. Characteristics of the interaction of a synthetic human tristetraprolin tandem zinc finger peptide with au-rich element-containing rna substrates. *J Biol Chem*, 278(22):19947–19955, May 2003.

[144] Mathias A E. Frevel, Tala Bakheet, Aristobolo M. Silva, John G. Hissong, Khalid S A. Khabar, and Bryan R G. Williams. p38 mitogen-activated protein kinase-dependent and -independent signaling of mrna stability of au-rich element-containing transcripts. *Mol Cell Biol*, 23(2):425–436, Jan 2003.

[145] Arvind Raghavan, Mohammed Dhalla, Tala Bakheet, Rachel L. Ogilvie, Irina A. Vlasova, Khalid S A. Khabar, Bryan R G. Williams, and Paul R. Bohjanen. Patterns of coordinate down-regulation of are-containing transcripts following immune cell activation. *Genomics*, 84(6):1002–1013, Dec 2004.

[146] Debashish Ray, Hilal Kazan, Esther T. Chan, Lourdes Peña Castillo, Sidharth Chaudhry, Shaheynoor Talukder, Benjamin J. Blencowe, Quaid Morris, and Timothy R. Hughes. Rapid and systematic analysis of the

rna recognition specificities of rna-binding proteins. *Nat Biotechnol*, 27(7):667–670, Jul 2009.

[147] Nicole-Claudia Meisner, Jörg Hackermüller, Volker Uhl, András Aszódi, Markus Jaritz, and Manfred Auer. mrna openers and closers: modulating au-rich element-controlled mrna stability by a molecular switch in mrna secondary structure. *Chembiochem*, 5(10):1432–1447, Oct 2004.

[148] Jörg Hackermüller, Nicole-Claudia Meisner, Manfred Auer, Markus Jaritz, and Peter F. Stadler. The effect of rna secondary structures on rna-ligand binding and the modifier rna mechanism: a quantitative model. *Gene*, 345(1):3–12, Jan 2005.

[149] Isabel López de Silanes, Ming Zhan, Ashish Lal, Xiaoling Yang, and Myriam Gorospe. Identification of a target rna motif for rna-binding protein hur. *Proc Natl Acad Sci U S A*, 101(9):2987–2992, Mar 2004.

[150] Sungmin Park-Lee, Soyoun Kim, and Ite A. Laird-Offringa. Characterization of the interaction between neuronal rna-binding protein hud and au-rich rna. *J Biol Chem*, 278(41):39801–39808, Oct 2003.

[151] Brandy Y. Brewer, Joanna Malicka, Perry J. Blackshear, and Gerald M. Wilson. Rna sequence elements required for high affinity binding by the zinc finger domain of tristetraprolin: conformational changes coupled to the bipartite nature of au-rich mrna-destabilizing motifs. *J Biol Chem*, 279(27):27870–27877, Jul 2004.

[152] Mark T. Worthington, Jared W. Pelo, Muhammadreza A. Sachedina, Joan L. Applegate, Kristen O. Arseneau, and Theresa T. Pizarro. Rna binding properties of the au-rich element-binding recombinant nup475/tis11/tristetraprolin protein. *J Biol Chem*, 277(50):48558–48564, Dec 2002.

[153] Fahad Al-Zoghaibi, Tareef Ashour, Wijdan Al-Ahmadi, Hana Abulleef, Omar Demirkaya, and Khalid S A. Khabar. Bioinformatics and experimental derivation of an efficient hybrid 3' untranslated region and use in expression active linear dna with minimum poly(a) region. *Gene*, 391(1-2):130–139, Apr 2007.

[154] Neelanjan Mukherjee, Patrick J. Lager, Matthew B. Friedersdorf, Marshall A. Thompson, and Jack D. Keene. Coordinated posttranscriptional mrna population dynamics during t-cell activation. *Mol Syst Biol*, 5:288, 2009.

[155] Georg Stoecklin, Scott a Tenenbaum, Thomas Mayo, Sridar V Chittur, Ajish D George, Timothy E Baroni, Perry J Blackshear, and Paul Anderson. Genome-wide analysis identifies interleukin-10 mRNA as target of tristetraprolin. *The Journal of biological chemistry*, 283(17):11689–99, April 2008.

[156] Qing Jing, Shuang Huang, Sabine Guth, Tyler Zarubin, Andrea Motoyama, Jianming Chen, Franco Di Padova, Sheng-Cai Lin, Hermann Gram, and Jiahuai Han. Involvement of microRNA in AU-rich element-mediated mRNA instability. *Cell*, 120(5):623–34, March 2005.

[157] Carine Barreau, Luc Paillard, and H Beverley Osborne. Au-rich elements and associated factors: are there unifying principles? *Nucleic Acids Res*, 33(22):7138–7150, 2005.

[158] P. J. Good, Q. Chen, S. J. Warner, and D. C. Herring. A family of human rna-binding proteins related to the drosophila bruno translational regulator. *J Biol Chem*, 275(37):28583–28592, Sep 2000.

[159] X. C. Fan and J. A. Steitz. Overexpression of hur, a nuclear-cytoplasmic shuttling protein, increases the in vivo stability of are-containing mrnas. *EMBO J*, 17(12):3448–3460, Jun 1998.

[160] X. C. Fan and J. A. Steitz. Hns, a nuclear-cytoplasmic shuttling sequence in hur. *Proc Natl Acad Sci U S A*, 95(26):15293–15298, Dec 1998.

[161] I. E. Gallouzi and J. A. Steitz. Delineation of mrna export pathways by the use of cell-permeable peptides. *Science*, 294(5548):1895–1901, Nov 2001.

[162] D. Antic and J. D. Keene. Embryonic lethal abnormal visual rna-binding proteins involved in growth, differentiation, and posttranscriptional gene expression. *Am J Hum Genet*, 61(2):273–278, Aug 1997.

[163] Zhu Yuan, Andrew J. Sanders, Lin Ye, Yu Wang, and Wen G. Jiang. Knockdown of human antigen r reduces the growth and invasion of breast cancer cells in vitro and affects expression of cyclin d1 and mmp-9. *Oncol Rep*, 26(1):237–245, Jul 2011.

[164] Kyle D. Mansfield and Jack D. Keene. Neuron-specific elav/hu proteins suppress hur mrna during neuronal differentiation by alternative polyadenylation. *Nucleic Acids Res*, Dec 2011.

[165] Sudha Talwar, Junfei Jin, Brittany Carroll, Angen Liu, Marion Boyd Gillespie, and Viswanathan Palanisamy. Caspase-mediated cleavage of rna-binding protein hur regulates c-myc protein expression after hypoxic stress. *J Biol Chem*, 286(37):32333–32343, Sep 2011.

[166] Rachid Mazroui, Sergio Di Marco, Eveline Clair, Christopher von Roretz, Scott A. Tenenbaum, Jack D. Keene, Maya Saleh, and Imed-Eddine Gallouzi. Caspase-mediated cleavage of hur in the cytoplasm contributes to pp32/phap-i regulation of apoptosis. *J Cell Biol*, 180(1):113–127, Jan 2008.

[167] Na Chang, Jie Yi, Gaier Guo, Xinwen Liu, Yongfeng Shang, Tanjun Tong, Qinghua Cui, Ming Zhan, Myriam Gorospe, and Wengong Wang.

Hur uses auf1 as a cofactor to promote p16ink4 mrna decay. *Mol Cell Biol*, 30(15):3875–3886, Aug 2010.

[168] C. Zheng and Bj Baum. Including the p53 elav-like protein-binding site in vector cassettes enhances transgene expression in rat submandibular gland. *Oral Dis*, Dec 2011.

[169] G. M. Wilson and G. Brewer. The search for trans-acting factors controlling messenger rna decay. *Prog Nucleic Acid Res Mol Biol*, 62:257–291, 1999.

[170] A. Sela-Brown, J. Silver, G. Brewer, and T. Naveh-Many. Identification of auf1 as a parathyroid hormone mrna 3'-untranslated region-binding protein that determines parathyroid hormone mrna stability. *J Biol Chem*, 275(10):7424–7429, Mar 2000.

[171] Ines Raineri, Daniel Wegmueller, Brigitte Gross, Ulrich Certa, and Christoph Moroni. Roles of auf1 isoforms, hur and brf1 in are-dependent mrna turnover studied by rna interference. *Nucleic Acids Res*, 32(4):1279–1288, 2004.

[172] N. Xu, C. Y. Chen, and A. B. Shyu. Versatile role for hnrnp d isoforms in the differential regulation of cytoplasmic mrna turnover. *Mol Cell Biol*, 21(20):6960–6971, Oct 2001.

[173] Vishram P. Kedar, Beth E. Zucconi, Gerald M. Wilson, and Perry J. Blackshear. Direct binding of specific auf1 isoforms to the tandem zinc finger domains of tristetraprolin (ttp) family proteins. *J Biol Chem*, Dec 2011.

[174] Hong Xin, Julie A. Brown, Changning Gong, Hao Fan, Gary Brewer, and James R. Gnarra. Association of the von hippel-lindau protein with auf1 and posttranscriptional regulation of vegfa mrna. *Mol Cancer Res*, 10(1):108–120, Jan 2012.

[175] Jin-Yu Lu, Navid Sadri, and Robert J. Schneider. Endotoxic shock in auf1 knockout mice mediated by failure to degrade proinflammatory cytokine mrnas. *Genes Dev*, 20(22):3174–3184, Nov 2006.

[176] B C Varnum, Q F Ma, T H Chi, B Fletcher, and H R Herschman. The TIS11 primary response gene is a member of a gene family that encodes proteins with a highly conserved sequence containing an unusual Cys-His repeat. *Molecular and cellular biology*, 11(3):1754–8, March 1991.

[177] Wi S Lai, Elizabeth a Kennington, and Perry J Blackshear. Interactions of CCCH zinc finger proteins with mRNA: non-binding tristetraprolin mutants exert an inhibitory effect on degradation of AU-rich element-containing mRNAs. *The Journal of biological chemistry*, 277(11):9606–13, March 2002.

[178] B. A. Johnson, M. Geha, and T. K. Blackwell. Similar but distinct effects of the tristetraprolin/tis11 immediate-early proteins on cell survival. *Oncogene*, 19(13):1657–1664, Mar 2000.

[179] Jens Lykke-Andersen and Eileen Wagner. Recruitment and activation of mRNA decay enzymes by two ARE-mediated decay activation domains in the proteins TTP and BRF-1. *Genes & development*, 19(3):351–61, February 2005.

[180] Perry J Blackshear, Ruth S Phillips, Sanjukta Ghosh, Silvia B V Ramos, Silvia V B Ramos, Eric K Richfield, and Wi S Lai. Zfp36l3, a rodent X chromosome gene encoding a placenta-specific member of the Tristetraprolin family of CCCH tandem zinc finger proteins. *Biology of reproduction*, 73(2):297–307, August 2005.

[181] Heping Cao, Joseph F Urban, and Richard a Anderson. Insulin increases tristetraprolin and decreases VEGF gene expression in mouse 3T3-L1 adipocytes. *Obesity (Silver Spring, Md.)*, 16(6):1208–18, June 2008.

[182] Ruth S Phillips, Silvia B V Ramos, and Perry J Blackshear. Members of the tristetraprolin family of tandem CCCH zinc finger proteins exhibit CRM1-dependent nucleocytoplasmic shuttling. *The Journal of biological chemistry*, 277(13):11606–13, March 2002.

[183] W. S. Lai, D. J. Stumpo, and P. J. Blackshear. Rapid insulin-stimulated accumulation of an mrna encoding a proline-rich protein. *J Biol Chem*, 265(27):16556–16563, Sep 1990.

[184] R. N. DuBois, M. W. McLane, K. Ryder, L. F. Lau, and D. Nathans. A growth factor-inducible nuclear protein with a novel cysteine/histidine repetitive sequence. *J Biol Chem*, 265(31):19185–19191, Nov 1990.

[185] Danielle M Carrick, Wi S Lai, and Perry J Blackshear. The tandem CCCH zinc finger protein tristetraprolin and its relevance to cytokine mRNA turnover and arthritis. *Arthritis research & therapy*, 6(6):248–64, January 2004.

[186] Wi S. Lai, Joel S. Parker, Sherry F. Grissom, Deborah J. Stumpo, and Perry J. Blackshear. Novel mrna targets for tristetraprolin (ttp) identified by global analysis of stabilized transcripts in ttp-deficient fibroblasts. *Mol Cell Biol*, 26(24):9196–9208, Dec 2006.

[187] Carmen R. Tchen, Matthew Brook, Jeremy Saklatvala, and Andrew R. Clark. The stability of tristetraprolin mrna is regulated by mitogen-activated protein kinase p38 and by tristetraprolin itself. *J Biol Chem*, 279(31):32393–32400, Jul 2004.

[188] Seth A. Brooks, John E. Connolly, and William F C. Rigby. The role of mrna turnover in the regulation of tristetraprolin expression: evidence

for an extracellular signal-regulated kinase-specific, au-rich element-dependent, autoregulatory pathway. *J Immunol*, 172(12):7263–7271, Jun 2004.

[189] Kai Yin, Xiang Deng, Zhong-Cheng Mo, Guo-Jun Zhao, Jin Jiang, Li-Bao Cui, Chun-Zhi Tan, Ge-Bo Wen, Yuchang Fu, and Chao-Ke Tang. Tristetraprolin-dependent post-transcriptional regulation of inflammatory cytokine mrna expression by apolipoprotein a-i: role of atp-binding membrane cassette transporter a1 and signal transducer and activator of transcription 3. *J Biol Chem*, 286(16):13834–13845, Apr 2011.

[190] G a Taylor, E Carballo, D M Lee, W S Lai, M J Thompson, D D Patel, D I Schenkman, G S Gilkeson, H E Broxmeyer, B F Haynes, and P J Blackshear. A pathogenetic role for TNF alpha in the syndrome of cachexia, arthritis, and autoimmunity resulting from tristetraprolin (TTP) deficiency. *Immunity*, 4(5):445–54, May 1996.

[191] Ian M. Kaplan, Sebastien Morisot, Diane Heiser, Wen-Chih Cheng, Min Jung Kim, and Curt I. Civin. Deletion of tristetraprolin caused spontaneous reactive granulopoiesis by a non-cell-autonomous mechanism without disturbing long-term hematopoietic stem cell quiescence. *J Immunol*, 186(5):2826–2834, Mar 2011.

[192] Wi S. Lai, Elizabeth A. Kennington, and Perry J. Blackshear. Interactions of ccch zinc finger proteins with mrna: non-binding tristetraprolin mutants exert an inhibitory effect on degradation of au-rich element-containing mrnas. *J Biol Chem*, 277(11):9606–9613, Mar 2002.

[193] Tobias M Franks and Jens Lykke-Andersen. TTP and BRF proteins nucleate processing body formation to silence mRNAs with AU-rich elements. *Genes & development*, 21(6):719–35, March 2007.

[194] Georg Stoecklin, Tiffany Stubbs, Nancy Kedersha, Stephen Wax, William F C Rigby, T Keith Blackwell, and Paul Anderson. MK2-induced tristetraprolin:14-3-3 complexes prevent stress granule association and ARE-mRNA decay. *The EMBO journal*, 23(6):1313–24, March 2004.

[195] Sandra L. Clement, Claudia Scheckel, Georg Stoecklin, and Jens Lykke-Andersen. Phosphorylation of tristetraprolin by mk2 impairs au-rich element mrna decay by preventing deadenylase recruitment. *Mol Cell Biol*, 31(2):256–266, Jan 2011.

[196] Francesco P. Marchese, Anna Aubareda, Corina Tudor, Jeremy Saklatvala, Andrew R. Clark, and Jonathan L E. Dean. Mapkap kinase 2 blocks tristetraprolin-directed mrna decay by inhibiting caf1 deadenylase recruitment. *J Biol Chem*, 285(36):27590–27600, Sep 2010.

[197] Wi S Lai, Elizabeth A Kennington, and Perry J Blackshear. Tristetraprolin and Its Family Members Can Promote the Cell-Free Deadenylation of AU-Rich Element-Containing mRNAs by Poly (A) Ribonuclease. *Cell*, 23(11):3798–3812, 2003.

[198] Heike Sandler, Jochen Kreth, H Th Marc Timmers, and Georg Stoecklin. Not1 mediates recruitment of the deadenylase Caf1 to mRNAs targeted for degradation by tristetraprolin. *Nucleic acids research*, 39(10):4373–86, May 2011.

[199] Sandhya Sanduja, Fernando F Blanco, and Dan a Dixon. The roles of TTP and BRF proteins in regulated mRNA decay. *Wiley interdisciplinary reviews. RNA*, 2(1):42–57, January 2010.

[200] Mei-Yan Qi, Zhi-Zhang Wang, Zhuo Zhang, Qin Shao, An Zeng, Xiang-Qi Li, Wen-Qing Li, Chen Wang, Fu-Ju Tian, Qing Li, Jun Zou, Yong-Wen Qin, Gary Brewer, Shuang Huang, and Qing Jing. Au-rich-element-dependent translation repression requires the cooperation of tristetraprolin and rck/p54. *Mol Cell Biol*, 32(5):913–928, Mar 2012.

[201] W S Lai, E Carballo, J R Strum, E a Kennington, R S Phillips, and P J Blackshear. Evidence that tristetraprolin binds to AU-rich elements and promotes the deadenylation and destabilization of tumor necrosis factor alpha mRNA. *Molecular and cellular biology*, 19(6):4311–23, June 1999.

[202] Edward Hitti, Tatiana Iakovleva, Matthew Brook, Stefanie Deppenmeier, Achim D Gruber, Danuta Radzioch, Andrew R Clark, Perry J Blackshear, Alexey Kotlyarov, and Matthias Gaestel. Mitogen-Activated Protein Kinase-Activated Protein Kinase 2 Regulates Tumor Necrosis Factor mRNA Stability and Translation Mainly by Altering Tristetraprolin Expression , Stability , and Binding to Adenine / Uridine-Rich Element. *Society*, 26(6):2399–2407, 2006.

[203] A. Kotlyarov, A. Neininger, C. Schubert, R. Eckert, C. Birchmeier, H. D. Volk, and M. Gaestel. Mapkap kinase 2 is essential for lps-induced tnf-alpha biosynthesis. *Nat Cell Biol*, 1(2):94–97, Jun 1999.

[204] Armin Neininger, Dimitris Kontoyiannis, Alexey Kotlyarov, Reinhard Winzen, Rolf Eckert, Hans-Dieter Volk, Helmut Holtmann, George Kollias, and Matthias Gaestel. Mk2 targets au-rich elements and regulates biosynthesis of tumor necrosis factor and interleukin-6 independently at different post-transcriptional levels. *J Biol Chem*, 277(5):3065–3068, Feb 2002.

[205] K. R. Mahtani, M. Brook, J. L. Dean, G. Sully, J. Saklatvala, and A. R. Clark. Mitogen-activated protein kinase p38 controls the expression and posttranslational modification of tristetraprolin, a regulator of tumor

necrosis factor alpha mrna stability. *Mol Cell Biol*, 21(19):6461–6469, Oct 2001.

[206] E. Carballo, H. Cao, W. S. Lai, E. A. Kennington, D. Campbell, and P. J. Blackshear. Decreased sensitivity of tristetraprolin-deficient cells to p38 inhibitors suggests the involvement of tristetraprolin in the p38 signaling pathway. *J Biol Chem*, 276(45):42580–42587, Nov 2001.

[207] Heping Cao. Expression, purification, and biochemical characterization of the antiinflammatory tristetraprolin: a zinc-dependent mrna binding protein affected by posttranslational modifications. *Biochemistry*, 43(43):13724–13738, Nov 2004.

[208] Heping Cao, Frederick Dzineku, and Perry J. Blackshear. Expression and purification of recombinant tristetraprolin that can bind to tumor necrosis factor-alpha mrna and serve as a substrate for mitogen-activated protein kinases. *Arch Biochem Biophys*, 412(1):106–120, Apr 2003.

[209] Heping Cao, Leesa J. Deterding, and Perry J. Blackshear. Phosphorylation site analysis of the anti-inflammatory and mrna-destabilizing protein tristetraprolin. *Expert Rev Proteomics*, 4(6):711–726, Dec 2007.

[210] Carol A. Chrestensen, Melanie J. Schroeder, Jeffrey Shabanowitz, Donald F. Hunt, Jared W. Pelo, Mark T. Worthington, and Thomas W. Sturgill. Mapkap kinase 2 phosphorylates tristetraprolin on in vivo sites including ser178, a site required for 14-3-3 binding. *J Biol Chem*, 279(11):10176–10184, Mar 2004.

[211] Don Benjamin, Martin Schmidlin, Lu Min, Brigitte Gross, and Christoph Moroni. Brf1 protein turnover and mrna decay activity are regulated by protein kinase b at the same phosphorylation sites. *Mol Cell Biol*, 26(24):9497–9507, Dec 2006.

[212] Lei Sun, Georg Stoecklin, Susan Van Way, Vania Hinkovska-Galcheva, Ren-Feng Guo, Paul Anderson, and Thomas Patrick Shanley. Tristetraprolin (TTP)-14-3-3 complex formation protects TTP from dephosphorylation by protein phosphatase 2a and stabilizes tumor necrosis factor-alpha mRNA. *The Journal of biological chemistry*, 282(6):3766–77, March 2007.

[213] Barbra A. Johnson, Justine R. Stehn, Michael B. Yaffe, and T Keith Blackwell. Cytoplasmic localization of tristetraprolin involves 14-3-3-dependent and -independent mechanisms. *J Biol Chem*, 277(20):18029–18036, May 2002.

[214] Lei Sun, Georg Stoecklin, Susan Van Way, Vania Hinkovska-Galcheva, Ren-Feng Guo, Paul Anderson, and Thomas Patrick Shanley. Tristetraprolin (ttp)-14-3-3 complex formation protects ttp from dephospho-

rylation by protein phosphatase 2a and stabilizes tumor necrosis factor-alpha mrna. *J Biol Chem*, 282(6):3766–3777, Feb 2007.

[215] A. J. Muslin, J. W. Tanner, P. M. Allen, and A. S. Shaw. Interaction of 14-3-3 with signaling proteins is mediated by the recognition of phosphoserine. *Cell*, 84(6):889–897, Mar 1996.

[216] M. B. Yaffe, K. Rittinger, S. Volinia, P. R. Caron, A. Aitken, H. Leffers, S. J. Gamblin, S. J. Smerdon, and L. C. Cantley. The structural basis for 14-3-3:phosphopeptide binding specificity. *Cell*, 91(7):961–971, Dec 1997.

[217] K. Rittinger, J. Budman, J. Xu, S. Volinia, L. C. Cantley, S. J. Smerdon, S. J. Gamblin, and M. B. Yaffe. Structural analysis of 14-3-3 phosphopeptide complexes identifies a dual role for the nuclear export signal of 14-3-3 in ligand binding. *Mol Cell*, 4(2):153–166, Aug 1999.

[218] Surajit Ganguly, Joan L. Weller, Anthony Ho, Philippe Chemineau, Benoit Malpaux, and David C. Klein. Melatonin synthesis: 14-3-3-dependent activation and inhibition of arylalkylamine n-acetyltransferase mediated by phosphoserine-205. *Proc Natl Acad Sci U S A*, 102(4):1222–1227, Jan 2005.

[219] Sojin Shikano, Brian Coblitz, Haiyan Sun, and Min Li. Genetic isolation of transport signals directing cell surface expression. *Nat Cell Biol*, 7(10):985–992, Oct 2005.

[220] Brian Coblitz, Sojin Shikano, Meng Wu, Sandra B. Gabelli, Lisa M. Cockrell, Matt Spieker, Yoshiro Hanyu, Haian Fu, L Mario Amzel, and Min Li. C-terminal recognition by 14-3-3 proteins for surface expression of membrane receptors. *J Biol Chem*, 280(43):36263–36272, Oct 2005.

[221] Marina Uhart, Alberto A. Iglesias, and Diego M. Bustos. Structurally constrained residues outside the binding motif are essential in the interaction of 14-3-3 and phosphorylated partner. *J Mol Biol*, 406(4):552–557, Mar 2011.

[222] Diego M. Bustos. The role of protein disorder in the 14-3-3 interaction network. *Mol Biosyst*, 8(1):178–184, Jan 2012.

[223] Catherine Johnson, Sandra Crowther, Margaret J. Stafford, David G. Campbell, Rachel Toth, and Carol MacKintosh. Bioinformatic and experimental survey of 14-3-3-binding sites. *Biochem J*, 427(1):69–78, Apr 2010.

[224] Shang-Yi Chiu, Guillaume Serin, Osamu Ohara, and Lynne E. Maquat. Characterization of human smg5/7a: a protein with similarities to caenorhabditis elegans smg5 and smg7 that functions in the dephosphorylation of upf1. *RNA*, 9(1):77–87, Jan 2003.

[225] Noemi Fukuhara, Judith Ebert, Leonie Unterholzner, Doris Lindner, Elisa Izaurralde, and Elena Conti. Smg7 is a 14-3-3-like adaptor in the nonsense-mediated mrna decay pathway. *Mol Cell*, 17(4):537–547, Feb 2005.

[226] G. Stoecklin, X. F. Ming, R. Looser, and C. Moroni. Somatic mrna turnover mutants implicate tristetraprolin in the interleukin-3 mrna degradation pathway. *Mol Cell Biol*, 20(11):3753–3763, Jun 2000.

[227] Georg Stoecklin, Marco Colombi, Ines Raineri, Sabrina Leuenberger, Michel Mallaun, Martin Schmidlin, Brigitte Gross, Min Lu, Toshio Kitamura, and Christoph Moroni. Functional cloning of BRF1 , a regulator of ARE-dependent mRNA turnover. *EMBO Journal*, 21(17):4709–4718, 2002.

[228] Deborah J Stumpo, Noah A Byrd, Ruth S Phillips, Sanjukta Ghosh, Robert R Maronpot, Trisha Castranio, Erik N Meyers, Yuji Mishina, and Perry J Blackshear. Chorioallantoic Fusion Defects and Embryonic Lethality Resulting from Disruption of Zfp36L1 , a Gene Encoding a CCCH Tandem Zinc Finger Protein of the Tristetraprolin Family. *Society*, 24(14):6445–6455, 2004.

[229] Sarah E Bell, Maria Jose Sanchez, Olivera Spasic-Boskovic, Tomas Santalucia, Laure Gambardella, Graham J Burton, John J Murphy, John D Norton, Andrew R Clark, and Martin Turner. The RNA binding protein Zfp36l1 is required for normal vascularisation and post-transcriptionally regulates VEGF expression. *Developmental dynamics : an official publication of the American Association of Anatomists*, 235(11):3144–55, November 2006.

[230] Tatiana Vignudelli, Tommaso Selmi, Andrea Martello, Sandra Parenti, Alexis Grande, Claudia Gemelli, Tommaso Zanocco-Marani, and Sergio Ferrari. Zfp36l1 negatively regulates erythroid differentiation of cd34+ hematopoietic stem cells by interfering with the stat5b pathway. *Mol Biol Cell*, 21(19):3340–3351, Oct 2010.

[231] Sjur Reppe, Ole K Olstad, Edith Rian, Vigdis T Gautvik, Kaare M Gautvik, and Rune Jemtland. Butyrate response factor 1 is regulated by parathyroid hormone and bone morphogenetic protein-2 in osteoblastic cells. *Biochemical and Biophysical Research Communications*, 324:218–223, 2004.

[232] Martin Schmidlin, Min Lu, Sabrina a Leuenberger, Georg Stoecklin, Michel Mallaun, Brigitte Gross, Roberto Gherzi, Daniel Hess, Brian a Hemmings, and Christoph Moroni. The ARE-dependent mRNA-destabilizing activity of BRF1 is regulated by protein kinase B. *The EMBO journal*, 23(24):4760–9, December 2004.

[233] Sushmit Maitra, Chu-Fang Chou, Christian a Luber, Kyung-Yeol Lee, Matthias Mann, and Ching-Yi Chen. The AU-rich element mRNA decay-promoting activity of BRF1 is regulated by mitogen-activated protein kinase-activated protein kinase 2. *RNA (New York, N.Y.)*, 14(5):950–9, May 2008.

[234] Silvia B V Ramos, Deborah J Stumpo, Elizabeth A Kennington, Ruth S Phillips, Cheryl B Bock, Fernando Ribeiro-neto, and Perry J Blackshear. The CCCH tandem zinc-finger protein Zfp36l2 is crucial for female fertility and early embryonic development. *Development*, 2004.

[235] Deborah J Stumpo, Hal E Broxmeyer, Toni Ward, Scott Cooper, Giao Hangoc, Yang Jo Chung, William C Shelley, Eric K Richfield, Manas K Ray, Mervin C Yoder, Peter D Aplan, and Perry J Blackshear. Targeted disruption of Zfp36l2, encoding a CCCH tandem zinc finger RNA-binding protein, results in defective hematopoiesis. *Blood*, 114(12):2401–10, September 2009.

[236] Eisaku Iwanaga, Tomoko Nanri, Hiroaki Mitsuya, and Norio Asou. Mutation in the RNA binding protein TIS11D / ZFP36L2 is associated with the pathogenesis of acute leukemia. *International Journal of Oncology*, pages 25–31, 2011.

[237] Daniel J Hodson, Michelle L Janas, Alison Galloway, Sarah E Bell, Simon Andrews, Cheuk M Li, Richard Pannell, Christian W Siebel, H Robson MacDonald, Kim De Keersmaecker, Adolfo a Ferrando, Gerald Grutz, and Martin Turner. Deletion of the RNA-binding proteins ZFP36L1 and ZFP36L2 leads to perturbed thymic development and T lymphoblastic leukemia. *Nature immunology*, 11(8):717–24, August 2010.

[238] Danielle M Carrick and Perry J Blackshear. Comparative expression of tristetraprolin (TTP) family member transcripts in normal human tissues and cancer cell lines. *Archives of biochemistry and biophysics*, 462(2):278–85, June 2007.

[239] Ines Raineri, Daniel Wegmueller, Brigitte Gross, Ulrich Certa, and Christoph Moroni. Roles of AUF1 isoforms , HuR and BRF1 in ARE-dependent mRNA turnover studied by RNA interference. *Development*, 32(4), 2004.

[240] M. Gossen and H. Bujard. Tight control of gene expression in mammalian cells by tetracycline-responsive promoters. *Proc Natl Acad Sci U S A*, 89(12):5547–5551, Jun 1992.

[241] Milan Spasic, Caroline C. Friedel, Johanna Schott, Jochen Kreth, Kathrin Leppek, Sarah Hofmann, Sevim Ozgur, and Georg Stoecklin. Genome-wide assessment of au-rich elements by the arescore algorithm. *PLoS Genet*, 8(1):e1002433, Jan 2012.

[242] Roger S Jackson, Yong-Jig Cho, and Peng Liang. TIS11D is a candidate pro-apoptotic p53 target gene. *Cell cycle (Georgetown, Tex.)*, 5(24):2889–93, December 2006.

[243] Guri Tzivion and Joseph Avruch. 14-3-3 Proteins: Active Cofactors in Cellular Regulation By Serine/Threonine Phosphorylation. *The Journal of biological chemistry*, 277(5):3061–4, February 2002.

[244] Ulrich Rothbauer, Kourosh Zolghadr, Serge Muyldermans, Aloys Schepers, M Cristina Cardoso, and Heinrich Leonhardt. A versatile nanotrap for biochemical and functional studies with fluorescent fusion proteins. *Mol Cell Proteomics*, 7(2):282–289, Feb 2008.

[245] Carol a Chrestensen, Melanie J Schroeder, Jeffrey Shabanowitz, Donald F Hunt, Jared W Pelo, Mark T Worthington, and Thomas W Sturgill. MAPKAP kinase 2 phosphorylates tristetraprolin on in vivo sites including Ser178, a site required for 14-3-3 binding. *The Journal of biological chemistry*, 279(11):10176–84, March 2004.

[246] Meeta Kulkarni, Sevim Ozgur, and Georg Stoecklin. On track with p-bodies. *Biochem Soc Trans*, 38(Pt 1):242–251, Feb 2010.

[247] N Kudo, B Wolff, T Sekimoto, E P Schreiner, Y Yoneda, M Yanagida, S Horinouchi, and M Yoshida. Leptomycin B inhibition of signal-mediated nuclear export by direct binding to CRM1. *Experimental cell research*, 242(2):540–7, August 1998.

[248] C. M. Cahill, G. Tzivion, N. Nasrin, S. Ogg, J. Dore, G. Ruvkun, and M. Alexander-Bridges. Phosphatidylinositol 3-kinase signaling inhibits daf-16 dna binding and function via 14-3-3-dependent and 14-3-3-independent pathways. *J Biol Chem*, 276(16):13402–13410, Apr 2001.

[249] David W. Powell, Madhavi J. Rane, Brian A. Joughin, Ralitsa Kalmukova, Jeong-Ho Hong, Bruce Tidor, William L. Dean, William M. Pierce, Jon B. Klein, Michael B. Yaffe, and Kenneth R. McLeish. Proteomic identification of 14-3-3zeta as a mitogen-activated protein kinase-activated protein kinase 2 substrate: role in dimer formation and ligand binding. *Mol Cell Biol*, 23(15):5376–5387, Aug 2003.

[250] G. A. Seluja, L. Elias, and S. F. Pietromonaco. Two unique 5' untranslated regions in mrnas encoding human 14-3-3 zeta: differential expression in hemopoietic cells. *Biochim Biophys Acta*, 1395(3):281–287, Feb 1998.

[251] Berlinda Verdoodt, Anne Benzinger, Grzegorz M. Popowicz, Tad A. Holak, and Heiko Hermeking. Characterization of 14-3-3sigma dimerization determinants: requirement of homodimerization for inhibition of cell proliferation. *Cell Cycle*, 5(24):2920–2926, Dec 2006.

[252] Roger S Jackson, 2nd, Yong-Jig Cho, and Peng Liang. Tis11d is a candidate pro-apoptotic p53 target gene. *Cell Cycle*, 5(24):2889–2893, Dec 2006.

[253] A. J. Muslin and H. Xing. 14-3-3 proteins: regulation of subcellular localization by molecular interference. *Cell Signal*, 12(11-12):703–709, Dec 2000.

[254] Ramars Amanchy, Balamurugan Periaswamy, Suresh Mathivanan, Raghunath Reddy, Sudhir Gopal Tattikota, and Akhilesh Pandey. A curated compendium of phosphorylation motifs. *Nat Biotechnol*, 25(3):285–286, Mar 2007.

[255] S a Barker, K K Caldwell, a Hall, a M Martinez, J R Pfeiffer, J M Oliver, and B S Wilson. Wortmannin blocks lipid and protein kinase activities associated with PI 3-kinase and inhibits a subset of responses induced by Fc epsilon R1 cross-linking. *Molecular biology of the cell*, 6(9):1145–58, September 1995.

[256] C L Manthey, S W Wang, S D Kinney, and Z Yao. SB202190, a selective inhibitor of p38 mitogen-activated protein kinase, is a powerful regulator of LPS-induced mRNAs in monocytes. *Journal of leukocyte biology*, 64(3):409–17, September 1998.

[257] R. Winzen, M. Kracht, B. Ritter, A. Wilhelm, C. Y. Chen, A. B. Shyu, M. Müller, M. Gaestel, K. Resch, and H. Holtmann. The p38 map kinase pathway signals for cytokine-induced mrna stabilization via map kinase-activated protein kinase 2 and an au-rich region-targeted mechanism. *EMBO J*, 18(18):4969–4980, Sep 1999.

[258] R. Moll and W. W. Franke. Intermediate filaments and their interaction with membranes. the desmosome-cytokeratin filament complex and epithelial differentiation. *Pathol Res Pract*, 175(2-3):146–161, 1982.

[259] Ting-Jen Cheng, Yu-Fang Tseng, Whei-Meih Chang, Margaret Dah-Tsyr Chang, and Yiu-Kay Lai. Retaining of the assembly capability of vimentin phosphorylated by mitogen-activated protein kinase-activated protein kinase-2. *J Cell Biochem*, 89(3):589–602, Jun 2003.

[260] Katrin Engel, Heidi Schultz, Falk Martin, Alexey Kotlyarov, Kathrin Plath, Michael Hahn, Udo Heinemann, and Matthias Gaestel. Constitutive Activation of Mitogen-activated Protein Kinase-activated Protein Kinase 2 by Mutation of Phosphorylation Sites and an A-helix Motif *. *Biochemistry*, 270(45):27213–27221, 1995.

[261] Sandra L Clement, Claudia Scheckel, Georg Stoecklin, and Jens Lykke-Andersen. Phosphorylation of tristetraprolin by MK2 impairs AU-rich element mRNA decay by preventing deadenylase recruitment. *Molecular and cellular biology*, 31(2):256–66, January 2011.

[262] Clyde L. Denis and Junji Chen. The ccr4-not complex plays diverse roles in mrna metabolism. *Prog Nucleic Acid Res Mol Biol*, 73:221–250, 2003.

[263] Brian P Hudson, Maria a Martinez-Yamout, H Jane Dyson, and Peter E Wright. Recognition of the mRNA AU-rich element by the zinc finger domain of TIS11d. *Nature structural & molecular biology*, 11(3):257–64, March 2004.

[264] S. C. Huang and T. C. Lee. Arsenite inhibits mitotic division and perturbs spindle dynamics in hela s3 cells. *Carcinogenesis*, 19(5):889–896, May 1998.

[265] S. R. Datta, A. Brunet, and M. E. Greenberg. Cellular survival: a play in three akts. *Genes Dev*, 13(22):2905–2927, Nov 1999.

[266] A. X. Liu, J. R. Testa, T. C. Hamilton, R. Jove, S. V. Nicosia, and J. Q. Cheng. Akt2, a member of the protein kinase b family, is activated by growth factors, v-ha-ras, and v-src through phosphatidylinositol 3-kinase in human ovarian epithelial cancer cells. *Cancer Res*, 58(14):2973–2977, Jul 1998.